

**MULTIFUNCTIONAL CONDUCTING POLYMER COATINGS FOR MAGNESIUM
IMPLANTS**

by

Kasey Catt

B.S. Bioengineering, The Pennsylvania State University, 2010

Submitted to the Graduate Faculty of
Swanson School of Engineering in partial fulfillment
of the requirements for the degree of
Doctor of Philosophy

University of Pittsburgh

2016

UNIVERSITY OF PITTSBURGH
SWANSON SCHOOL OF ENGINEERING

This dissertation was presented

by

Kasey Catt

It was defended on

June 23, 2016

and approved by

Prashant Kumta, Ph.D., Edward R. Weidlein Chair Professor, Departments of
Bioengineering, Chemical and Petroleum Engineering, Mechanical Engineering

Kacey Marra, Ph.D., Associate Professor, Departments of Plastic Surgery and Bioengineering

Yeoheung Yun, Ph.D., Associate Professor, Department of Chemical and Biological
Engineering, North Carolina A&T State University

Dissertation Director: Tracy Cui, Ph.D., William Kepler Witeford Professor, Department of
Bioengineering

Copyright © by Kasey Catt

2016

MULTIFUNCTIONAL CONDUCTING POLYMER COATINGS FOR MAGNESIUM IMPLANTS

Kasey Catt, PhD

University of Pittsburgh, 2016

Magnesium's potential to degrade completely *in vivo* with safe corrosion byproducts make it a promising biomaterial for use in a wide array of implants from orthopedic fixation devices that do not require a removal surgery to peripheral nerve guides that degrade away after regeneration. However, a few issues need to be addressed before widespread clinical use can be realized. Firstly, Mg often degrades too rapidly *in vivo*. Rapid degradation can result in the mechanical instability and gas bubbles that may separate the implant from the tissue. Secondly, Mg implants lack the ability to combat potential infection and the inflammatory foreign body response. Lastly, Mg alone lacks a versatile functionalization method to incorporate tissue specific cues that better guide tissue growth and regeneration. To overcome these issues, conducting polymer based coatings with a combination of functionalities in corrosion control, drug release, and biofunctionalization are investigated in this thesis.

A composite coating of conducting polymer poly 3,4-ethylene dioxythiophene (PEDOT) doped with Graphene Oxide (GO) has been developed for improving Mg implant performance for applications such as orthopedic fixation, stents, and peripheral nerve regeneration. The PEDOT/GO coating decreased Mg corrosion throughout 22days of immersion in a phosphate buffered solution. Corrosion protection is attributed to an initial passive barrier followed by electrochemical coupling of the coating with the Mg to form a more protective Mg phosphate layer. Additionally, anti-inflammatory drug Dexamethasone was incorporated into the PEDOT/GO film and it was shown that Mg corrosion current could drive drug

release. Lastly, the carboxylic acid groups of the GO sheets exposed at the surface of the PEDOT/GO coating were used to immobilize multiple bioactive molecules. Specifically, immobilized poly ethylene glycol (PEG) prevented both bacterial and fibroblast attachment, while nerve growth factor (NGF) attachment increased neurite sprouting from PC12 cells. These results suggest that the PEDOT/GO coating has the potential to be a versatile coating that can provide corrosion protection and add biologically relevant cues to the Mg implant.

TABLE OF CONTENTS

PREFACE.....	XIII
1.0 INTRODUCTION	1
1.1 MAGNESIUM AS A DEGRADABLE BIOMATERIAL	2
1.1.1 Biocompatibility and Biodegradation.....	2
1.1.2 Mechanical properties of Mg.....	4
1.1.3 History as a biomedical material.....	4
1.1.4 Mg modifications to improve performance.....	5
1.1.4.1 Mg Alloys	5
1.1.4.2 Conversion coatings	7
1.1.4.3 Polymer coatings	8
1.1.5 Summary	10
1.2 CONDUCTING POLYMERS.....	10
1.2.1 Polymerization of CP.....	11
1.2.2 Doping and conductivity of the CP	13
1.2.3 Applications of conducting polymers.....	14
1.2.4 Summary	16
1.3 GRAPHENE AND GRAPHENE OXIDE	17
1.4 CONDUCTING POLYMER AND GRAPHENE COMPOSITES	19

1.5	THESIS ORGANIZATION.....	20
2.0	POLY (3,4-ETHYLENEDIOXYTHIOPHENE) GRAPHENE OXIDE COMPOSITE COATINGS FOR CONTROLLING MAGNEISUM IMPLANT CORROSION	22
2.1	ABSTRACT.....	22
2.2	INTRODUCTION	23
2.3	MATERIALS AND METHODS	25
2.3.1	Materials.....	25
2.3.2	Polymerization of the PEDOT/GO film.....	26
2.3.3	Tafel Scan	27
2.3.4	Long term corrosion tests (pH, Mg ion, OCP, and EIS).....	28
2.3.4.1	OCP and EIS	28
2.3.4.2	pH and Mg ion concentration measurement	29
2.3.5	Hydrogen evolution measurement	29
2.3.6	SEM and EDX analysis	30
2.3.7	Neuron culture	30
2.3.7.1	LDH Assay	31
2.3.7.2	Live dead staining	31
2.3.8	Statistics	31
2.4	RESULTS.....	32
2.4.1	Film formation	32
2.4.2	SEM and EDX analysis	35
2.4.3	Corrosion Characterization.....	37
2.4.3.1	Tafel Scan.....	38
2.4.3.2	Magnesium ion analysis.....	39

2.4.3.3	pH analysis.....	40
2.4.3.4	Electrochemical tests.....	42
2.4.3.6	EIS	43
2.4.3.7	Equivalent circuit analysis	44
2.4.4	Hydrogen evolution	48
2.4.5	Cytotoxicity	49
2.4.5.1	LDH.....	49
2.4.5.2	Live/Dead assay	50
2.5	DISCUSSION.....	52
2.6	CONCLUSION	57
3.0	SELF-POWERED THERAPUTIC RELEASE FROM CONDUCTING POLYMER FILMS ON MAGNESIUM	59
3.1	ABSTRACT.....	59
3.2	INTRODUCTION	60
3.3	MATERIALS AND METHODS.....	65
3.3.1	Materials.....	65
3.3.2	PEDOT/GO/DEX film polymerization.....	65
3.3.3	SEM.....	66
3.3.4	Impedance spectroscopy	66
3.3.5	Tafel Scan	67
3.3.6	Hydrogen evolution	67
3.3.7	Powered release.....	68
3.3.8	Corrosion triggered release	68
3.3.9	Bioactivity assessment	69

3.4	RESULTS	70
3.4.1	SEM.....	70
3.4.2	Impedance Spectroscopy.....	72
3.4.3	Tafel scan.....	74
3.4.4	Hydrogen evolution	75
3.4.5	Externally powered drug release.....	76
3.4.6	Corrosion triggered drug release	77
3.4.7	Bioactivity of release Dex	79
3.5	DISCUSSION.....	81
3.6	CONCLUSION	86
4.0	PEDOT/GO COATINGS AS A METHOD FOR ADDING BIO-FUNCTIONAL SURFACE CUES	87
4.1	ABSTRACT.....	87
4.2	INTRODUCTION	88
4.2.1	Problems that can be addressed by surface functionalization	88
4.2.2	Prevention of infection	89
4.2.3	Mitigation of inflammation.....	90
4.2.4	Implant specific cues	91
4.2.5	EDC-NHS linking	94
4.3	MATERIALS AND METHODS.....	95
4.3.1	Materials.....	95
4.3.2	Polymerization of PEDOT/GO film.....	96
4.3.3	EDC-NHS functionalization	97
4.3.4	NIH-3T3 fibroblast	97

4.3.5	Live dead stain	98
4.3.6	PC12 cell culture	98
4.3.7	Cell Fixation for SEM	99
4.3.8	Cytochrome C assay	99
4.3.9	Bacteria culture.....	100
4.4	RESULTS	100
4.4.1	Albumin-Fluorescein	100
4.4.2	NIH 3T3 Fibroblast attachment.....	102
4.4.3	PC12 cell attachment and neurite sprouting.....	104
4.4.4	Cytochrome C Assay	109
4.4.5	Bacteria Culture	110
4.5	DISCUSSION.....	111
4.6	CONCLUSION	117
5.0	CONCLUSION	118
5.1	SUMMARY OF RESULTS	118
5.2	FUTURE DIRECTIONS.....	121
	BIBLIOGRAPHY	124

LIST OF FIGURES

Figure 2-1: Mg ribbon following polymerization.....	26
Figure 2-2: Tafel scan immersion.....	27
Figure 2-3: Mg samples for long term corrosion tests.....	28
Figure 2-4: Macroscopic morphology.	34
Figure 2-5: Micro morphology.	36
Figure 2-6: EDX post corrosion.....	37
Figure 2-7: Tafel scan.	39
Figure 2-8: Mg ion concentration.	40
Figure 2-9: Hydroxide in the corrosion solution.....	41
Figure 2-10: Open circuit potential.....	43
Figure 2-11: EIS.....	44
Figure 2-12: Equivalent Circuit Modeling.....	47
Figure 2-13: Hydrogen evolution.....	49
Figure 2-14: Cytotoxicity.....	51
Figure 2-15: Corrosion Protection Mechanism.....	57
Figure 3-1: PEDOT/GO/Dex Mg morphology.	71
Figure 3-2: PEDOT/GO/Dex on Mg EIS.....	73
Figure 3-3: Tafel Scan.	75

Figure 3-4: Hydrogen evolution.....	76
Figure 3-5: Powered drug release.	77
Figure 3-6: Corrosion powered drug release.	79
Figure 3-7: Dex Bioactivity.	80
Figure 4-1: Albumin-Fluorescein surface attachment.	101
Figure 4-2: NIH 3T3 on PEG surface.	103
Figure 4-3: PC12 control culture.	104
Figure 4-4: PC12 Cell culture.	106
Figure 4-5: PC12 SEM.....	108
Figure 4-6: Cytochrome C Assay.	110
Figure 4-7: E coli attachment and viability.....	111

PREFACE

This work, and my education here, was all graciously made possible by my advisor. For that, I would like to give my most sincere thanks to Dr. Tracy Cui for all the encouragement, support, guidance, and constructive criticism she has provided me over these last six years. I would also like to acknowledge all of the past and current members of the NTE Lab without who's help I would not have made it this far. Thanks to Dr. Xiliang Lou who showed me the ropes when it came to conducting polymers. Thanks to Dr. Christi Kolarcik who constantly provided the knowledge to take a step back and critically evaluate the situation. Thanks to Dr. Takashi Kozai who was always a wealth of knowledge. Thanks to Dr. Cassandra Weaver who taught me the ways of cell culture. Thanks to Dr. Jeff Du for always being someone I could bring my questions to. Thanks to Dr. Nick Alba for helping with the Autolab. Thanks to Dr. Noah Snyder for being a great motivator. Thanks to Dr. Ian Mitch Taylor for always saying exactly what he was thinking. Resounding thank you to Dr. Xia Li who constantly made sure the lab was stocked and running smoothly. Thanks to Mr. James Eles for always being able to make light of the situation. Thanks to Mr. Patrick Cody for his help in cell culture. I would also like to thank the undergrad students who worked with me over the year. Thank you to Huaxiu Li who has worked on these projects for the past three years and could always be relied on. Thank you to Victor Hoang and Roland Beard who greatly helped with the drug release experiments.

My work here could not have been completed without the support of my loving family. Thank you to my wife who was always there to celebrate when an experiment worked and console me when it did not. Thanks to my parents who continually supported me in many ways throughout my grad school journey.

Without you all I would have never made it this far!

1.0 INTRODUCTION

Implantable medical devices have become a standard in the current healthcare system. From pacemakers to deep brain stimulators, implanted devices have improved the lives of countless patients. However, for certain applications, continual presence of the device is not ideal, due to chronic inflammation, the foreign body response, and device specific issues such as increased thrombogenicity and restenosis for stents and potential metal particulate toxicity from current orthopedic materials. For these implantable devices that are only temporarily needed, the requirement of surgical implant removal once the tissue has healed minimizes their current applications. Making a temporary device out of biodegradable materials would eliminate the need to surgically remove these devices and consequently increase device implementation as well as improve patient outcomes. To accomplish this, a variety of degradable materials including polymers and ceramics have been developed, however, Magnesium's (Mg) superior mechanical properties and safe degradation byproducts, provided the corrosion rate is controlled, make it a continually promising material. Mg corrodes naturally *in vivo* and results in safe degradation products provided the corrosion rate is appropriately controlled. Mg devices such as stents, orthopedic fixation screws and plates, and nerve guides provide the opportunity to promote proper patient healing without the need for surgical intervention to remove the device once its presence is no longer required. Additionally, *in vivo* device degradation decreases potential complications of long-term device presence such as restenosis and chronic

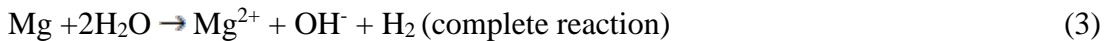
inflammation. If the corrosion rate of Mg is properly controlled, these Mg devices could be designed in such a way that they only exist for the period the specific tissue needs to regenerate and following this period they degrade away safely in the body. This thesis describes use of conducting polymers for corrosion control and improvement of Mg implant interactions with native tissue.

1.1 MAGNESIUM AS A DEGRADABLE BIOMATERIAL

1.1.1 Biocompatibility and Biodegradation

Magnesium is an extraordinarily promising material for use in biomedical implants due to a multiple factors. Firstly, Mg is considered an essential human nutrient[1]. Mg is the fourth most abundant cation in the human body and has been shown to be present at different concentrations in nearly all cells[2, 3]. The recommended dietary allowance, the average daily intake sufficient to meet the nutritional needs of ~98% of healthy individuals, of Mg for adults is 300-400mg[4]. The binding of Mg to ATP is required for energy generation[5]. Mg interacts with nucleic acids in a variety of ways and is required in the synthesis of DNA[6, 7]. Mg is utilized in at least 300 enzymes that are involved in a wide variety of biochemical processes that dictate things such as neural activity, muscular contraction, and proper blood glucose and pressure[6]. Magnesium also facilitates membrane transport of additional important ions calcium and phosphorus[8]. This excessive presence of Mg in the human body lends to the expectation that Mg implants will be an exceptionally biocompatible material.

In addition to its prevalence in the human body, Mg has the potential to completely corrode *in vivo* without toxic side effects. When placed *in vivo*, the corrosion of Mg proceeds as follows.



Here the anodic dissolution of Mg (equation 2) generates electrons that reduce water through the cathodic reduction of H₂O (equation 1). The complete reaction (equation 3) results in the formation of hydrogen gas, hydroxide ions, and Mg²⁺ ions. Provided the Mg corrosion is slow enough, the hydrogen gas is free to diffuse away through the tissue[9]. The hydroxide ion will either be buffered by the body's many buffering systems or will react with the Mg²⁺ ions to form Mg hydroxide (equation 4).



Mg(OH)₂ is insoluble and will be deposited on the surface of the corroding magnesium. Mg(OH)₂ has a porous and amorphous morphology that does not provide a significant improvement in corrosion protection[10, 11]. *In vivo* this Mg(OH)₂ layer is easily converted by the chloride ions in the body to a soluble MgCl₂[1, 12, 13]. This corrosion product can be excreted through urination minimizing potential toxicity issues as the implant degrades[14, 15]. This process of *in vivo* degradation resulting in safe byproducts Mg²⁺, OH⁻, and hydrogen is one of the main benefits of using Mg as an implant material.

1.1.2 Mechanical properties of Mg

The superior mechanical properties of Mg are also alluring for implementation as a biomedical implant. Mg and its alloys have a Young's moduli of around 41-45 GPa and densities of around 1.74-2 g/cm³ which outperform current degradable polymers such as poly L-lactic acid(PLA), Polyglycolic acid(PGA), and the combinations of PLA and PGA which have young's moduli of 2.5-6.5 GPa and a specific densities of 1.24-1.61 g/cm²[3, 16, 17]. This gives Mg a superior strength to weight ratio advantage over current degradable polymers making it a more viable option for structures like stents. Also Mg's mechanical properties match those of bone, young's moduli 3-20 GPa and density 1.8-2.1 g/cm², much more closely than current orthopedic biomaterials such as Ti (110-117 GPa & 4.4-4.5 g/cm²), Co-Cr alloy (230 GPa & 8.3-9.2 g/cm²), and stainless steel (189-205 GPa & 7.9-8.1 g/cm²)[15]. This close mechanical match between Mg and bone has the potential to minimize stress shielding observed with current orthopedic implant metals[3, 15].

1.1.3 History as a biomedical material

The first use of Mg in medicine was in 1878 when physician Edward C. Huse used Mg wire, originally designed for pyrotechnics and early photography, as ligatures to stop bleeding in human patients[18]. Following Huse, Austrian physician Dr. Erwin Payr pioneered the testing of magnesium for multiple applications starting in 1892[18]. Payr tested Mg structures for connection of vessel anastomosis, as well as use of screws, plates, and pegs for orthopedic fixation and a variety of general surgery closure and suture applications. Payr also used Mg for the connection of nerves during neurolysis. Early issues with Mg wires that limited their use

resulted from the Mg being brittle and their breaking when tied in a knot. Investigators explored a variety of alloys to improve the ductility of these Mg wires. Following Payr's work, researchers in the 20th century continued to test various Mg alloys for a multitude of applications with varied success. In 1917 Andrews tested Mg clips as substitutes for ligatures for wound closure and suggested while it safely degrades, the degradation is too rapid and the mechanical properties of Mg are not sufficiently strong[19]. In the 1930s Verbrugge experimented with the use of Mg alloys as plates bands and screws[18]. In 1951 Stone & Lord investigated the ability of Mg-Al alloy wires for clotting aneurisms[20]. In 1981 Hussel *et al* looked at the degradation rate of Mg rods in both rat and rabbit subcutaneously and intramuscularly[21]. Of all the work completed in the late 19th and throughout the 20th century, while Mg showed it could be a valuable tool to act as a degradable fixation device, researchers noted rapid degradation and a buildup of gas bubble pockets surrounding the degrading device[18].

1.1.4 Mg modifications to improve performance

To realize the goal of a fully degradable implant material where the corrosion rate can be controlled and with minimal generation of hydrogen gas, many techniques have been employed. These involve alloying Mg with other elements, generating different surface coatings, or applying organic coatings on top of the Mg.

1.1.4.1 Mg Alloys

Alloying Mg with different elements can improve corrosion resistance, ductility, as well as mechanical strength[11, 22-27]. These alloys, frequently taken from the aerospace and automotive industries, often use elements that are considerably more toxic than Mg itself such as

aluminum and rare earth elements. While Mg alloys with these elements can present favorable mechanical properties and corrosion rates, the concern for toxicity of the alloying elements upon corrosion has minimized their use in biomedical applications. To address the biocompatibility concerns, elements that are considered less toxic have been recently investigated[28-32]. These include elements like essential nutrients calcium, zinc, and manganese, as well as potentially essential metals that are used in other biomedical applications like Strontium, Tin, and Silicon[1]. A wide variety of Calcium (Ca) based alloys have been investigated. Mg-Ca binary alloys have shown good mechanical properties as well as biocompatibility[33]. Zinc is also considered to be a biocompatible metal[34]. Mg-Zn alloys have improved mechanical properties as well as a decreased corrosion rate[35, 36]. Manganese alloys of Mg have been shown to decrease the effects of impurities on Mg, decreasing the damaging effects of galvanic coupling with impurities and consequently decreasing corrosion rates[36, 37]. Silicon, while having low solubility, has been reported as an optimal alloy for improving Mg's yield strength and ultimate tensile strength[38]. Mg Zirconium alloys have also improved Mg's mechanical properties as well as resulted in a 50% decrease in corrosion rate[38]. While binary alloys of Mg minimize the potential for corrosion byproduct cytotoxicity, Mg alloys with many different combinations of alloying elements have been tested to further improve corrosion resistance and mechanical properties[17, 32, 36, 39-42]. Despite the potential issues associated with the release of alloying elements during corrosion, some companies have received the CE mark for use of their proprietary Mg alloys in biomedical applications. Syntellix AG received the CE mark for their Mg based screw *Magnezix*[®] in 2013, and Trans Luminal Technologies LLC received the CE mark in 2014 for their Mg based vascular closure device *Velox CD*[™] [43, 44]. In summary, alloying represents a promising way to improve Mg performance for biomedical applications.

1.1.4.2 Conversion coatings

In addition to alloying, multiple surface treatments have been tested to further adjust the corrosion rate of Mg. These include conversion coatings that are created by immersing the Mg in a salt bath to facilitate specific corrosion products via the inherent corrosion of Mg. The most simple conversion coating is that of alkali treatment where the inherent MgO and Mg(OH)₂ surface products are further altered[45]. These coatings show an initial decrease in corrosion rate but can be easily broken down by Cl in the body[2]. Calcium phosphate coatings as well as hydroxyapatite coatings have been investigated due to their similarity to bone[46-48]. Fluoride treatments are also of interest to orthopedic applications due to improved bone interactions[49, 50]. Fluoride conversion coatings have shown improved corrosion resistance on both pure Mg and Mg alloys[51-53]. These and a variety of other conversion coatings have been investigated on Mg alloys as well as pure Mg, however corrosion protection is still inadequate[2, 54-57]. Further techniques involve electrochemical anodization to generate surface coatings with improved properties. Anodization of Mg samples takes conversion coatings one step further in that, in addition to facilitating a corrosion product by immersing the Mg in different media, an electrical potential is applied which can change the morphology and structure of the deposited corrosion layer. Anodization in basic solutions results in the growth of a more stable variant of the MgO and Mg(OH)₂ layer[58, 59]. Calcium phosphate and hydroxyapatite coatings have also been deposited on Mg substrates through anodization[60, 61]. Another anodization paradigm used is plasma electrolytic oxidation (PEO), or microarc oxidation, where anodization is conducted above the breakdown potential resulting in films that are generally more protective than conversion coatings[2]. PEO treatments in biologically relevant media, Hanks solution and simulated body fluid, have shown an improvement in corrosion protection as well as improved

wear resistance[62-64]. PEO has also been used to deposit calcium phosphate coatings[65-67] as well as fluoride coatings[68]. A variety of different coatings have been applied to Mg and its alloys through PEO in the effort to improve corrosion and wear performance[69-71]. The benefit of anodization and PEO over conversion coatings is that the energy applied during formation results in a more dense and uniform film with a complete coverage of the sample that results in superior corrosion protection.

1.1.4.3 Polymer coatings

Other techniques used to improve Mg corrosion resistance include the application of an additional surface coating, commonly a polymer, either degradable or non-degradable. These polymer coatings provide added benefits of potential mechanisms for drug release as well as methods for adding functional biomolecules to Mg [2, 72]. Coatings of non-degradable poly(ether imide) PEI have improved Mg corrosion resistance[73, 74]. PLGA degradable polymer coatings have been effective at slowing Mg corrosion as well as improving Mg alloy in vitro interactions with osteoblast-like MC3T3 cells[75]. Applications of other degradable polymers PLA and polycaprilactone(PCL) have also shown the ability to improve corrosion resistance of Mg and improve cytocompatibility with osteoblasts[76, 77]. Xu and Yamamoto[78] compared Mg coated with PLLA or PCL via spin coating and concluded that both coatings improve cytocompatibility while PLLA was better adhered to the Mg substrate. Prior to organic coating application, Mg and its alloys are often pretreated with a conversion coating or PEO surface treatments to improve the adhesion of these organic coatings[2, 72, 79]. This dual protection paradigm can combine the corrosion protection of the conversion coating and polymer coating in addition to providing a system for drug release and surface functionalization.

Drug release from these polymer coatings is another potentially powerful technique to improve in vivo Mg implant performance. The most common techniques for drug release is diffusion of the drug from the film or release of the drug from the film as the polymer degrades[72]. Lu et al [80] deposited PLGA coatings on pretreated Mg which released drug at different rates based on the ratio of lactic and glycolic acids. These drug releasing PLGA coatings also improved corrosion resistance of the coated Mg. Mg based stents coated with degradable polymer from Biotronic SE & Co. have shown the ability to release paclitaxel and degrade away safely[81]. Adjusting the polymer ratios in PLGA coatings on degradable stents can tailor the release rate of drugs like paclitaxel[82]. Cross-linked gelatin with degradable PLGA drug containing nanoparticles have also been used as a drug releasing platform on Mg where the release rate could be controlled through the crosslinking density[83]. Polymer coatings also provide loci for further functionalization. PLLA coatings on Mg allowed for the attachment of fibronectin which improved the attachment of MC3T3 osteoblast like cells[84]. While these different polymer coatings provide a viable method of controlled drug release there is minimal corrosion protection. Once the polymer has degraded away, corrosion of the underlying Mg substrate proceeds unhindered. Additionally, these drug releasing coatings do not provide an on demand release, once in contact with body fluid, the polymer begins to degrade and release the drug. A drug releasing platform that can respond to changes around the implant and release drugs at specific events could help to improve the local tissue response and minimize potential toxic side effects of the continual drug delivery of current coatings. It would be ideal if a coating could provide both active corrosion control as well as a method for releasing drugs on demand.

1.1.5 Summary

Mg has a potential multitude of applications in the biomedical field due to its biocompatibility, biodegradation, and superior mechanical properties compared to current biodegradable materials. Since the 1870s, Mg materials have been investigated for these applications, however rapid degradation and buildup of gas bubbles surrounding the implants have limited the clinical use of Mg. To combat these issues different techniques such as, alloying, conversion coating, anodizing, and coating with polymers have been tested. While promising, these techniques still leave room for improvement in terms of biocompatibility and corrosion protection performance. In addition, the current techniques have limited abilities to deliver drugs around the implant in an on demand way. Current polymer coatings simply release drug as the polymer is degraded in vivo. A technique that could both control Mg corrosion and provide an on demand method for drug release could facilitate the transition of Mg implants from academic research to clinical applications.

1.2 CONDUCTING POLYMERS

Electro-active conducting polymers (CP) are a unique set of materials that possess both conductivity and redox properties. Since first being reported by Henry Letheby, a British chemist, in 1862, CPs have found uses in many applications[85]. Largely developed from the 1970s onward, CPs have been used in thin film transistors[86], fuel cells[87], super capacitors[88], corrosion control[89, 90], and sensors[91, 92]. In addition, CPs have been investigated for a wide range of biomedical applications[93-95]. From improving the charge

transfer on microelectrodes[96-99], to acting as a controllable drug releasing platform[100-102], to facilitating the addition of surface cues[103], CP structure and function have the ability to suit many different applications through careful tailoring of the chemistry.

1.2.1 Polymerization of CP

CP synthesis is one of the attractive aspects of these unique polymers with the ability to be both chemically driven as well as electrochemically driven. In both instances, oxidation of the monomer is followed by free radical polymerization where the new polymer will precipitate out of the polymerization solution upon its increase in molecular weight[104]. The chemical polymerization method utilizes strong oxidizing agents to facilitate polymerization that are ideal for large-scale solution polymerization. To create a thin film from CPs polymerized with this technique, the CP is placed on the sample and the sample is then spun at a consistent speed resulting in a thin polymer film. This technique is good for flat surfaces without much topography. In some cases oxidizing agents have been immobilized on the surface to generate a thin film of polymer, however uniformity and thickness are difficult to control making thin films of CP difficult to fabricate with chemical polymerization methods[105]. To overcome some of the issues associated with chemical polymerization, electrochemical polymerization has been investigated. While limited in that the surface to be coated must be conductive and not effective for bulk polymerization, electro-polymerization allows for a more controlled deposition of thin films of CPs on more complex geometries. Electro-polymerization utilizes an oxidizing potential on an electrode immersed in a monomer solution. This potential drives the radical polymerization at the surface of the electrode on which the potential is applied resulting in the deposition of thin films of the polymer on the surface[105]. This dissertation utilizes this method

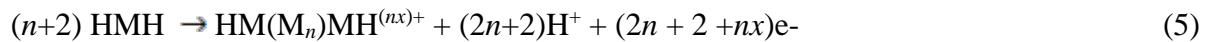
of electro-polymerization due to its ability to coat the potentially complex geometries of structures like stents.

Electro-polymerization provides additional control over the deposition parameters in that the intensity of the applied potential or current as well as the duration can be carefully controlled through the hardware of the electrochemical system. Electro-polymerization has been conducted in three different ways, potentiodynamic, galvanostatic, and potentiostatic each with its benefits and drawbacks. Potentiodynamic involves the sweeping of applied potentials between magnitudes that would drive polymerization and those that are too weak to drive polymerization. This allows for the deposition of very thin films of CP via one sweep and in order to build up a thicker layer multiple cycles are often conducted. The repeated deposition of thin layers of polymer with a wait time in-between, as the potential is not strong enough to drive polymerization, allows for the entrapment of solvents and other molecules present in the polymerization solution[106]. Entrapped anion and solvent molecules then affect the resulting CP in terms of compactness or degree of swelling and electrical performance. Galvanostatic polymerization applies a set current for a set duration in which the current results in a potential that is sufficiently intense to drive polymerization. This constant current method allows for the same total charge to be delivered during film creation resulting in the same amount of polymer being deposited and consequently films of the same thickness. Despite the control over the current, the potential is free to fluctuate during polymerization resulting in films with differing degrees of oxidation and consequently different electrochemical behavior. Potentiostatic methods set the applied potential during polymerization, which prevents over oxidation of the CP. However, the current, and therefore total charge, are allowed to fluctuate making it difficult to create coatings of uniform thickness. To remedy these drawbacks of potentiostatic and

galvanostatic polymerization, a method called chronocoulometry uses potentiostatic polymerization with built in integrator that allows for the continual calculation of the total charge used during the polymerization. This method allows for precise control of the potential applied as well as consistent total charge and resulting film thickness. This chronocoulometry method was used for the polymerizations presented in this thesis due to optimal potential control as well as the ability to polymerize multiple films with the same total charge.

1.2.2 Doping and conductivity of the CP

Deposition of CP alone results in films with minimal conductivity, however further reducing or oxidizing the polymer backbone can improve the conductivity of these polymers to levels of metals[105]. This thesis will focus on the further oxidation of the polymer backbone as it is accomplished in a one-step electropolymerization where an oxidizing potential is used to both drive polymerization and oxidize the polymerized CP backbone. Oxidation of the polymer backbone results in a positive charge on the backbone that, during polymerization, is balanced by incorporating negative molecules into polymer film termed ‘dopants’. These dopants are incorporated into the film and associated with the positive charges located on the CP backbone. The reaction depicting this polymerization, oxidation, and doping process can be seen in equation 5 where HMH is the CP monomer.



Doping levels of conducting polymers typically fall between 0.25 and 0.4 represented as x in the above equation[107].

Following doping of the film, CP conductivity is attributed to both the conjugated backbone as well as the formation of polarons and bipolarons on the oxidized backbone which are neutralized by the dopant molecules. The conjugated backbone of the CP consists of alternating double and single bonded sp^2 hybridized atoms with overlapping p-orbitals[105]. These overlapping p-orbitals result in the formation of π molecular orbitals and the ability to share electrons through this continuous supramolecular orbital [108]. Upon further oxidation, electric holes are created in the polymer backbone. Polarons and bipolarons are created by these holes upon addition of the dopant. This results in mobile charge carriers consisting of loosely localized electrons surrounded by distortion of the lattice on the CP backbone which further improves conductivity[109].

A unique property of these CPs is their ability to undergo reversible redox reactions. After electro-polymerization, the polymer backbone is in an oxidized state with positive charge on the backbone and negatively charged dopants trapped in the CP to neutralize this charge. If a reducing potential is then applied to the polymer, the positive charge on the CP backbone can be neutralized resulting in no electrostatic force holding the negative dopant in the film. These dopants then have the ability to diffuse out of the film into the surrounding media. This process has been used extensively as a method for controlled drug delivery[101, 102, 110-113]. It has also been shown that larger dopants can remain trapped in the film resulting in the intake of positive ions to balance the negative charge left behind upon polymer reduction[114].

1.2.3 Applications of conducting polymers

The reversible redox properties make CPs useful micro actuators. Mechanical changes are facilitated by the insertion and expulsion of counter ions during reduction and oxidation[115].

Smela et al first showed the ability to use CP redox reactions as actuators by creating bi-layered structures of gold and CP[116]. Upon reduction of the polymer, the expulsion of anions, and shrinkage of the CP caused the structures to curl. This was further elaborated to a box design where the entire gold/CP box could be opened and closed. Jager et al used a complex micro fabricated structure of gold and CP to create a micrometer sized manipulator[117]. The combined actuation of CP gold structures could pick up and move a 100 μm glass bead a distance of 250 μm . In addition to the μm motion of objects, these CP actuators have been used as strain sensors [118, 119] and for the detection of acid/base[120].

Redox properties of CPs have also been used for electrochromic devices where the optical properties of the CP are dependent on its redox state. Devices consisting of layers of different CPs have shown fast response times and long-term stability as electrochromic devices[121]. These CP electrochromic devices have also shown improvements in bleached vs. colored switching time and improved contrast[122, 123].

CPs have also shown promise as a useful technology for biomedical applications including sensors[124, 125], tissue engineering[94, 95, 126-128], and electrodes that interface with tissue[96, 97, 113, 129-131]. Conducting polymer morphology is highly dependent on the dopant incorporated, however, even small dopants result in a rough surface morphology. This rough surface increases the effective surface area and consequently decreases electrode resistance and improves capacitive charge transfer. The lower resistance provided by CP coatings on neural electrodes has been shown to improve the recording of these electrodes[96]. CPs also facilitate more effective charge transfer through faradaic charge transfer mechanisms. For metal electrodes, faradaic charge transfer takes place through the oxidation of the metal which can result in electrode damage[129]. CPs on the other hand can facilitate charge transfer

through the reduction and oxidation of its backbone that is accompanied by the expulsion and incorporation of ions. This results in improved charge transfer for stimulation electrodes in that lower voltages are required to pass the same amount of charge which minimizes potential tissue damage from high potentials[99]. Conducting polymers also can improve the tissue reaction to implanted electrodes by providing a mechanical buffer between the generally hard electrodes and soft neural tissue[132]. The release of entrapped ions during polymer reduction has also been investigated as a way to locally deliver drugs to improve tissue reactions around CP coated electrodes[110]. Release of anti-inflammatory dexamethasone from CP coated electrodes has been used to decrease inflammation around implanted electrodes[98, 133]. Conducting polymers also provide mechanisms for functionalization with bioactive molecules that can improve the interaction of local tissue with the polymer or be used to elicit specific changes in the local tissue[97, 103, 134].

1.2.4 Summary

CPs can be deposited on to conducting substrates of different geometries through electropolymerization. This results in a CP film that is both electrically and ionically conductive. These CPs can undergo reversible redox reactions where the polymer backbone is reduced and the charged dopants are released from the film. These properties of CPs have resulted in their application in a wide variety of application including exploration for many biomedical applications.

1.3 GRAPHENE AND GRAPHENE OXIDE

Graphene is a relatively new carbon structure that was first synthesized in 2004 and consists of a single atomic layer of carbon arranged in a 2 dimensional honeycomb lattice[135, 136]. This unique structure presents a myriad of new properties including exceptional electronic, mechanical, and optical properties[137-139]. The properties of graphene are highly dependent on the purity and as a result, a variety of methods for developing graphene have been introduced. One of the more popular methods is that of chemical exfoliation because it is relatively low cost and more easily scaled than other methods. This process uses strong oxidizing agents to separate graphene from graphite resulting in graphene sheets that are highly oxidized referred to as graphene oxide (GO)[140]. In an effort to convert GO to graphene, different chemical, thermal, and electrochemical treatments have been tested to create reduced GO (rGO) which has similar performance characteristics to graphene. The intermediate GO has also garnered interest due to the large number of reactive oxygen functional groups which allow for the addition of different chemical groups[140].

While the exact chemical structure of GO is dependent on its fabrication route and still debated, the generally accepted model of GO is that proposed by Lerf-Klinowski[140]. This consists of the carbon honeycomb sheet of graphene with dislocations of hydroxyl (C-OH) and epoxide (C-O-C) as well as carboxyl (C-O-OH) groups on the edges of the carbon sheet[141]. This structure provides numerous active sites while also maintaining some areas of sp^2 hybridized domains that can partake in π - π stacking of aromatic rings. Consequently, GO has been investigated for a wide range of applications including acting as a catalyst[142], guided cancer therapy[143], sensors[144-146], super capacitors[147, 148], electronics[149], and solution processing[150] to name a few.

Graphene Oxide has also been used as a barrier layer to protect surfaces from corrosion. Graphene sheets provide good barriers that prevent corrosion media from reacting with the underlying substrate[151-153]. The additional negative charges on the GO can further inhibit the corrosion by preventing aggressive negative ions from reaching the surface [154, 155].

Graphene and Graphene oxide have also seen a great deal of use in the drug delivery field[156, 157]. The combination of high surface area, hydrophilicity, presence of aromatic regions, and presence of functional epoxy, hydroxide, and carboxyl groups make GO an ideal candidate for different drug delivery applications. Anti-cancer drug doxorubicin showed strong bonding with GO sheets through both π - π stacking of aromatic regions and hydrogen bonding with the functional groups[158]. GO sheets have also been used to transport aptamers into cells for in situ molecular analysis[145]. Functionalization of GO's reactive groups with polyacrylic acid has also facilitated improved loading and release of a chemotherapeutic agents[159].

Graphene and GO have seen varying reports on their biocompatibility [160] with some researchers suggesting toxicity while others showing varying levels of biocompatibility. Notably the biocompatibility of graphene and GO is heavily dependent on the size of the sheets, the concentration of exposure, and purity of the sample[161]. Despite the varying results in reports of graphene and GO toxicity, for GO specifically, where the hydroxyl, epoxide, and carboxyl groups interrupt the carbon structure, there is evidence that these structures can be degraded in vivo. Phagocytotic cells have shown the ability to uptake GO structures[162], and certain enzymes facilitate degradation of the GO sheets[163, 164]. These reports suggest that GO could be degraded in vivo with minimal toxicity. Additionally, the toxicity of graphene and GO structures have been markedly reduced through the attachment of additional groups such as Polyethylene glycol[160].

1.4 CONDUCTING POLYMER AND GRAPHENE COMPOSITES

With the unique properties of both CP and Graphene, combinations of the two have been investigated for multiple applications including batteries[165, 166], super capacitors[148, 167], heavy metal removal filters[168, 169], and improved sensors[125, 170] to name a few. These applications often take advantage of the coupling of the electrical properties of Graphene with CP to create materials of superior conductivity and increased surface area due to the roughness added to CP films when incorporating the Graphene sheets[171]. These high surface area electrochemically stable CP/Graphene composites have been explored as super capacitors with the ability to have high power densities and high cycle lifetimes[167, 172]. One method of creating these films is through the polymerization of CP doped with GO followed by the reduction of GO to rGO which has superior electrical properties[171]. CP films doped with GO that were subsequently reduced to form CP/rGO films exhibited a high rate of charge transfer and excellent cycling stability when used as a cathode for a lithium ion battery[165]. In addition, high surface area CP/rGO composites have been shown to be effective at adsorbing heavy metals for removal during water treatment[168, 169]. Our lab has taken advantage of the improved properties when incorporating GO into CP coatings for sensors. CP/GO sensors showed improved Dopamine detection sensitivity due to improved electrochemical properties of the sensor as well as electrostatic interactions between the dopamine molecule and the CP/GO surface[125]. The superior electrochemical properties of CP/Graphene composites result in a wide array of potential applications.

1.5 THESIS ORGANIZATION

The work described in this thesis explores the use of a CP/GO composite coating for improving the properties of Mg for biomedical implants. While much work has been done utilizing CPs on other metals, there has been little exploration of CPs on Mg. A composite coating of CP/GO on Mg will be fabricated and investigated. The coating's ability to satisfy the current needs for improvement of Mg implants including, corrosion control, drug delivery, and improved tissue reaction will be examined. This effort seeks to provide insight into technology that can help Mg devices transition clinical use.

Chapter 1 will focus on the use of CP and GO composite as a method of decreasing corrosion on Mg substrates. Both CPs and GO have shown individual abilities to prevent corrosion, this work investigates the synergistic effect of combining the two. Firstly this work will describe the electrochemical polymerization method determined to deposit the CP/GO film on the Mg surface. Then the corrosion protection of the film will be investigated through multiple methods to determine the mechanisms of corrosion control. Lastly the effect of the CP/GO film on cytotoxicity of Mg samples will be assessed.

Chapter 2 will focus on the use of CP/GO films as a platform for self-powered drug release. Here, Anti-inflammatory drug dexamethasone (Dex) will be incorporated into the CP/GO film on Mg developed in Chapter 1. The ability of the CP/GO/Dex film on Mg to release drug will be investigated. Different methods of controlling drug release from the CP/GO/Dex films will be explored through the use of Mg corrosion current as a source of electrons to reduce the polymer backbone and facilitate drug release.

Chapter 3 will begin to explore the ability to use CP/GO films as a method to add surface functionalized cues on to Mg. The exposed carboxyl groups on the GO protruding from the CP

film will be used to functionalize bioactive molecules on the surface of CP/GO coated Mg. The presence of the functionalized moiety on the surface will be confirmed and the ability of this surface cue to elicit a cellular response will be evaluated.

2.0 POLY (3,4-ETHYLENEDIOXYTHIOPHENE) GRAPHENE OXIDE COMPOSITE COATINGS FOR CONTROLLING MAGNEISUM IMPLANT CORROSION

2.1 ABSTRACT

Magnesium (Mg) is a promising biodegradable implant material because of its appropriate mechanical properties and safe degradation products. However, *in vivo* corrosion speed and hydrogen gas production need to be controlled for uses in biomedical applications. Here we report the development of a conducting polymer 3,4-ethylenedioxythiophene (PEDOT) and graphene oxide (GO) composite coating as a corrosion control layer. PEDOT/GO was electropolymerized on Mg samples in ethanol media. The coated Mg samples were subjected to various corrosion tests. The PEDOT/GO coating significantly reduced the rate of corrosion as evidenced by lower Mg ion concentration and pH of the corrosion media. In addition, the coating decreased the evolved hydrogen. Electrochemical analysis of the corroding samples showed a more positive corrosion potential, a decreased corrosion current, and an increase in the polarization resistance. PEDOT/GO corrosion protection is attributed to three factors; an initial passive layer preventing solution ingress, buildup of negative charges in the film, and formation of corrosion protective Mg phosphate layer through redox coupling with Mg corrosion. To explore the biocompatibility of the coated implants *in vitro*, corrosion media from PEDOT/GO

coated or uncoated Mg samples were exposed to cultured neurons where PEDOT/GO coated samples showed decreased toxicity. These results suggest that PEDOT/GO coating will be an effective treatment for controlling corrosion of Mg based medical implants.

2.2 INTRODUCTION

High strength to weight ratio, excellent mechanical properties, and biodegradability makes magnesium attractive for a variety of biomedical implant applications[11, 173, 174]. The ability of Mg implants to completely degrade in the body prevents the need for implant removal surgery and minimizes the side effects due to the chronic presence[3, 39, 175-177]. In vivo corrosion of Mg implants result in harmless byproducts, granted that the corrosion rate is appropriately controlled[2, 174, 175, 178]. In addition, Mg is essential in numerous biological processes and increased levels of Mg have been shown to be beneficial to osseointegration as well as neural protection and regeneration[176, 179-181]. Mg's mechanical properties are also superior to current biodegradable polymers[16]. Despite the promise of Mg as a biodegradable implant material; there have been multiple reports on rapid in vivo corrosion of Mg [9, 11, 17, 18, 39, 41, 42, 182, 183]. Rapid degradation results in premature mechanical failure and can lead to harmful buildup of corrosion products, such as hydroxide ions, which increases the local pH, and hydrogen gas that can result in gas bubble formation around the implant. In order to prevent such uncontrolled and rapid in vivo degradation, many approaches have been investigated to control corrosion, including alloying, coatings, and surface treatments.

Conducting polymer (CP) coatings have shown promise in their ability to increase corrosion resistance of metals. CPs can be electropolymerized directly on metal surface along

with appropriate dopant molecules resulting in a conductive and electroactive film that can have unique redox reactions with the underlying metal[114]. With multiple different types of CPs and a greater number of dopants, many mechanisms have been proposed to explain CP corrosion control. These mechanisms have been thoroughly reviewed elsewhere [89, 90, 114] and include: a barrier layer, ennobling, anodic protection, formation of a modified CP metal interface, facilitation of a protective oxide, shifting of the electrochemical interface, and use of dopant released from the CP to facilitate a more corrosion resistant surface layer. Some research also suggests that CPs can electrochemically protect exposed areas of the substrate and act as a self-healing coating[184, 185].

In addition to CPs, graphene and graphene oxide (GO) have been shown to provide effective corrosion control. Layers of graphene sheets alone can act as a barrier to prevent corrosion[151-153]. GO sheets, due to negatively charged functional groups, can repel anions that normally facilitate corrosion[154]. We hypothesize, that when GO is coupled with the CP coating as immobile anionic dopant, additional corrosion protection benefits may be obtained. As the positive backbone of the CP is reduced via the electrons generated by metal corrosion, large dopants will remain physically trapped in the film resulting in a net negatively charged film. Such an effect has been previously reported with polypyrrole CP doped with dodecylsulfate [114].

The aforementioned corrosion studies involving conducting polymers have been mostly focused on metals such as aluminum and stainless steel, while few have investigated the use of CPs to control Mg corrosion[186, 187]. In our previous work we show that PEDOT film electrodeposited on Mg surfaces in ionic liquid reduced the corrosion current[186]. In this work we developed a method to electrochemically polymerize poly 3,4-ethylenedioxythiophene

(PEDOT) doped with GO on Mg to utilize the synergistic properties of both CP and GO. The effect of the PEDOT/GO coating on Mg corrosion was evaluated and the mechanism of corrosion protection investigated. Additionally, the effect of the coating on cellular toxicity of Mg was assessed with primary neuron cultures.

2.3 MATERIALS AND METHODS

2.3.1 Materials

Single layer graphene oxide sheets were purchased from Cheap Tubes (Cambridgeport, VT). 200 proof ethanol was purchased from Decon Labs Inc. (King of Prussia, PA). Magnesium ribbon $\geq 99.5\%$ (3 mm wide x 0.2 mm thick), 3,4-Ethylenedioxythiophene (EDOT) monomer, methanol, laminin (from Engelbreth-holm-swarm murine sarcoma basement membrane), and nitrocellulose were purchased from Sigma-Aldrich. PBS 10x concentrate (136 mM NaCl, 2.7 mM Potassium chloride, 10 mM Phosphate Buffer) was purchased from EMD Millipore (Billerica, MA) and diluted using de-ionized water from a Millipore Milli-Q system. StanBio Liquicolor Magnesium Test and Live Dead stain were purchased from Fisher Scientific. Conductive silver paint was purchased from Electron Microscopy Sciences (Hatfield, PA). Two part epoxy was purchased from Leco (St. Joseph, MI). Glutamax 100x, B27 supplement, and Neurobasal media for neuron culture were purchased from Gibco (Grand Island, NY). Primary neurons were isolated from e18 rat cortices from Brain Bits (Springfield, IL).

2.3.2 Polymerization of the PEDOT/GO film

GO was added to ethanol at a concentration of 10 mg/ml and the resulting solution was sonicated for 30 minutes in a bath sonicator FS110H (Fisher Scientific). Following sonication, 20 μ l/ml EDOT and 35 μ l/ml deionized water were added and dissolved into the GO ethanol solution to create the polymerization solution. Magnesium ribbon was cut into 2 cm long strips, rinsed with ethanol, and blotted dry. Polymerizations, and all electrochemical measurements, were conducted on a Gamry Potentiostat FAS2/Femtostat using Gamry Framework Software (Warminster, PA). Polymerization consisted of a two-electrode system with Mg ribbon working electrode and a gold counter/reference electrode. Polymerization was conducted in 300 μ l of fresh polymerization solution and a potential of 0.6 V vs. counter was applied until a charge of 10 mC was reached. Coated length was 9 mm (Fig.2-1). Following polymerization, electrodes were gently dipped in ethanol then dried at -20°C for two days, followed by drying at 3°C for one day. Following this drying process, the PEDOT/GO forms a thin adherent black film on the Mg ribbon. Samples were stored at ambient temperature following drying process.



Figure 2-1: Mg ribbon following polymerization

2.3.3 Tafel Scan

A three-electrode system was utilized with Ag/AgCl reference, platinum counter, and Mg working electrode. Coated or uncoated samples were immersed 5mm into PBS for the scan. This ensured only the coated portion of the PEDOT/GO sample was exposed to the PBS (Fig. 2-2). Open circuit potential (OCP) was recorded for 600 s, or until it reached a stability of 0.05 mV/s. Following OCP determination, the sample was scanned from -0.25 V to +0.25 V vs. OCP. This scan provides a current vs. voltage graph displaying the anodic and cathodic half reactions. The low current valley in the graph is the position where the anodic and cathodic half reactions are in equilibrium. The potential where this occurs is the corrosion potential (E_{corr}). Additionally, the current where the half reactions are in equilibrium can be extrapolated from the linear portions of the cathodic and anodic arms of the tafel scan. The point of intersection of these linear extrapolations is the corrosion current (i_{corr}).

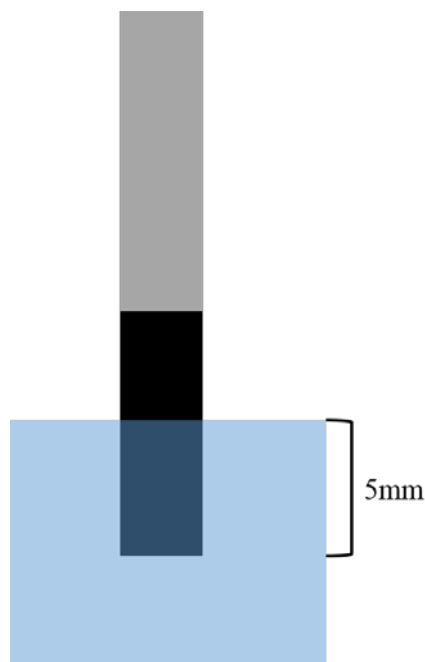


Figure 2-2: Tafel scan immersion

2.3.4 Long term corrosion tests (pH, Mg ion, OCP, and EIS)

PEDOT/GO coated and uncoated Mg samples were electrically connected using conductive silver paste and copper wire to the back of the Mg sample (Fig. 2-3). Samples were then mounted in epoxy only leaving 5mm length exposed. This resulted in a fixed area of the sample being exposed to the corrosion solution, with only coated portions being exposed for PEDOT/GO samples. Corrosion was conducted in PBS using 20 ml/cm² media volume to surface area ratio. Each day samples were transferred to fresh PBS and OCP and Electrochemical Impedance Spectroscopy (EIS) measurements were conducted in fresh PBS. Mg ion concentration and pH measurements were taken from the PBS of the previous day.

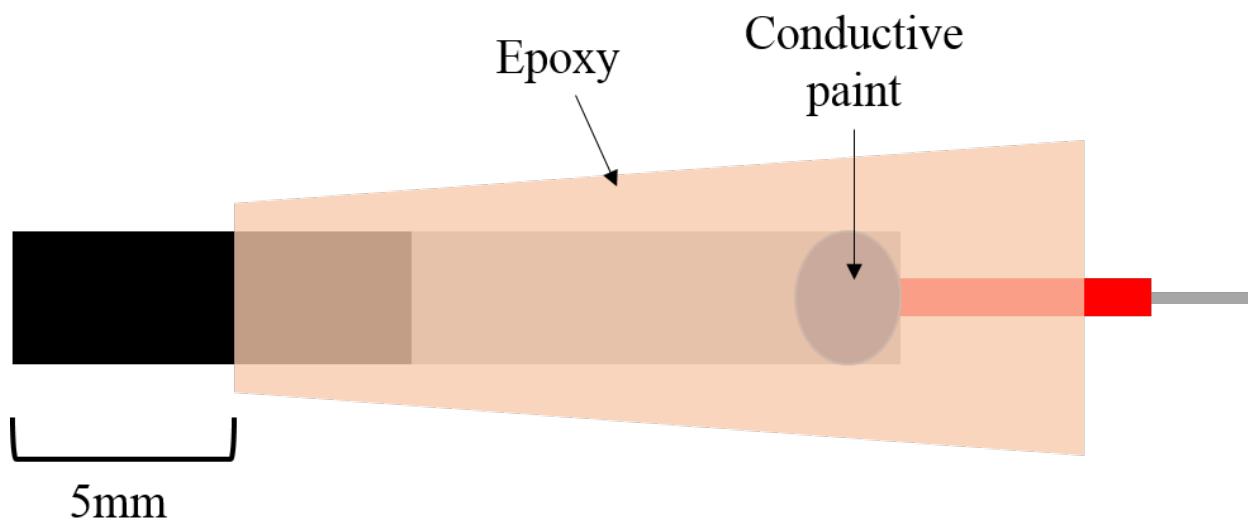


Figure 2-3: Mg samples for long term corrosion tests

2.3.4.1 OCP and EIS

In fresh PBS, a three-electrode system was used to measure the OCP and EIS with an Ag/AgCl reference, platinum counter, and Mg working electrode. OCP was recorded for 600 s, or until it reached a stability of 0.05 mV/s. Following OCP, EIS was taken from 100 kHz to 0.1 Hz with

an applied potential of 0 V vs. OCP and a voltage amplitude of 10 mV. Equivalent circuit analysis was conducted using Gamry Echem Analyst software.

2.3.4.2 pH and Mg ion concentration measurement

The pH of the daily corrosion media was measured using Fisher Scientific Accumet Ab15. Magnesium Ion analysis was conducted using StanBio Magnesium Liquicolor (Xylidyl Blue assay). 200 μ l of the liquicolor assay was added to each well 96 well plate. Corrosion solution was diluted in half with PBS. Three 10 μ l samples were taken from each dilute corrosion solution and placed into individual wells containing the liquicolor solution and gently mixed. Samples were allowed to react at room temperature for 10 minutes. Absorbance at 520 nm was then tested, after ensuring there were no bubbles in the wells, using a Spectromax M5 spectrophotometer.

2.3.5 Hydrogen evolution measurement

PEDOT/GO coated Mg and uncoated Mg samples were mounted in epoxy on glass microscope slides leaving 5 mm of the sample exposed. Samples were then placed in a 2 L crystallization dish filled with PBS. 2 ml plastic pipettes were modified so that the tip was closed and the opposite end was flared out. These pipettes were filled with PBS and placed over the corroding Mg samples. Hydrogen evolved from the samples was collected at the top of the pipette allowing for quantification of the total volume of evolved hydrogen gas.

2.3.6 SEM and EDX analysis

SEM analysis was conducted using a Jeol JSM 6330F SEM. Accelerating voltage was 3kV unless otherwise noted. Samples were analyzed before corrosion and after 22 days of corrosion in PBS, refreshing PBS every day. Following corrosion, samples were rinsed in DI water followed by ethanol rinse and air-dry, and stored in a desiccator until imaging. Coating integrity and surface morphology of coated and uncoated samples were analyzed. Due to lack of EDX analysis capability on JEOL JSM 6330F, further chemical analysis was conducted on a Jeol JSM6510 SEM using an Oxford Instruments X-ray analyzer and Inca Software. Working distance was 10 mm and accelerating voltage was 20 kV for elemental analysis. Elemental identification was conducted automatically through the Inca EDX software.

2.3.7 Neuron culture

Coated and uncoated Mg samples were placed in culture media (Neurobasal media, 10% Horse serum, 2 mM L-alanyl-L-glutamine, 4 ml b27 50x per ml media, and 1% PennStrep) at a surface area to volume ratio of 1.25 ml/cm². Corrosion was conducted in a cell culture incubator at 37°C and 5% CO₂. Following corrosion for 24 or 72 hours, different amount of corrosion media were added to neurons cultures.

96 well plates were pre-coated with nitrocellulose, cast from 1 cm²/ml methanol solution, followed by laminin (40 µl/ml) adsorption then rinsed with PBS. Following pretreatment, primary neurons from e18 rat cortices were dissociated via trituration and were plated at 30,000 cells/well. Neurons were allowed to grow in unaltered media for 1 day. After one day, the

media was replaced with non-dilute (100%) corrosion media as well as corrosion media diluted to 50 and 10% with fresh culture media.

2.3.7.1 LDH Assay

Following exposure for 24 hours, cytotoxicity was also assessed using the LDH assay. 50 μ l cell supernatant was removed and combined with 50 μ l assay reaction solution. Reaction proceeded for 30 minutes at room temperature followed by addition of 50 μ l of the assay stop solution. Absorbance was measured at 490 nm (for LDH) and 680 nm (for background) using a Molecular Device Spectromax M5 plate reader.

2.3.7.2 Live dead staining

Following exposure to corrosion solution, media was removed and replaced with staining solution 2 μ M calceinAM and 2 μ M ethidium homodimer-1 in PBS. After 10 min of incubation, images were taken on a Leica DMI 4000B inverted scope. Counting was conducted with ImageJ manually using 'Cell Counter' add-on by Kurt De Vos.

2.3.8 Statistics

Statistical analysis was conducted using a two-tailed Student's T-Test. Significance is considered $p < 0.05$. Data is represented as mean (\pm SEM).

2.4 RESULTS

2.4.1 Film formation

Electropolymerization of PEDOT requires an oxidizing potential that can drive Mg corrosion. To minimize this corrosion and increase PEDOT/GO film adhesion, polymerization was conducted in ethanol. Initially, pure ethanol was utilized as the sole solvent as it does not facilitate Mg corrosion[188]. However, film growth was not achieved. Previous reports of polymerization in non-aqueous media noted the effect of small amounts of water on polymer growth[189-191]. Addition of water to the polymerization solution serves to decrease the electrostatic repulsion of the radical mer units during polymerization by increasing the permittivity of the polymerization solution. To that end, water was added at increasing concentrations in the polymerization solution until uniform film growth was observed. If excessive water was present, films showed visible bubbles due to Mg corrosion during the polymerization.

The film drying protocol following polymerization was also optimized. PEDOT/GO films after polymerization were in a solvated form and showed a significant volume decrease during drying. Drying at ambient temperatures resulted in rapid evaporation of the ethanol and prompt drying of the film. These quickly dried films displayed non-uniform thicknesses, visually observed as darker patches, as well as bubbles and cracks in the coating. To slow the drying, samples were placed at -20°C for two days followed by storage at 4°C for one day. Following this process, films presented uniform color and no appearance of cracks or bubbles. Polymerization at optimized conditions resulted in uniform films with a rough surface texture (Fig. 2-4A and 2-5 A&C) compared to Mg (Fig. 2-4B and 2-5B). This rough surface

texture resembles that shown previously by our lab and is a result of the GO sheets protruding from the surface of the polymer film[103]. Following the above drying protocol the thickness of the coating was quantified using SEM and comparing coated and uncoated Mg ribbon thicknesses. It was determined that the PEDOT/GO coating procedure resulted in a 50nm thick coating once dried.

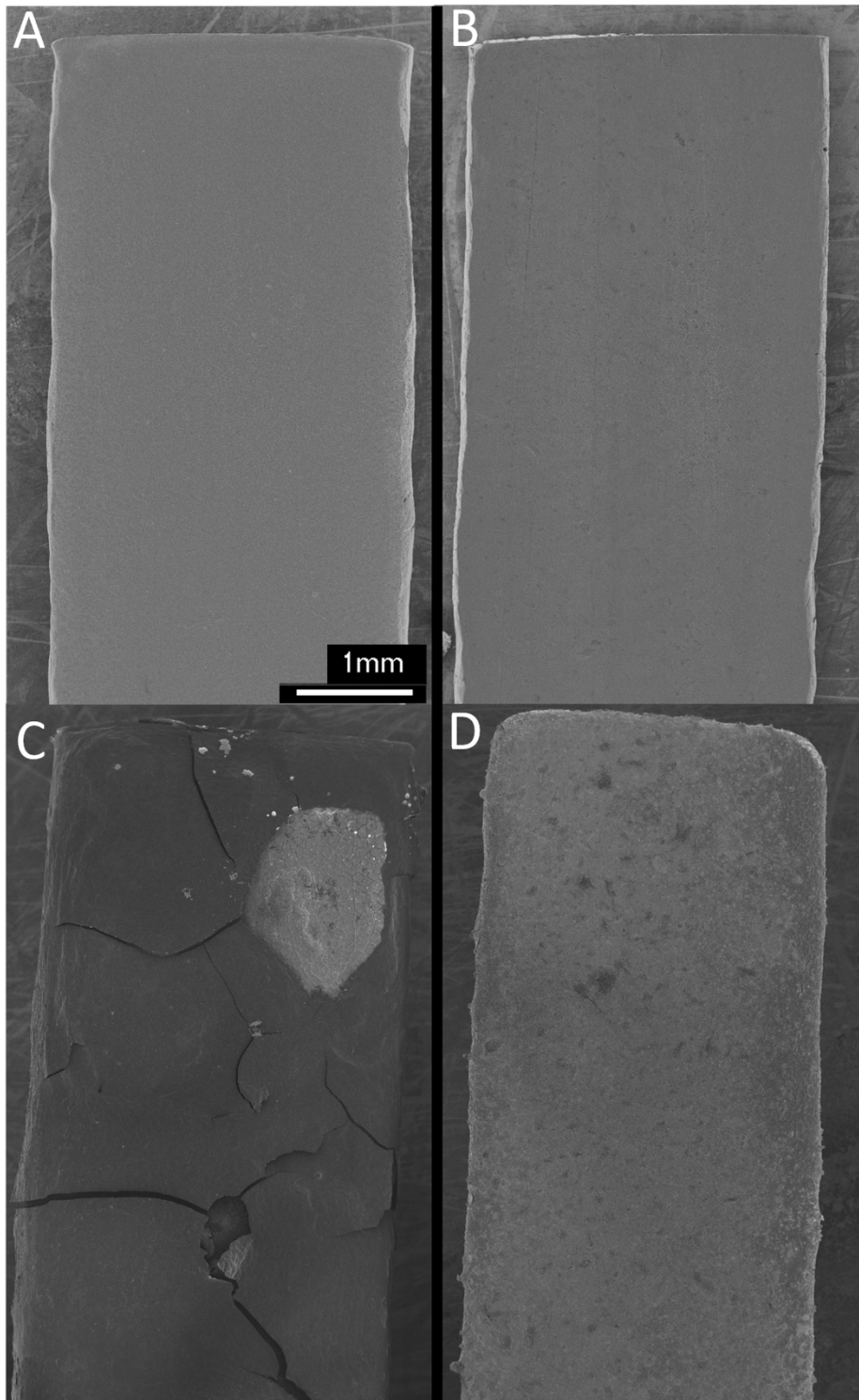


Figure 2-4: Macroscopic morphology. (A) PEDOT/GO coated Mg before corrosion (B) Mg sample before corrosion (C) PEDOT/GO sample post corrosion (D) Mg sample post corrosion

2.4.2 SEM and EDX analysis

Images of un-corroded samples as well as samples corroded in PBS for 22 days were analyzed under SEM (Figs. 2-4 and 2-5). Pre corrosion, Mg samples exhibited a rough surface morphology presumably due to oxides and hydroxides formed upon exposure to ambient air. The PEDOT/GO coated samples show uniform coverage with a rough surface morphology resulting from the GO sheets being exposed at the surface[103]. Following corrosion, PEDOT/GO coated samples display cracks in the coating as well as areas where the coating delaminated. PEDOT/GO samples showed coating delamination of varying degrees with one sample having a large portion of the coating removed and two remaining largely intact throughout the 22 day corrosion. It is likely that the cracking of the film visualized under SEM was exacerbated by the SEM sample drying preparation. Of interest is the morphology of the underlying Mg after corrosion. Images revealed cracked plate like morphology of exposed Mg around the PEDOT/GO coated areas (Fig. 2-5D). Uncoated Mg samples, however, predominantly displayed an amorphous morphology with only some areas of cracked plate like morphology on the edge (Fig. 2-5E). There is also evidence that the cracked plate like morphology was present underneath the PEDOT/GO coating as seen through the cracks in the coating (Fig. 2-5F). EDX analysis was conducted on both the cracked and amorphous morphologies and it was found that the scale morphology displayed higher percentage of oxygen and phosphorus than the amorphous areas (Fig. 2-6). This suggests that the uncoated samples were predominantly coated with a $\text{Mg}(\text{OH})_2$ while the PEDOT/GO coated samples displayed a $\text{Mg}_3(\text{PO}_4)_2$ in the areas where the PEDOT/GO coating began to fail.

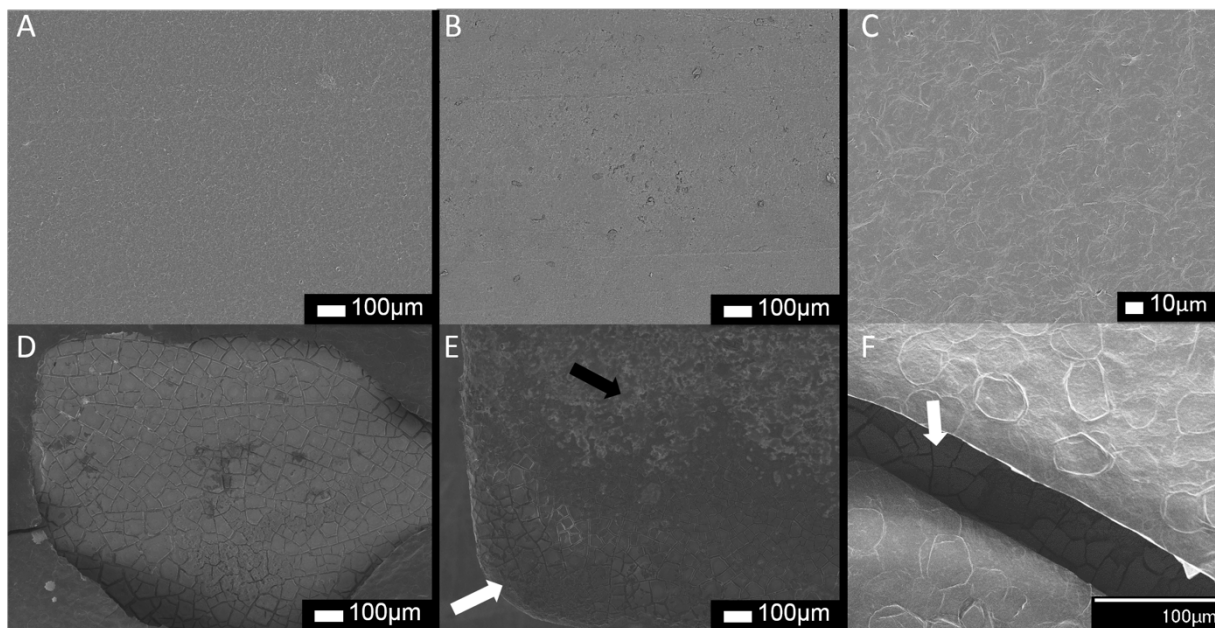


Figure 2-5: Micro morphology. (A) PEDOT/GO coated sample before corrosion. A rough surface morphology can be seen indicative of GO sheets exposed at the surface. (B) Untreated Mg surface. (C) High magnification image of PEDOT/GO coating to better illustrate surface roughness. (D) Delaminated area on PEDOT/GO coated sample after corrosion showing the cracked scale like morphology taking up the entire delaminated area. (E) Uncoated Mg after corrosion. White arrow indicates similar cracked morphology predominantly present on the edges of the sample while the majority of the sample displayed a more amorphous morphology indicated by the black arrow. (F) Image of a crack in the PEDOT/GO film after corrosion where the cracked scale like morphology can also be seen as indicated by the white arrow.

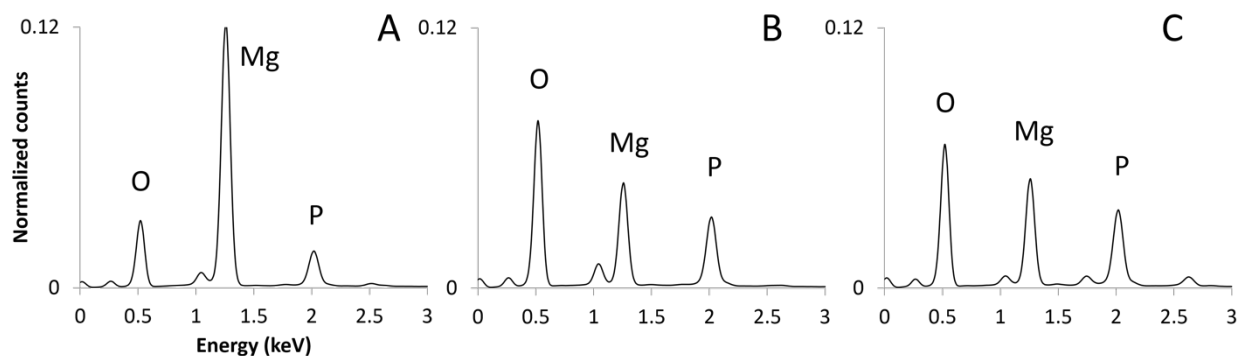


Figure 2-6: EDX post corrosion. (A) EDX of the dominant amorphous morphology on uncoated Mg after corrosion. (B) Elemental analysis of the scale morphology present on the edge of uncoated Mg. (C) Elemental analysis of scale morphology on PEDOT/GO coated Mg where the coating had delaminated.

2.4.3 Corrosion Characterization

Mg corrosion in aqueous solution, with or without the PEDOT/GO coating, involves several anodic and cathodic reactions as shown in equations 1-4 below. The assessments of corrosion often target different reaction products. Multiple methods to characterize corrosion have been reported in literature [11, 173, 178, 192, 193]. To obtain a comprehensive understanding, we utilized multiple metrics to analyze the corrosion of PEDOT/GO coated and uncoated samples.



2.4.3.1 Tafel Scan

Potentiodynamic Tafel scans indicate the balance of the cathodic and anodic half reactions. Representative Tafel scans for coated and uncoated Mg samples can be seen in Fig. 2-7. The PEDOT/GO coated Mg showed a positive shift in the corrosion potential (the point of minimal current). This shift is indicative of a decrease in the sample's tendency for corrosion. Additionally, the PEDOT/GO coating decreased the corrosion current, the current where anodic and cathodic half reactions are in equilibrium as determined by the intersection of lines extrapolated from the linear portions of the cathodic and anodic arms of the scan. This too is indicative of a decrease in the corrosion rate for the coated samples.

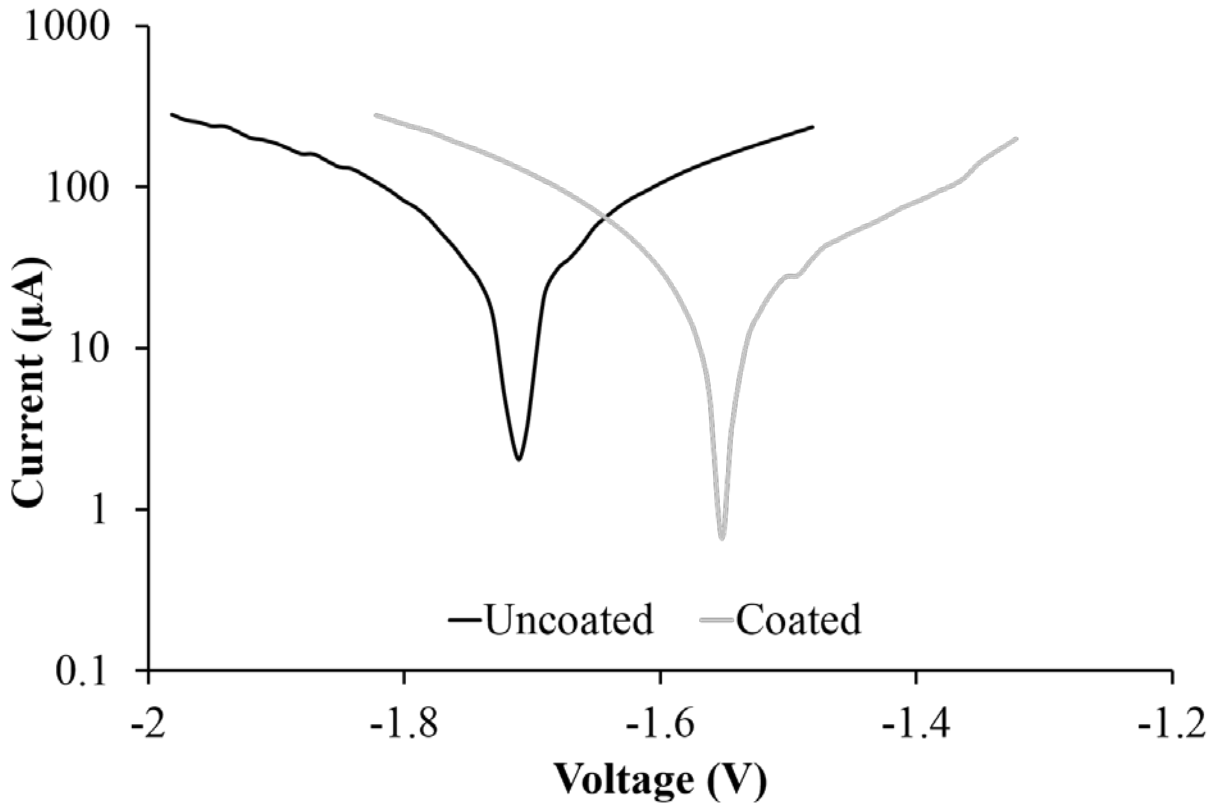


Figure 2-7: Tafel scan. Representative curves for uncoated Mg and PEDOT/GO coated Mg. It can be seen that the corrosion potential for the coated sample is more positive than uncoated and that the corrosion current is slightly lower.

2.4.3.2 Magnesium ion analysis

Tafel scan is a one-time analysis method that damages the sample and affects further readings. For long-term quantification of corrosion, Mg ion concentrations in the corrosion solution were analyzed using Magnesium Liquicolor assay. The reaction of untreated Mg in solution can be seen in equation 3. Oxidation of Mg (equation 2) is balanced by the reduction of water and formation of hydrogen bubbles (equation 1). Mg^{2+} may then react with anions at the surface, most commonly OH^- , to form an additional hydroxide layer that is only somewhat corrosion protective (equation 4). Mg ion concentration values, summed over days, can be seen in Fig. 2-

8. PEDOT/GO coated Mg had significantly less Mg ions in the corrosion media than untreated Mg for all measurements. PEDOT/GO coatings showed a $37.7\pm 4.3\%$ decrease in the daily release of Mg ion in the corrosion media. Rates of Mg ion release over the first 7 days were 30% lower for PEDOT/GO coated samples. The increase in error of the PEDOT/GO coatings is a result of the coating delamination occurring at slightly different rates.

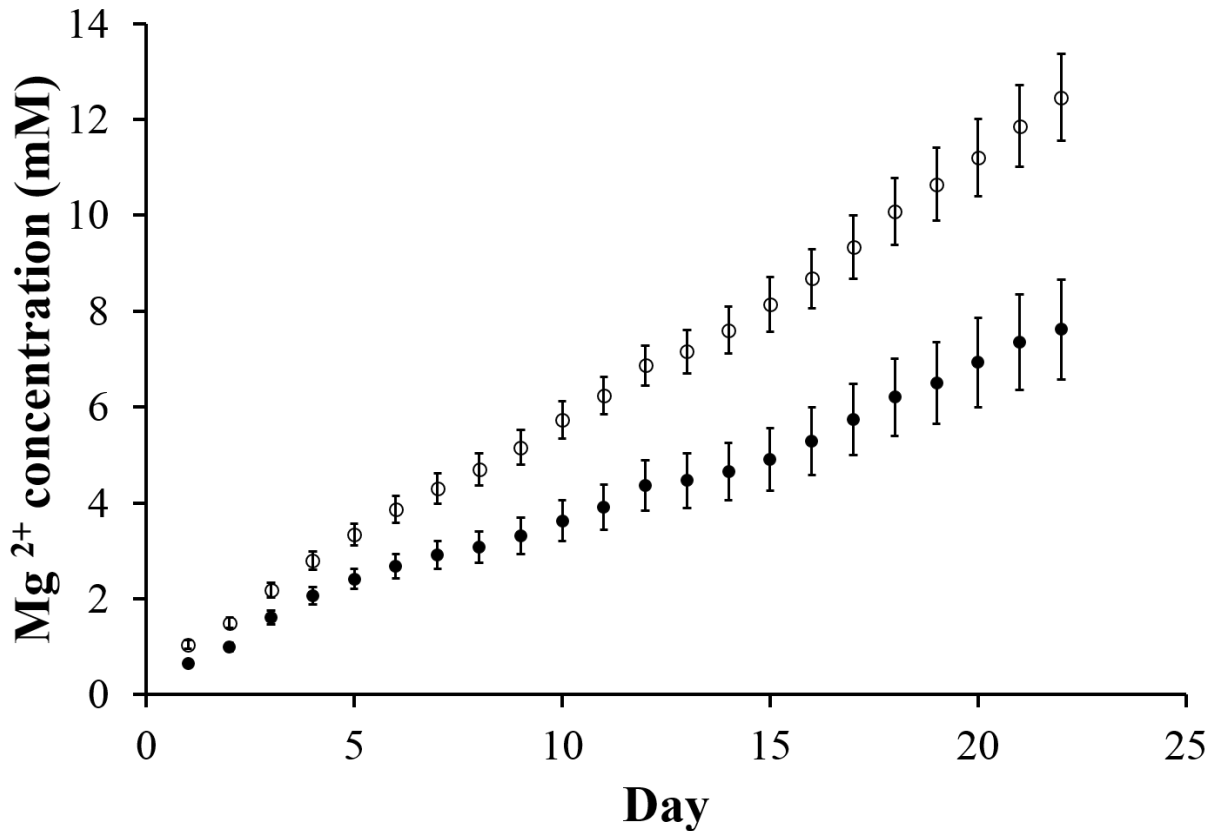


Figure 2-8: Mg ion concentration. Summed Mg ion concentration in the corrosion solution quantified daily using xylydyl blue assay. (all $p < 0.05$)

2.4.3.3 pH analysis

In addition to Mg ion quantification, pH of the corrosion solution was tested daily. Mg corrosion involves the reduction of water as the cathodic partial reaction (equation 1)[11, 193]. This

produces hydroxyl anions and consequently an increase in pH. Summed OH^- present in the corrosion solution can be seen in Fig. 2-9. Uncoated samples displayed a significantly greater amount of OH^- in the corrosion solution than the PEDOT/GO coated samples. This reduction in OH^- production is the result of the overall decrease in corrosion rate. Additionally, the reduction of the PEDOT backbone (equation 5) replacing the water reduction partial reaction (equation 1) will affect this metric. Coated samples resulted in a 43% decrease in the rate of OH^- production and showed a $46\pm 2\%$ decrease in the daily OH^- generated.

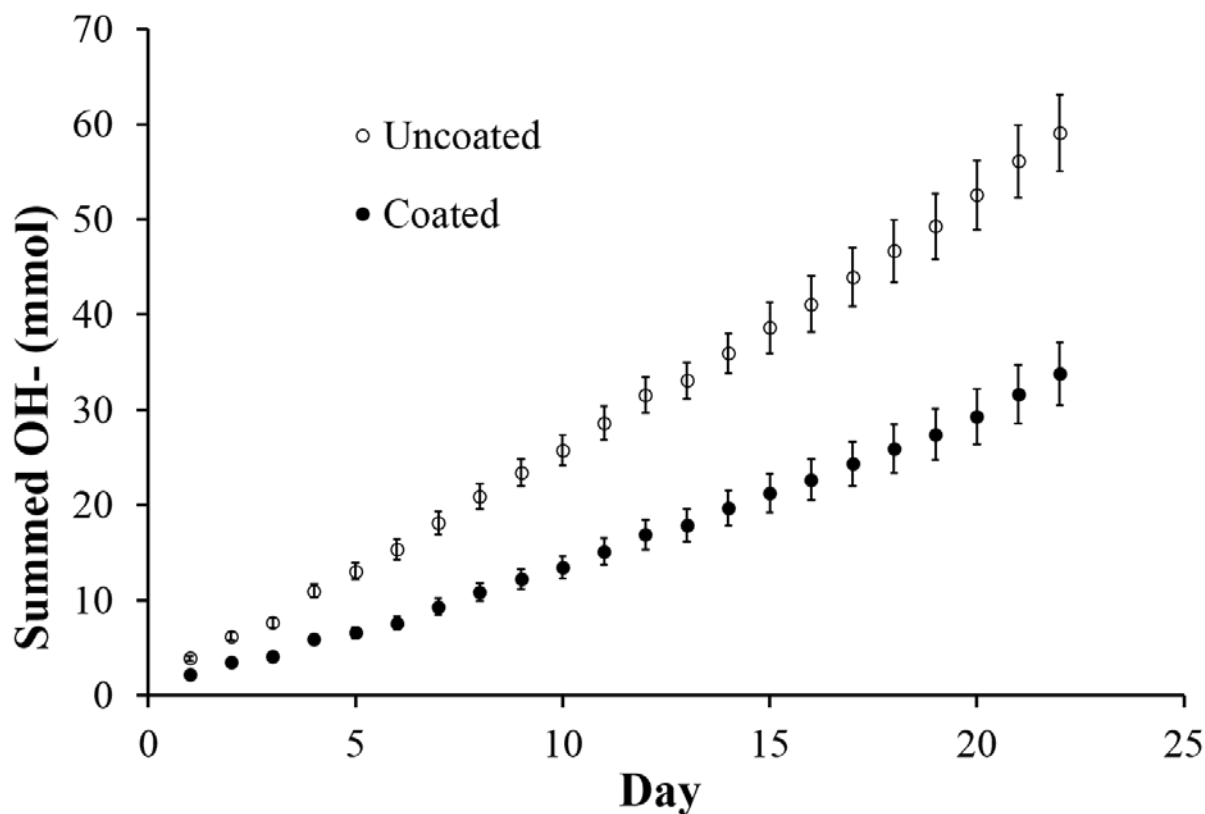


Figure 2-9: Hydroxide in the corrosion solution. Summed OH^- concentration in the corrosion solution calculated daily from pH measurements. (all $p < 0.05$)

2.4.3.4 Electrochemical tests

The long term corrosion samples were also subject to daily electrochemical tests. These tests include OCP and EIS measurement and were performed immediately after transferring the corroding samples to fresh PBS. These tests were designed to have a negligible effect on the corrosion reaction and could be repeated each day without affecting the samples.

2.4.3.5 OCP

OCP is a real time representation of corrosion potential displayed in the Tafel scans. It can be seen in Fig. 2-10 that the OCP values for the PEDOT/GO coated samples were more positive than the uncoated samples at all time points, which is indicative of lower corrosion rates. There was a sharp negative shift in corrosion potential in the first 24 hours for the PEDOT/GO coated samples. This drop is likely due to film cracking during the first 24 hours leading to a compromised barrier function. However, despite the drop, the OCP of the coated sample is still more positive than the uncoated and remained more positive throughout the 22-day experiment. Small isolated stagnant bubbles were visible after 24 hours on some of the PEDOT/GO coated samples. Following the film damage, the PEDOT/GO facilitated the formation of the $\text{Mg}_3(\text{PO}_4)_2$ layer, while on the untreated samples a less stable $\text{Mg}(\text{OH})_2$ layer was formed. The barrier layer protection provided by the PEDOT/GO, as well as the formation of the magnesium phosphate resulted in the higher OCP when compared to the uncoated samples.

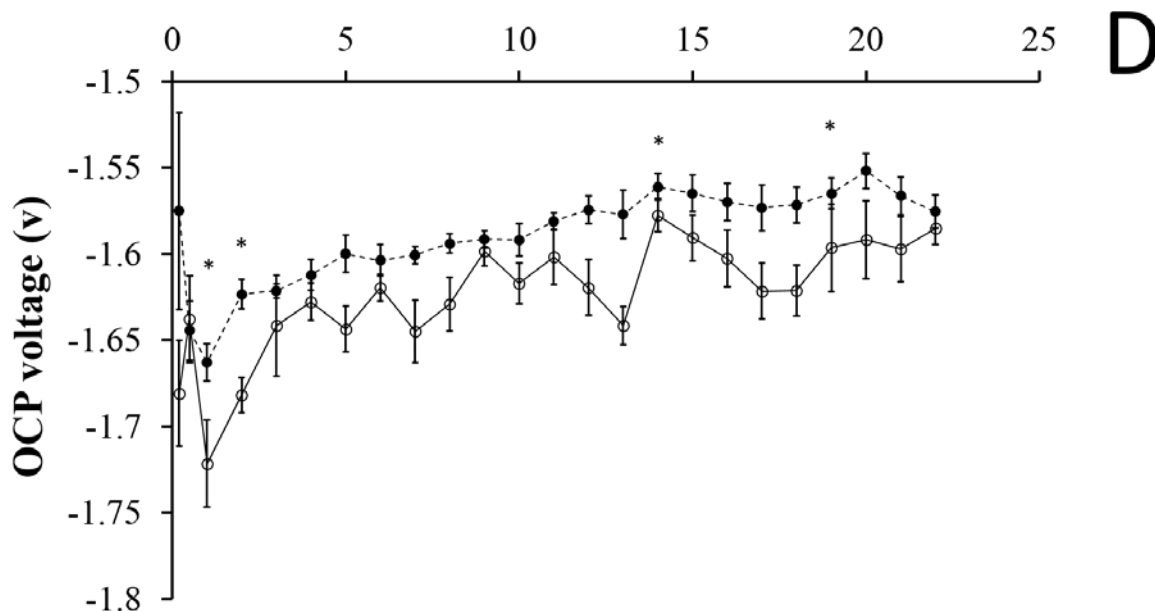


Figure 2-10: Open circuit potential Average OCP recorded daily for PEDOT/GO coated Mg and uncoated Mg. (* p<0.05)

2.4.3.6 EIS

Immediately after OCP readings, EIS was recorded. EIS and equivalent circuit modeling can provide better understanding of the sample/electrolyte interface and the effect of the coating on corrosion. Nyquist plots for uncoated and coated samples over the course of the experiment can be seen in Fig 2-11. The radius of the Nyquist plot is attributed to the corrosion resistance with larger radii indicating higher corrosion resistance[194, 195]. Here the uncoated sample shows an initial increase in the radius of the Nyquist arc followed by a decrease towards the end of the experiment. This is likely due to the initial formation of a $Mg(OH)_2$ (equation 4) layer on the uncoated samples after immersion in the corrosion media. This hydroxide layer is known to be unstable in chloride solutions [11] and the decrease in protection is likely due to the attack of the Cl^- from the corrosion solution facilitating corrosion. Conversely, the PEDOT/GO coatings

showed an increase in the radius of the Nyquist arc over initial days and the protection was maintained for the duration of the experiment. This is due to the barrier layer properties as well as the formation and continued maintenance of the $Mg_3(PO_4)_2$ corrosion protection layer.

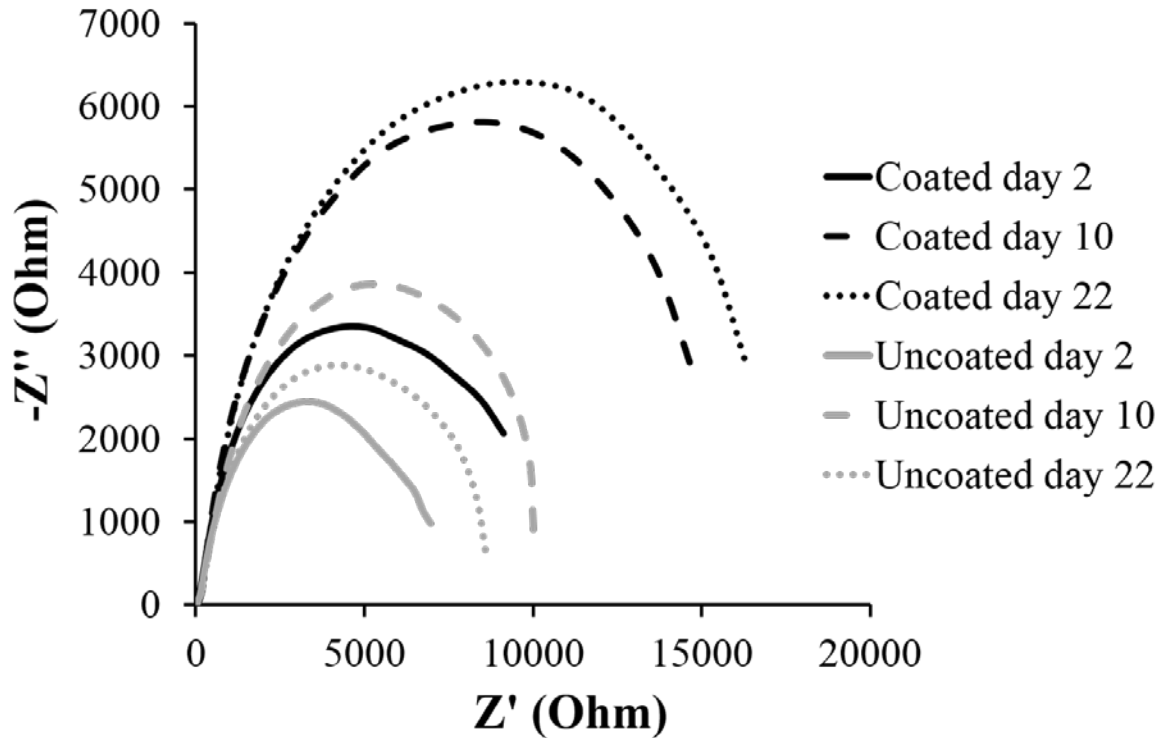


Figure 2-11: EIS. Representative Nyquist plots from EIS data taken on the same coated and uncoated samples at days 2, 10, and 22.

2.4.3.7 Equivalent circuit analysis

The equivalent circuit used to describe coated and uncoated samples can be seen in Fig 2-12. This is a common circuit used to describe corroding samples with coatings [90, 196-200], and has particularly been applied to magnesium with either an inherent oxide/hydroxide layer or other topically applied coatings[56, 201-203]. This circuit consists of solution resistance (R_s), coating capacitance (CPE_c), resistance of ion conduction through the coating (R_c), double layer

capacitance (CPE_{dl}), and polarization resistance (R_p). Both CPE_c and CPE_{dl} are constant phase elements, non-ideal capacitors, where an $n=1$ is ideal capacitor behavior[204].

Equivalent circuit analysis employed constant solution resistance due to constant PBS concentration and low resistance of the solution. Values R_p and CPE_{dl} describe the electrochemical reactions occurring at the Mg interface, where R_p is the faradaic charge transfer reaction of Mg corrosion. R_p is therefore the sample's corrosion resistance. As can be seen in Fig. 2-12 B, PEDOT/GO coated samples had a significantly higher R_p than uncoated samples indicating resistance to faradic corrosion. Double layer capacitance (CPE_{dl}) is another component representing the metal/solution interface. Uncoated samples exhibited increased CPE_{dl} indicating a greater surface area of metal in contact with the corrosion solution. This is likely due to the increased pitting corrosion and the more amorphous morphology of the corrosion products on the surface of the uncoated samples. Circuit components R_c and CPE_c represent properties of the coatings on the surface of the Mg. For PEDOT/GO, R_c and CPE_c are affected by both the PEDOT/GO coating and the passive phosphate layer. For the uncoated samples, R_c and CPE_c are affected by only oxide and hydroxide layers formed on the surface. There is very little difference between the coated and uncoated samples for the (R_c) indicating that the $Mg(OH)_2$ coating on the uncoated samples had similar ability to prevent the solution from reaching the underlying Mg as did the passive layer in combination with the PEDOT/GO coating. This is likely due to the amorphous morphology of the $Mg(OH)_2$, the visible damage to the conducting polymer during corrosion, and the cracks of the phosphate layer visualized under SEM. Additionally, while the magnesium hydroxide may have prevented corrosion media infiltration, it is continually being eroded away by the chloride ions in the corrosion media. Coating capacitance (CPE_c) was greater for coated samples during initial time points which is

attributed to the increase in surface area facilitated by the conducting polymer and its nanotopography [125]. Excessive water infiltration of the oxide/hydroxide film on the uncoated samples likely caused the increase in capacitance at later time points. CPE_{dl} and CPE_c are constant phase elements that are mathematical expressions to indicate non-ideal capacitor behavior. Here where n value indicates how closely they behave to an ideal capacitor with $n=1$ representing an ideal capacitor with a phase angle of 90° and $n=0.5$ representing a capacitor with a phase angle of 45° , n values displayed in Fig. 2-12 F & G. This data, especially the continually significant increase in R_p of the coated samples, serves as further evidence that the PEDOT/GO coating improves Mg corrosion resistance.

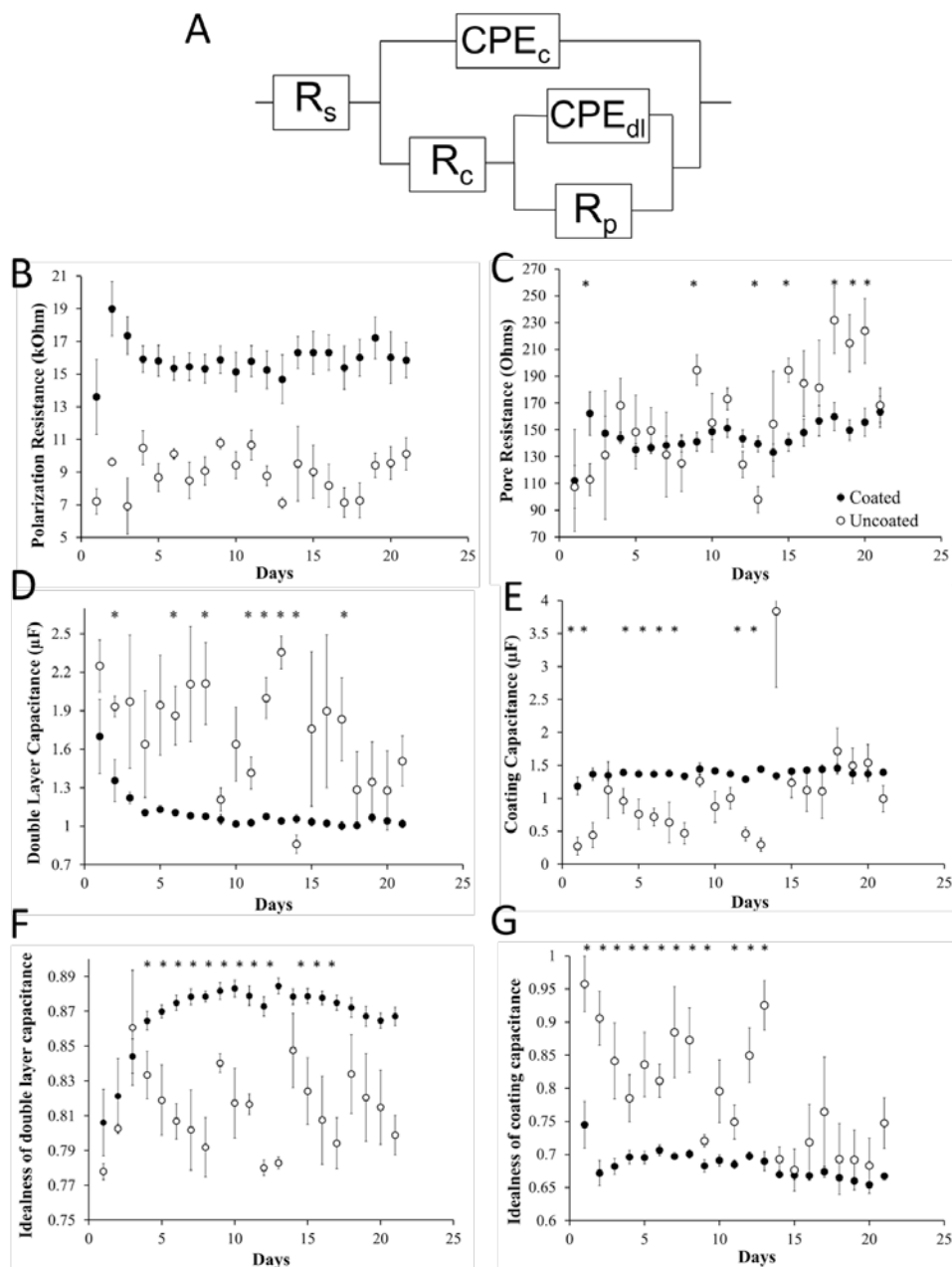


Figure 2-12: Equivalent Circuit Modeling. (A) Equivalent circuit used for subsequent modeling. (B) Polarization resistance [Rp] representing the samples resistance to faradaic charge transfer through corrosion. (all $p < 0.05$) (C) Pore resistance [Rc] indicative of the resistance of ion travel through the coatings on Mg. ($*p < 0.05$) (D) Double layer capacitance [CPEdl] indicative of the charge on the surface of the Mg. ($*p < 0.05$) (E) Coating capacitance [CPEc] indicative of charge on surface of any coating on the samples. ($*p < 0.05$) (F & G) Ideality of the constant phase element representing double layer capacitance and coating capacitance respectively indicating how closely samples behaved to acting like a perfect capacitor. ($*p < 0.05$)

2.4.4 Hydrogen evolution

Similar to Mg ion concentration and pH, hydrogen evolution measurements monitor a byproduct of the Mg corrosion reactions. Cumulative H₂ evolution from coated and uncoated samples can be seen in Fig. 2-13. Coated samples released less hydrogen than the uncoated samples, indicating that the coating is preventing corrosion or bypassing the water reduction reaction by PEDOT/GO reduction. As noted above the PEDOT/GO coated samples did display small isolated bubbles after about 24 hours of immersion, however those bubbles were stagnant and increased in volume much more slowly than the bubbles being released from the uncoated Mg samples.

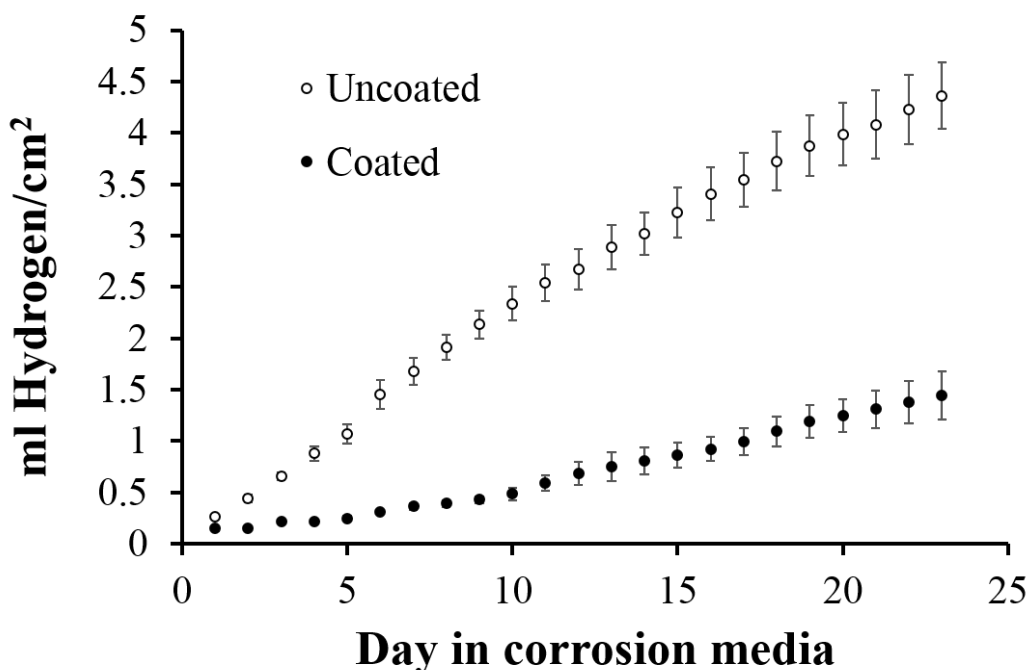


Figure 2-13: Hydrogen evolution. Cumulative hydrogen evolution of coated and uncoated samples corroded in PBS. (all $p < 0.05$)

2.4.5 Cytotoxicity

Assessment of corrosion byproduct cytotoxicity was conducted with the LDH assay as well as Live/dead staining. As can be seen in Fig. 2-14, both methods show a significant decrease in toxicity for the PEDOT/GO coated Mg corrosion media.

2.4.5.1 LDH

Initially, cytotoxicity was tested utilizing an LDH assay where the amount of LDH released by damaged cells into the media was quantified after exposure to 24-hour corrosion media. Results in Fig. 2-14A show a significant decrease in sample toxicity after coating. The PEDOT/GO coating significantly improved biocompatibility for both 100% and 50% corrosion media

samples. 100% corrosion media exposure showed a 40% decrease in toxicity as a result of PEDOT/GO coating. Cytotoxicity of cells exposed to 50% corrosion media showed an 86% decrease in toxicity. 10% corrosion solutions showed a trend of the coated samples being less toxic, though not significant. Presumably, at such high dilution, the differences between the coated and uncoated samples are negated.

2.4.5.2 Live/Dead assay

To assess longer term corrosion media toxicity, analysis was also conducted where samples were allowed to corrode for 72 hours. Coated samples showed good stability during the corrosion period with no visible delamination. As can be seen in Fig. 2-14 B, corrosion media of coated samples showed a 25% reduction in cytotoxicity at 50% corrosion media dilution. With the 10% corrosion media, there is a slight trend towards coated samples being less toxic, though not statistically significant. Large amounts of death were observed for both coated and uncoated samples at 100% media concentration to the point where quantification could not be completed.

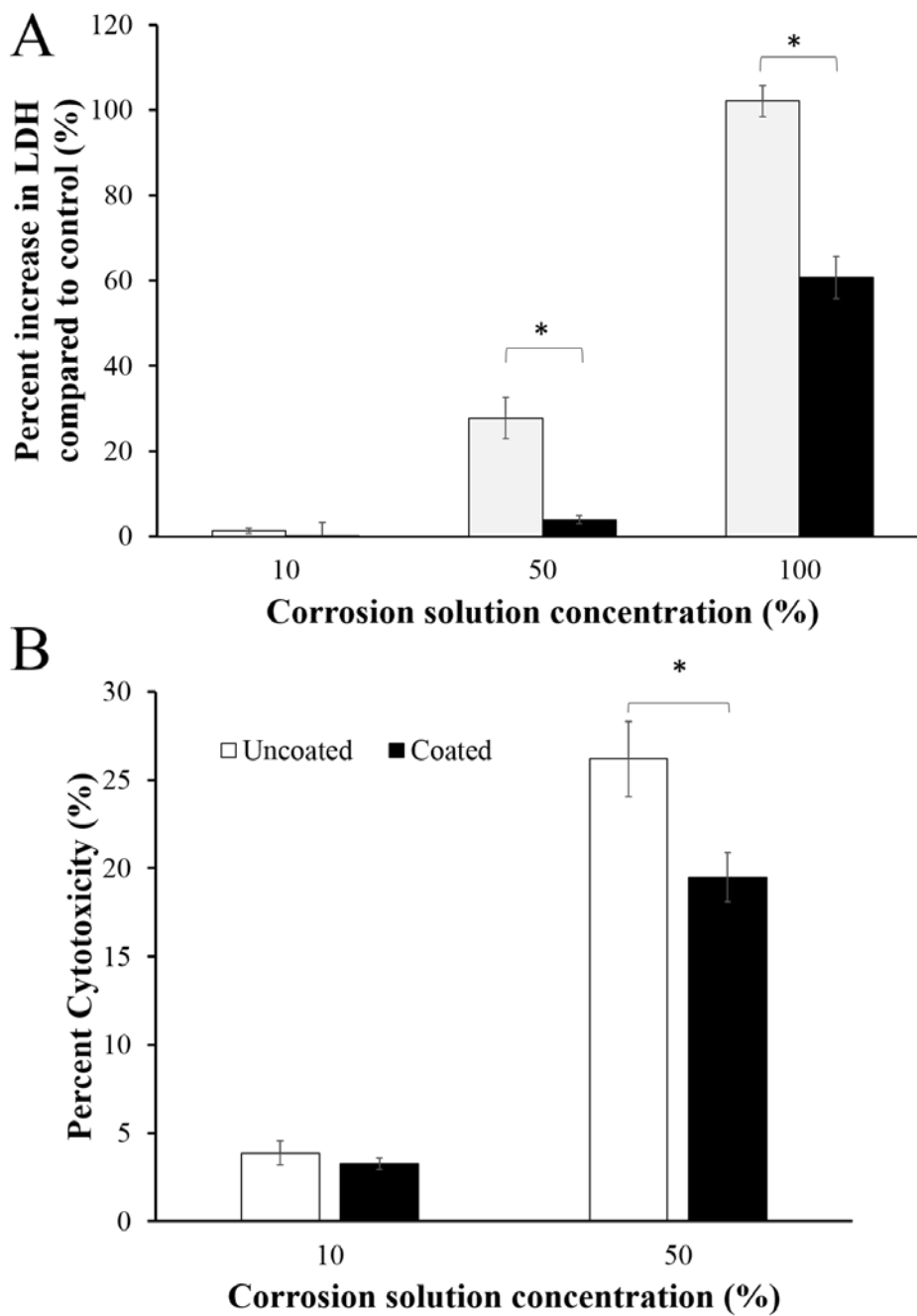


Figure 2-14: Cytotoxicity. (A) Cytotoxicity assessed through LDH quantification of neurons exposed for 24hours to corrosion media that had coated or uncoated samples corroded in it for 24 hours. (B) Percent cytotoxicity of neurons after 24 hour exposure to media that had coated and uncoated samples corroded in it for 3 days assessed through live dead staining. (* p<0.05)

2.5 DISCUSSION

Conducting polymers have demonstrated varying degrees of success as corrosion control coatings on metals other than Mg with potential mechanisms of protection varying widely [184, 205-213]. There has however been little investigation into the corrosion protection of CP on Mg[186, 187]. Here we show that PEDOT/GO can be electropolymerized on Mg, and the coating reduced corrosion rates and hydrogen evolution, as well as improved cytocompatibility.

Protocols for analyzing Mg corrosion are varied and can result in different interpretations of the corrosion rate[173]. To address these issues, multiple corrosion assessment techniques were conducted on the same set of samples. Damaging electrochemical tafel scans initially showed both a decrease in corrosion current as well as positive shift in corrosion potential indicative of greater resistance to corrosion. This test is a representation of early corrosion protection provided by the PEDOT/GO film and is likely largely due to the barrier properties of the coating. Non-damaging techniques were utilized for long term corrosion measurement. Both Mg ion and pH tests (Figs. 2-8 & 9) show a decreased corrosion rate for PEDOT/GO coated samples. Here, Mg ion assay assesses the presence of Mg ions in the corrosion solution resulting from the anodic reaction (equation 2) while pH represents products of the cathodic reaction (equation 1). Both of these metrics relate to the overall corrosion of the Mg.

Comparisons of the electrochemical data similarly indicated that the PEDOT/GO coating improved corrosion resistance. OCP data of PEDOT/GO coated samples displayed a positive corrosion potential at initial time points followed by a drop and recovery indicating the formation of the magnesium phosphate. Nyquist plots, as well as equivalent circuit analysis, also

revealed that the PEDOT/GO coatings were more resistant to corrosion displaying greater polarization resistance for the duration of the experiment.

SEM analysis of the coated and uncoated samples post corrosion revealed distinctly different surface morphology. Uncoated samples were largely covered in a layer of an amorphous morphology with a composition typical of $\text{Mg}(\text{OH})_2$. All PEDOT/GO coated samples had regions where the coating had begun to fail and the underlying Mg was exposed. These exposed regions showed a distinct scale morphology. EDX revealed increased phosphorous and oxygen content compared to the amorphous region. These data indicate that where the PEDOT/GO coating began fail, a unique corrosion byproduct $\text{Mg}_3(\text{PO}_4)_2$ was formed on the surface of the PEDOT/GO coated samples.

The PEDOT/GO coating facilitated this phosphate formation by utilizing its positively charged backbone as an alternate cathodic reduction reaction in the corrosion reaction. During corrosion on uncoated samples, Mg ions from the anodic half reaction and OH^- ions from the cathodic half reaction react with one another to form $\text{Mg}(\text{OH})_2$ on the surface (equation 4)[11, 193]. This mechanism is displayed in Fig. 2-15 A. This $\text{Mg}(\text{OH})_2$ film is generally porous, non-uniform, and chemically unstable making it a poor corrosion protection layer[214, 215]. By, replacing the traditional cathodic reaction (equation 1) with PEDOT/GO reduction, the positive backbone of the PEDOT is reduced to neutral and the generation of OH^- by equation 2 is diminished[216]. As a result, there is an increase probability that the Mg^{2+} will react with the phosphate in the solution. This mechanism is displayed in Fig. 2-15B. Previous reports have noted that the conducting polymer coatings facilitated the growth of a passive oxide layer on other metals[90, 217-221] in a manner similar to that proposed here. Additionally, reactions

displayed in Fig. 2-15B are similar to those proposed for certain anodized coatings containing phosphate[222].

These magnesium phosphate coatings provide increased corrosion resistance in that they are a denser and less soluble protection layer[223-228]. Phosphate conversion coatings are common techniques for improving corrosion resistance, and phosphate-based coatings on Mg have shown promise as corrosion prevention techniques [223, 224, 228-230]. Corrosion of Mg alloys in solutions containing phosphate at concentrations mimicking biologic fluids have resulted in the precipitation of a semi corrosion-protective phosphate layer[231, 232]. Phosphate containing layers have also been deposited on steel and Mg alloys by immersion into magnesium phosphate baths[222, 225, 226]. Both pure Mg and Mg alloys coated with these phosphate coatings demonstrated improved corrosion protection as well as a deposition of a phosphate protective coating in areas where the phosphate coating was damaged[222]. Phosphate coatings on Mg alloys have also been conducted through plasma electrolytic oxidation (PEO)[233]. Similar to the phosphate coatings deposited from solution, these PEO deposited coatings improved corrosion resistance and a re-passivation of damaged areas through the formation of a phosphate layer was observed. Both the solution deposited[222] and PEO deposited[233] phosphate protection layers displayed a surface with cracked morphology, similar to that observed here, where the coating had been damaged and a new phosphate layer formed. The facilitation of this phosphate intermediate in the area where the PEDOT/GO coating became damaged provides further corrosion protection even as the PEDOT/GO coating begins to fail.

The formation and maintenance of the phosphate layer is reliant on the polymer's ability to be reduced. As more Mg is exposed, there is a greater demand on the coating to generate the protective layer. Consequently, the polymer is further reduced. To increase the lifetime of

protection, PEDOT/GO films have the ability to be re-oxidized by dissolved oxygen in the solution, facilitating maintenance of the PEDOT protection[221]. It is however likely that this re-oxidation of the polymer backbone cannot maintain the same rate as the reduction provided by the Mg corrosion. Once the film has been completely reduced, it will act as a passive barrier layer in the areas where it is still adhered to the Mg.

For PEDOT/GO coated samples, early values for Mg^{2+} and OH^- concentrations indicate an initial low production of corrosion byproducts compared to the uncoated samples which had a high concentration of corrosion byproducts in the solution throughout the 23 days tested. This is likely due to initial passive barrier layer corrosion protection provided by the PEDOT/GO followed by reactions between the Mg, PEDOT/GO, and PBS that make the coating even more protective. Normally, following reduction of the polymer backbone, small negatively charged dopants are no longer held in the film and have the ability to diffuse out. However, with large graphene oxide sheets acting as the dopant in the PEDOT/GO film, the GO sheets remain trapped in the PEDOT matrix following reduction[102]. This causes the film to have a net negative charge which can further improve corrosion resistance by preventing aggressive negative ions like Cl^- from reaching the surface[114, 234].

Because of the allure of a degradable magnesium nerve guide implants[235, 236], in vitro primary neuronal culture was used as test bed to assess the effect of the PEDOT/GO coating on cytotoxicity of Mg implants. Reduced toxicity was observed by the PEDOT/GO coating in two different assays. Our lab has previously shown that PEDOT/GO film itself is exceptionally biocompatible and promotes the attachment and neurite extension of primary neurons[102, 103, 237]. The lowered toxicity afforded by the PEDOT/GO coating is likely due to two factors. Firstly, PEDOT/GO coatings decrease Mg ion concentration in solution, which at

elevated levels, has been shown to be toxic to neurons[238, 239]. Secondly, PEDOT/GO coatings maintained a more neutral pH due to the lack of OH⁻ production as the reduction of the polymer takes the place of water reduction[114]. Additionally, a potential benefit not demonstrated by corrosion media exposure tests is the prevention of hydrogen production. Hydrogen bubble formed during corrosion causes tissue dislocation from the implant and results in implant failure [9, 15, 17]. As discussed previously, the PEDOT/GO coating prevents water reduction and consequently decreases the formation of hydrogen bubbles. This benefit may serve to improve in vivo implant biocompatibility in future experiments.

This PEDOT/GO coating has demonstrated the ability to slow magnesium corrosion, improve biocompatibility, and electrochemically decrease the production of hydrogen gas, all of which are important properties for improving the clinical potential of Mg implants. In addition to these benefits, future exploration will involve the release of anti-inflammatory drugs from the coating to reduce the host tissue response [102]. Additionally, the GO sheets exposed at the surface of the film provide loci for surface functionalization which can allow for improved tissue interaction with the implant[103]. The combination of improved corrosion resistance, the ability to release drug at the site of corrosion, as well as improve tissue interaction through surface cues make this composite material a promising versatile coating for numerous potential applications of degradable Mg implants.

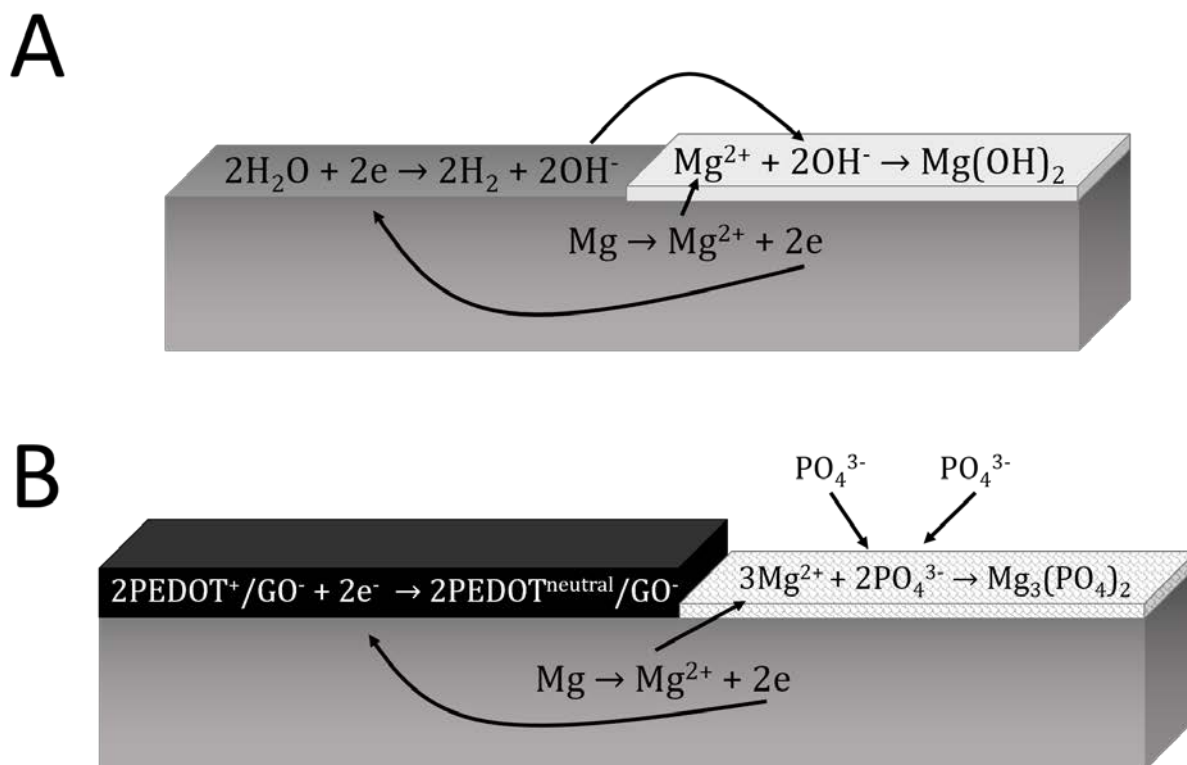


Figure 2-15: Corrosion Protection Mechanism. (A) Reactions facilitating the less corrosion protective Mg hydroxide formation for the uncoated samples. (B) Reactions occurring on the PEDOT/GO coated Mg samples in the area of film damage that lead to the formation of the corrosion protective magnesium phosphate layer.

2.6 CONCLUSION

Here PEDOT/GO coatings were electropolymerized on Mg ribbon as uniform and adherent coatings. Coated Mg samples showed decreased corrosion rates when evaluated with Mg ion concentration and pH of corrosion media, hydrogen evolution, and electrochemical techniques. Initially, PEDOT/GO coatings acted as passive barrier layers. Following diffusion of media through the film, the coating facilitated continued corrosion resistance through an increase in the

negative charge on the film and the formation of a magnesium phosphate layer. In vitro neuron cytotoxicity experiments demonstrated that the PEDOT/GO coating improves the biocompatibility of the Mg samples. This research provides new insight into the potential for conducting polymers to act as effective corrosion control coatings on magnesium biomedical implants through multiple mechanisms. Such coatings will be highly desired for various Mg implant applications from cardiovascular stents to nerve guides.

3.0 SELF-POWERED THERAPUTIC RELEASE FROM CONDUCTING POLYMER FILMS ON MAGNESIUM

3.1 ABSTRACT

Magnesium's ability to degrade away completely in vivo makes it an appealing material for medical applications. However, rapid corrosion, generation of hydrogen gas, and a lack of ability to add additional biomolecular cues have limited the clinical use of Mg. Here we report on the polymerization of a PEDOT/GO film on Mg with the addition of anti-inflammatory dexamethasone (Dex). The ability of this film to protect from corrosion and decrease hydrogen evolution is investigated. PEDOT/GO/Dex coatings on Mg improved corrosion resistance when evaluated through EIS, Tafel scans, and Hydrogen evolution. Additionally, the release of Dex from the film is explored both through application of external stimulation as well as through using the current generated during Mg corrosion. External electrical stimulation increased the rate of drug release. Corrosion generated current was also significant enough to drive release from the film and the amount of exposed Mg altered drug release rates. Bioactivity of the released Dex was confirmed through cell culture of released Dex with microglia stimulated with LPS. Here, released Dex was able to suppress the activation of the microglia. Not only does this PEDOT/GO/Dex coating have the ability to subdue Mg corrosion, it also can act as a smart releasing coating that delivers Dex at the site of corrosion to combat detrimental effects of

corrosion byproducts on local tissue. This self-powered smart coating could help combat the current issues preventing the use of Mg as medical implants.

3.2 INTRODUCTION

Implantable drug delivery devices have been drawing additional attention in recent years due to their benefits over oral and injectable therapeutics. By implanting a device that releases controlled amounts of drugs to the tissue local to the device, clinicians have the ability to deliver higher local dosages, minimize potential side effects, decrease total drug required to treat the patient, and protect drugs that may be too unstable to deliver with normal delivery methods[130, 240]. In addition, implantable devices may contain smart release systems as well as sensors and logic components to control drug delivery timing without the need for clinician supervision[241-243]. Implantable drug delivery devices have a wide variety of potential applications from cancer treatments to ingestible devices that deliver drug to the complex geometry of the small intestine[243-246]. These devices have initially taken advantage of microelectromechanical systems (MEMS) using silicon technology developed for the electronics industry[247-249]. However, these silicon based devices suffer from poor biocompatibility and require removal once the therapeutic reservoir is exhausted, or no longer needed [250, 251].

To address these issues, biodegradable materials are being investigated as drug delivery platforms. Conventional drug releasing systems largely include degradable polymers that serve as a reservoir for the drug of interest whereby the drug is released as the polymer degrades [252-255]. These systems however are not smart and cannot be precisely turned on and off according to the demand. There has recently been a push towards using degradable materials to form

MEMS devices that would allow the same sensors and logic as current devices but eliminate the need for removal surgery and minimize the biocompatibility issues from chronic presence[256-259]. In addition to the electronics for controlling the implantable drug delivery devices, safe power sources are needed to drive active drug release mechanisms[260, 261]. To that end a variety of power storage solutions that are more biologically friendly than current Lithium ion batteries are being explored. These include new sodium ion batteries[262, 263] as well as batteries that harness biomolecules to derive power[264].

Magnesium (Mg) is a promising material for use in implantable devices largely due to its safe biodegradation [15, 17, 173, 177, 192]. Additionally, Mg has a high strength to weight ratio, excellent electrical properties, and is compatible with some traditional MEMS fabrication processes [36, 39, 175, 265, 266]. As the fourth most common cation in the body, Mg takes part in a variety of biologic processes including ATP energy generation and DNA synthesis, and has been shown to promote bone growth and nerve regeneration[176, 179-181, 266]. Corrosion of a Mg implant results in local release of Mg ions, OH⁻, and hydrogen which can diffuse away provided the corrosion rate is slow[9]. This leads Mg to be a promising structural material for degradable implants as well as useful for developing degradable electronic systems. Furthermore, Mg is a potential anode for galvanically coupled power sources [267-269]. Here the electrons generated during corrosion can be utilized to power sensors and drug delivery devices. This combination of properties makes Mg a promising material for use in degradable self-powered drug delivery devices.

Biodegradable polymers that release therapeutics as they degrade have been deposited on the Mg surface to achieve the goal of a self-contained biodegradable drug releasing platform [80-82, 270-273]. This technique provides some control of drug release based on

polymer degradation rates but these coatings only act as a passive barrier layer preventing corrosion. Once the degradable polymer layer has been hydrolyzed away, Mg corrosion will proceed unhindered. While the eventual degradation of Mg is desired, previous reports have shown Mg is prone to rapid corrosion and loss of mechanical properties in addition to the excessive formation of hydrogen bubbles[15, 18, 42, 175, 182, 274]. Therefore, to address corrosion and maintain drug releasing properties, additional coatings and alloys are utilized in conjunction with the degradable polymer coatings. To better improve Mg's future potential, it would be ideal if a single coating could both protect Mg from corrosion as well as deliver therapeutics.

Conducting polymers (CP) offer a unique ability to accomplish both of these goals. CPs have been shown to be corrosion protective on a variety of different metals[89, 90, 114]. Mechanisms proposed for this protection however vary greatly depending on polymer, dopant, and sample pretreatment[184, 205-209, 212]. Proposed mechanisms for corrosion protection via conducting polymers include; a barrier layer, ennobling, anodic protection, formation of a modified CP metal interface, facilitation of a protective oxide, shifting of the electrochemical interface[89, 90, 114]. Additionally, CPs with corrosion inhibiting dopants have been used to decrease corrosion[114, 185, 207, 208]. Here, in the location where the CP begins to fail, the current generated by metal corrosion reduces the polymer and facilitates the release of dopant local to the site of film damage. When released, this dopant reacts with the corroding metal to form passive corrosion protecting layers. This corrosion triggered release of dopants from CPs has currently had little research in the use of bioactive dopants instead of corrosion protecting dopants.

Another mechanism of corrosion protection by CPs was reported in Chapter 2 where a CP film poly 3,4-ethylenedioxythiophene (PEDOT) doped with GO minimized corrosion of Mg through electrochemical interactions during corrosion. Here the conducting polymer is reduced as the underlying or exposed areas of metal are oxidized. This electrochemical interaction between the CP and the metal facilitates a corrosion protective layer to prevent further corrosion of the metal.

In addition to being used for corrosion protection, CP drug release through redox reactions has been well documented[98, 100, 101, 110, 133]. During polymerization, the polymer backbone is oxidized requiring negative dopants to provide charge balance. Following polymerization, reduction of the CP removes the positive charge on the backbone releasing the negative dopants. This electrically controlled release provides good temporal control of the drug release rate. Additionally, there are multiple ways in which CP dopant composites can be altered to adjust the release rate[100, 101, 113]. One mechanism previously reported in our lab is through the addition of graphene oxide (GO) sheets[102]. These sheets allow for altering both the amount of drug loaded into the film as well as the release rate of the drugs. Here, drug loading is accomplished via the π - π stacking of the drug molecule on the GO. In the polymer solution, the drug which has aromatic rings, stacks on the GO and is carried into the polymer as the negative charge on the GO facilitates GO doping into the CP film. The amount of drug that is carried into the polymer is dependent on the size of the GO sheets. Additionally, CPs with large immobile dopants, like GO sheets, can be used to incorporate positively charged therapeutics following polymerization[275-277] as well as carry in uncharged molecules.

Similar to CPs, GO has shown both corrosion control abilities as well as drug releasing properties. GO is an atomically thin layer of carbon functionalized with hydroxyl, epoxide, and

carboxylic acid groups[140]. GO alone has been used as a controlled drug release system largely for aromatic containing components[158, 278-281]. Here the drugs with aromatic rings in their structure are loaded on to the GO via π - π stacking in addition to hydrogen bonding. Release is typically accomplished via pH changes, however other methods including use of degradable ester bonds, degradable disulfide bonds, and ultrasound stimulation have been used to release drug from GO[156]. Electrical stimulation has also been used to enhance drug release from GO[278]. In addition to aromatic drugs, GO has been used for non-aromatic drug release[282], gene delivery[156], and aptamer delivery[145].

Graphene and GO have also been used as corrosion protection layers. Graphene sheets largely are used for their barrier properties and can provide corrosion protection both if they are grown on the substrate and if they are transferred to a new substrate[151-153]. The additional negative charges on the GO can further inhibit the corrosion by preventing aggressive negative ions from reaching the surface[154, 155]. GO coatings have even been used as barrier layers on Mg alloys following PEO treatment to further improve corrosion resistance[283].

A composite film of CP and GO may also be beneficial for corrosion protection. Doping the CP with GO traps the GO within the polymer network. Reduction of the CP/GO film then creates a net negative charge due to the GO's inability to diffuse away[114]. Consequently positive components from the solution are incorporated into the film. This process can be utilized to entrap and release neutral and positive dopants[112, 276]. These two cases show that the addition of GO to the CP helps diversify the films drug releasing properties making it applicable for different application needs.

Here we report the use of a CP film of poly 3,4-ethylenedioxythiophene (PEDOT) doped with GO containing Dex on Mg. Dex is a general steroidal anti-inflammatory that minimizes

inflammation around the implant site improving implant outcomes and has been shown to be effective in a variety of tissues[284-287]. We show that the PEDOT/GO/Dex film can control Mg corrosion, has a tunable drug release rate, and that the drug remains bioactive. Furthermore, previously reported electrically controlled release systems require a power source and wiring to the power the release, which may not be readily available. We show that drug release can be driven by the Mg corrosion current, consequently eliminating the need for external power.

3.3 MATERIALS AND METHODS

3.3.1 Materials

Single layer graphene oxide sheets were purchased from Cheap Tubes (Cambridgeport, VT). 200 proof ethanol was purchased from Decon Labs Inc. (King of Prussia, PA). Magnesium ribbon $\geq 99.5\%$ (3 mm wide x 0.2 mm thick), 3,4-ethylenedioxythiophene (EDOT) monomer, and dexamethasone were purchased from Sigma-Aldrich. PBS 10x concentrate (136 mM NaCl, 2.7 mM Potassium chloride, 10 mM Phosphate Buffer) was purchased from EMD Millipore (Billerica, MA) and diluted using de-ionized water from a Millipore Milli-Q system.

3.3.2 PEDOT/GO/DEX film polymerization

Composite films of PEDOT and GO, as well as PEDOT/GO/Dex were polymerized on Mg (20 mm x 3 mm x 0.2 mm, Sigma) and gold (20 mm x 3 mm x 0.1 mm, Ted Pella) strips. Prior to polymerization, samples were sonicated in ethanol briefly then dabbed dry. The polymerization

solution was created in two stages. Firstly, 10 mg/ml single layer GO (Cheap Tubes, Cambridgeport, VT) with and without 3.3 mg/ml Dex were added to 200 proof ethanol and sonicated for 30min. Sonication facilitated loading of the Dex on the GO for those samples with Dex. 35 μ l and 20 μ l of water and EDOT monomer respectively were then added per ml of the GO/ \pm Dex/ethanol solution and triturated to make the final polymerization solution.

Polymerization was conducted in this solution using a Gamry potentiostat/femtoostat on the Gamry Framework software. A two-electrode system was used with the sample to be coated as the working electrode and a gold counter/reference electrode. Polymerization was conducted at 0.6 V vs. Au until a total charge of 10 mC with samples immersed in the solution 9 mm. Following polymerization, samples were dipped in ethanol and stored at -20°C for 48 hours followed by 2°C for 24 hr. Samples were then stored at room temperature until release.

3.3.3 SEM

SEM analysis was conducted using a Jeol JSM 6330F SEM using an accelerating voltage of 3 kV. Samples were analyzed following above drying procedures in addition to an overnight storage in a vacuum desiccator. Coating integrity and surface morphology of coated and uncoated samples were analyzed.

3.3.4 Impedance spectroscopy

A three-electrode system was used to measure EIS with an Ag/AgCl reference, platinum counter, and Mg working electrode. PEDOT/GO and PEDOT/GO/Dex as well as uncoated Mg ribbon

samples were immersed 5 mm into PBS for the scan. This ensured only the coated portion of the sample was exposed to the PBS. Samples were allowed to sit in PBS for 5 minutes prior to running EIS analysis. Following the 5 minutes, OCP was recorded for 20 s or until it reached a stability of 0.05 mV/s. EIS was then taken from 100 kHz to 0.1 Hz with an applied potential of 0 V vs. OCP and a voltage amplitude of 10 mV.

3.3.5 Tafel Scan

Following EIS, using the same electrochemical cell, Tafel scans of the samples were conducted. Open circuit potential was recorded for 20 seconds prior to the scan. The scan was then run from -0.25 V to +0.25 V vs. OCP.

3.3.6 Hydrogen evolution

PEDOT/GO/Dex coated Mg as well as uncoated Mg samples were mounted in epoxy on glass microscope slides so that 5 mm of the sample was exposed. Samples were then placed in a 2 L crystallization dish that was filled with PBS. 2ml plastic pipettes were modified so that the tip was closed and the opposite end was flared out. These pipettes were filled with PBS and placed over the corroding samples. Hydrogen evolved from the samples rose up the pipette and collected at the top allowing for quantification of the total evolved hydrogen.

3.3.7 Powered release

Electrochemical release from PEDOT/GO/Dex on Mg was stimulated using the Gamry system with a three electrode system using a Pt counter electrode and Ag/AgCl reference electrode in 3ml PBS. Samples, immersed in the solution 5 mm, were subject to pulsatile stimulation of -0.25 V vs. open circuit potential (OCP) for 5s followed by 0 V vs. OCP for 5s. This stimulus was repeated 10 times. Following stimulation, the absorbance of the release solution was analyzed using SpectroMax M5 plate reader at the characteristic absorbance of Dex 242 nm and the analyzed solution was returned to the release solution. This 10 stimulation paradigm followed by solution analysis was repeated for a total of 50 simulations. The number of stimulations between solution analyses was then increased. The release solution was analyzed after a total of 100, 200, 400, and 600 simulations. Control samples were placed in PBS and measurements were taken at time intervals mimicking the stimulation paradigm but without the stimulation.

3.3.8 Corrosion triggered release

9 mm of the 20 mm long Mg ribbon samples were coated with PEDOT/GO/Dex. For passive release experiments, 'long' Mg samples were left un-altered while 'short' Mg samples had 10 mm of the uncoated portion removed. Gold samples were all in the 'long' form as the amount of exposed gold is not expected to affect drug release. Long Mg, short Mg and gold samples were completely immersed in 3 ml PBS. Samples of the release solution were taken at 5 min, 15 min, 30 min, 1 hr, 2 hr, and 3 hr and absorbance was analyzed with SpectroMax M5 plate reader at the wavelength of 242 nm.

3.3.9 Bioactivity assessment

Bioactivity of released dexamethasone was tested using previously reported methods[100]. A microglia cell line, Highly Aggressive Proliferating Immortalized (HAPI) cells, was challenged with a gram negative bacteria derived lipopolysaccharide (LPS) in combination with Interferon gamma. Nitrite content of the culture media was assessed using a Griess reagent kit to determine the level of microglial activation. Dex bioactivity was assessed by the drug's ability to suppress microglia activation and consequently decrease the nitrite production. Both dexamethasone as purchased and as released from the PEDOT/GO/DEX films were compared to assess the bioactivity of Dex released from the films.

HAPI cells (courtesy of Dr. Xiaoping Hu's lab, University Pittsburgh) were plated at 10^5 cells/well in a 24 well plate. After about 24 hours cells reached 80% confluence. Culture media was then removed and replaced with challenging solutions. These were as follows:

- (1) Control: 194 μ l PBS and 818 μ l DMEM F12
- (2) Released Dex: 182 μ l Dex in PBS (10.7 μ g/ml) released from PEDOT/GO/Dex coatings on Mg, 12 μ l PBS, 818 μ l DMEM F12
- (3) Control Dex: 182 μ l as purchased Dex in PBS (10.7 μ g/ml), 12 μ l PBS, 818 μ l DMEM F12
- (3) LPS only stimulation: 182 μ l PBS, 10 μ l of LPS in PBS (10 μ g/ml), 2 μ l IFN γ in PBS (1 μ l/ml), and 818 μ l DMEM F12
- (4) LPS + released Dex: 182 μ l Dex in PBS (10.7 μ g/ml) released from PEDOT/GO/Dex coatings on Mg, 10 μ l of LPS in PBS (10 μ g/ml), 2 μ l IFN γ in PBS (1 μ l/ml), and 818 μ l DMEM F12

(5) LPS + control Dex: 182 μ l as purchased Dex in PBS (10.7 μ g/ml), 10 μ l of LPS in PBS (10 μ g/ml), 2 μ l IFN γ in PBS (1 μ l/ml), and 818 μ l DMEM F12

Cells were incubated in the treatment media for 24 hours at 37°C. Following 24 hour incubation, culture media supernatant was removed and added to Griess reagent kit following instructions. Nitrite production was quantified by analyzing this solution with Spectromax M5 Spectrophotometer at an absorbance wavelength of 540 nm. Following removal of culture media cells were fixed in with 4% paraformaldehyde for 30 min. Cells were stained with DAPI cell nuclei stain for counting. Fixed and stained HAPI cells were imaged using a Leica DMI 4000 B inverted fluorescent microscope and counted in ImageJ using the particle analysis tool.

3.4 RESULTS

3.4.1 SEM

SEM imaging of the PEDOT/GO/Dex samples revealed a uniform coating on the Mg ribbon sample (Fig. 3-1 A & B). Higher magnification images (Fig. 3-1 C) show a rough surface morphology resulting from the edges of the GO sheets being exposed at the surface. This morphology is the same as that observed for PEDOT/GO only samples in section 2.4.2 indicating that GO sheets have been entrapped in the PEDOT matrix. Additionally, this morphology suggests the carboxylic acid functional groups on the edges of the GO sheets are still available for future functionalization.

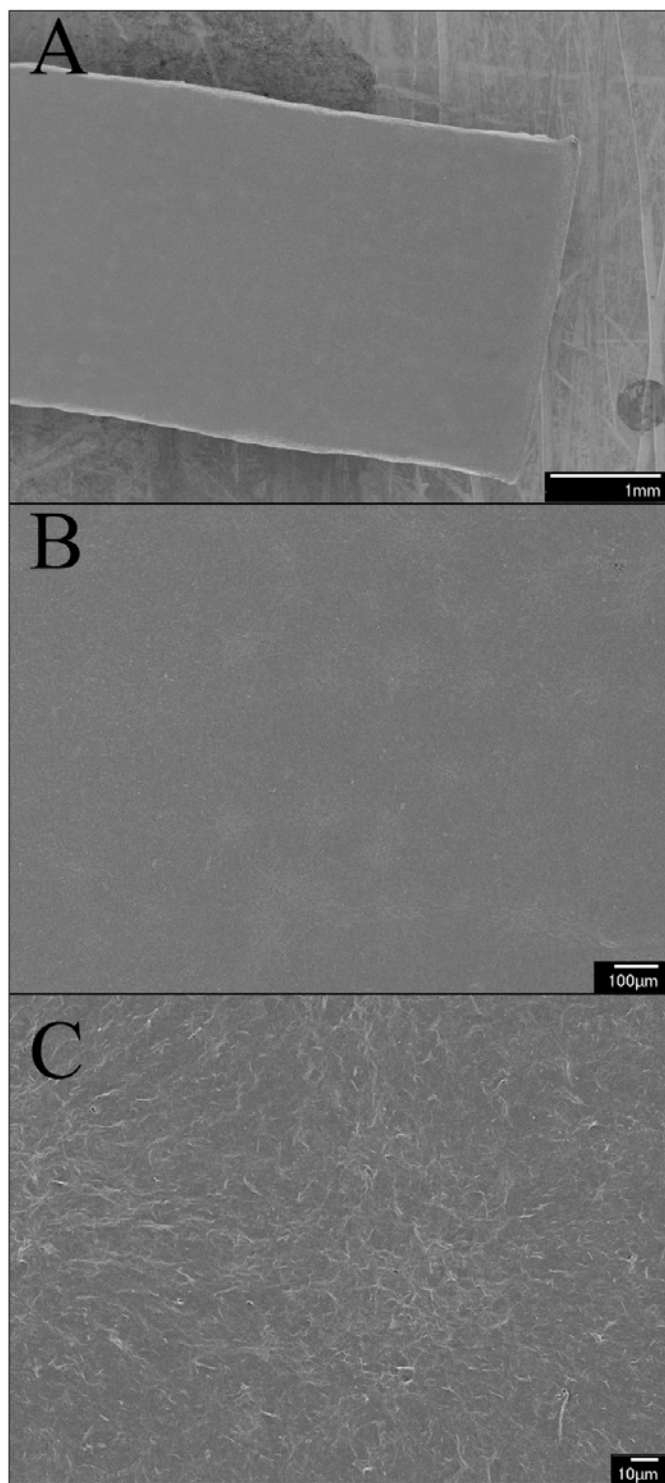


Figure 3-1: PEDOT/GO/Dex Mg morphology. (A) 20x image of PEDOT/GO/Dex coated Mg. (B) 100x image of PEDOT/GO/Dex coated Mg. (C) 500x image of PEDOT/GO/Dex coated Mg where the morphology provided by the GO sheets can be seen.

3.4.2 Impedance Spectroscopy

Immediately after OCP readings, EIS was recorded to provide additional assessment of corrosion protection afforded by the coating. Nyquist plots for uncoated and coated samples, with and without drug, following the 24hr OCP recording can be seen in Fig. 3-2. The radius of the Nyquist plot is attributed to the corrosion resistance with larger radii indicating more corrosion resistance[194, 195]. PEDOT/GO/Dex films show an increase in the arc radius when compared to uncoated Mg (Fig. 3-2 B). PEDOT/GO only films resulted in a Nyquist curve with a 90% greater arc radius than PEDOT/GO/Dex films suggesting much better corrosion protection performance (Fig. 3-2A).

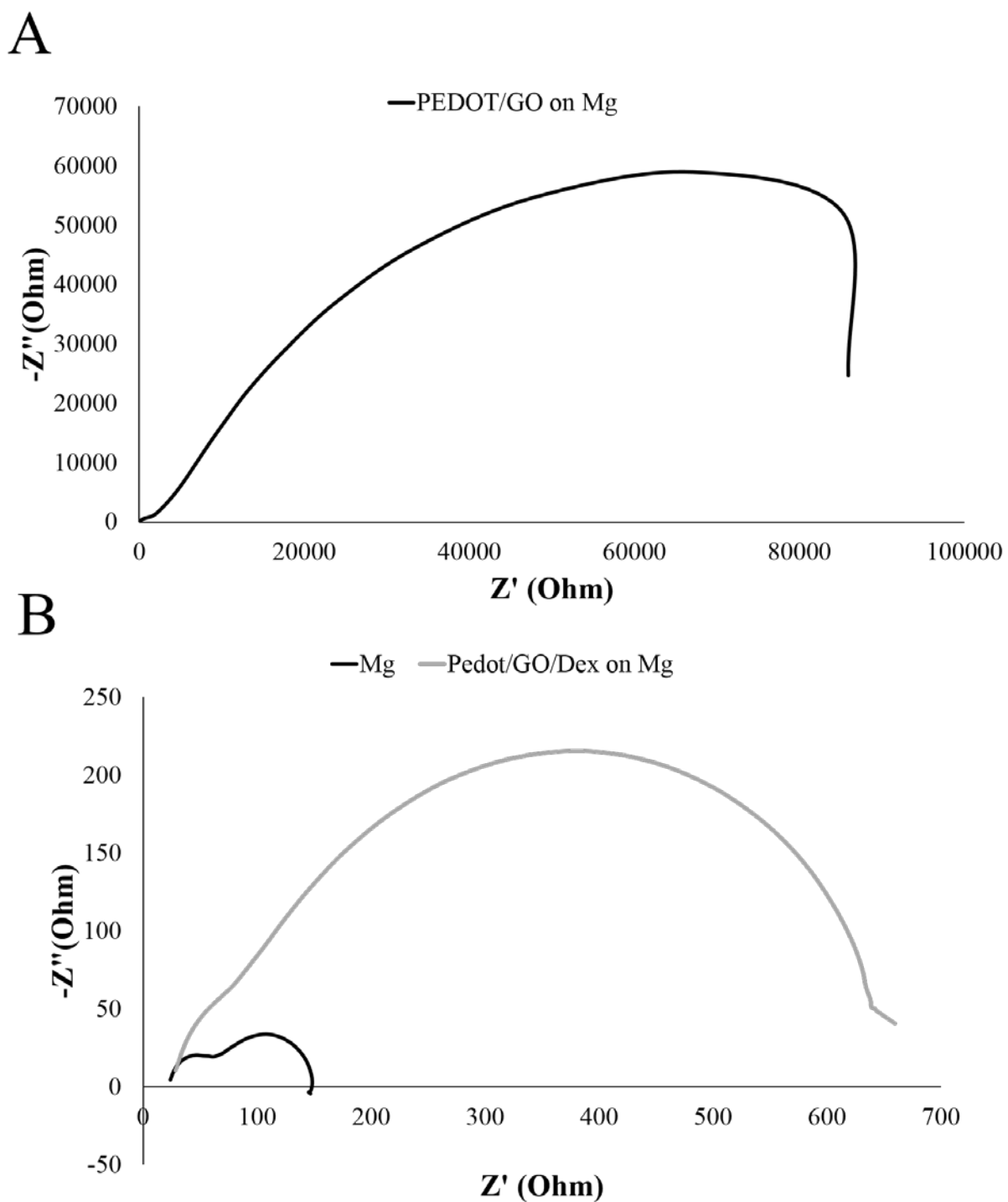


Figure 3-2: PEDOT/GO/Dex on Mg EIS. (A) Nyquist plots from EIS data collected for PEDOT/GO coatings on Mg. (B) Nyquist plots from EIS data collected for PEDOT/GO/Dex coated Mg and Uncoated Mg.

3.4.3 Tafel scan

Tafel scans represent the balance of anodic and cathodic half reactions of the corrosion reaction. From Tafel scans values for the corrosion current as well as corrosion potential can be extrapolated. A lower corrosion current as well as a more positive corrosion potential are both indicative of decreased corrosion. As can be seen in Fig. 3-3, Both PEDOT/GO and PEDOT/GO/Dex films show a positive shift in their corrosion potential. In addition, both of the coatings show a decrease in corrosion current when compared to the Mg only sample. The PEDOT/GO/Dex films do not show as significant of a positive corrosion potential shift or as dramatic of a decrease in corrosion current when compared to PEDOT/GO coatings. This suggests the Dex loaded films are not as effective at preventing corrosion of the Mg. The decrease in corrosion performance is most likely due to the addition of the Dex into the polymer creating an imperfect barrier layer.

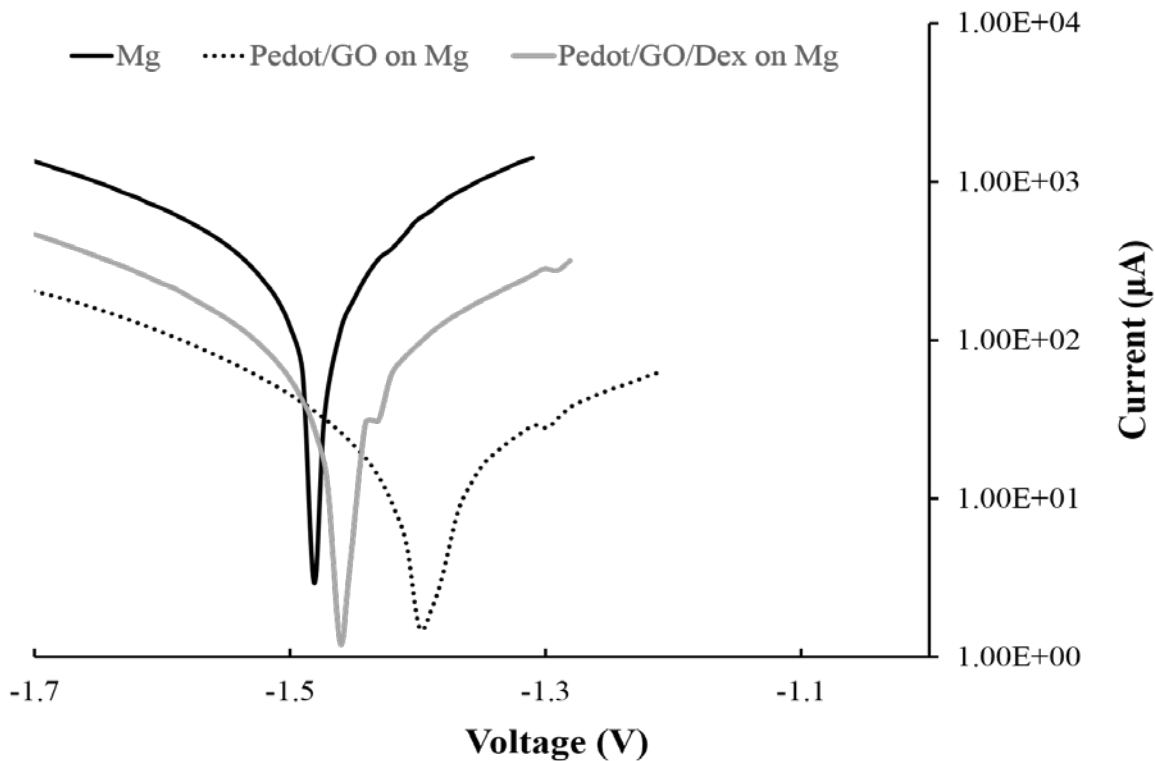


Figure 3-3: Tafel Scan. Current output from voltages applied during Tafel scan for PEDOT/GO on Mg, PEDOT/GO/Dex on Mg, and uncoated Mg.

3.4.4 Hydrogen evolution

Evolved hydrogen quantifies the byproduct of Mg corrosion resulting from water reduction. Here PEDOT/GO/Dex films act initially as a barrier layer to prevent corrosion followed by electrochemical coupling with the Mg to prevent further corrosion once the media inevitably reaches the underlying Mg. The PEDOT/GO/Dex films resulted in a 51% decrease in the rate of hydrogen evolution(Fig. 3-4). It must be noted that visible delamination of the film was observed on 75% of the PEDOT/GO/Dex samples within the first 24 hours. Despite this delamination, the decrease in hydrogen evolution was maintained.

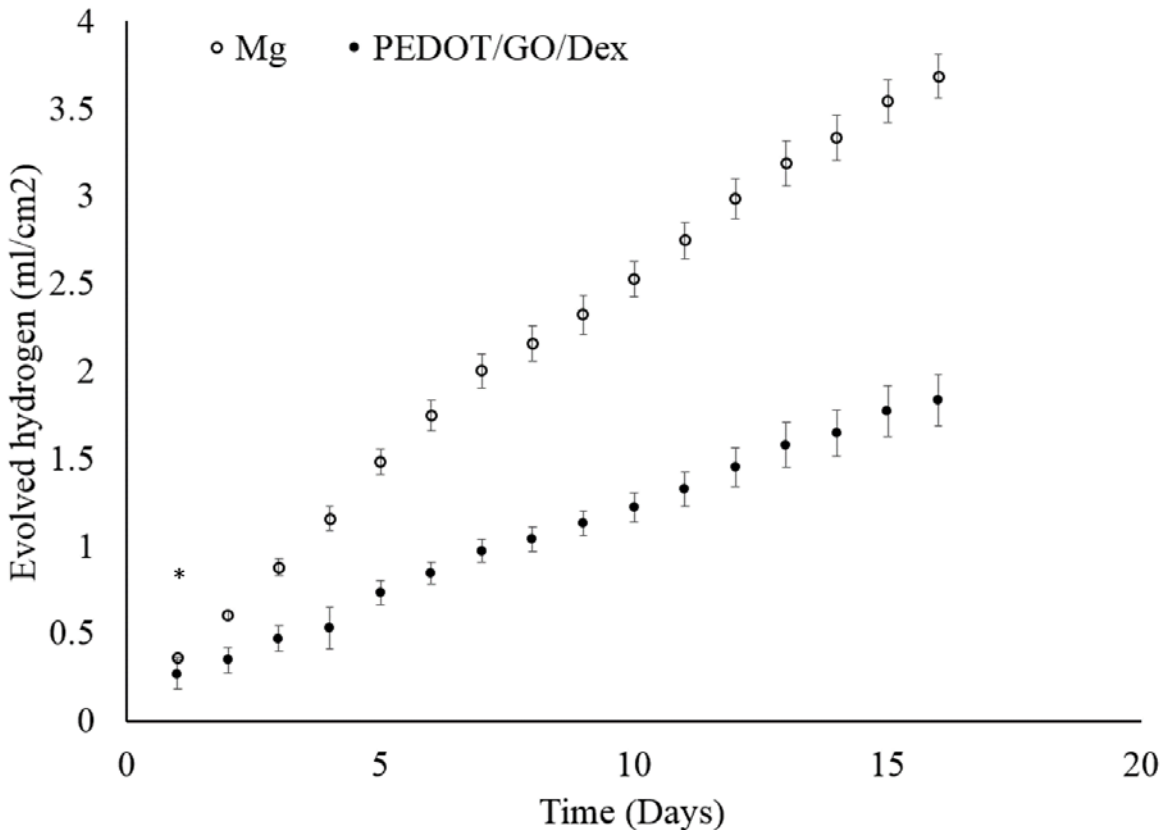


Figure 3-4: Hydrogen evolution. Evolved hydrogen from PEDOT/GO/Dex coated Mg and uncoated Mg. (* $p > 0.05$, all other $p < 0.05$)

3.4.5 Externally powered drug release

Powered drug release of CP Dex containing coatings on inert electrodes has shown that repeating reducing voltage stimulation (both biphasic and monophasic) is effective and that applying more negative potential results in increased drug release[100]. Here biphasic voltage stimulations are used to release Dex from the PEDOT/GO/Dex films on the more active Mg. As can be seen in Fig. 3-5, the Dex release rate is 10 fold greater for the stimulated sample for the first 100 stimulations. Following this, additional stimulations result in less drug release, likely because the majority of the drug that was near the surface was released and the drug that is released must

diffuse from deeper in the film. There is also a significant release of Dex from the non-stimulated samples. The initial spike in release is likely due to desorption of the loosely bound Dex on the surface and the following release is likely due to corrosion driven drug release described in 3.4.6 due to imperfect barrier properties of the PEDOT/GO/Dex film.

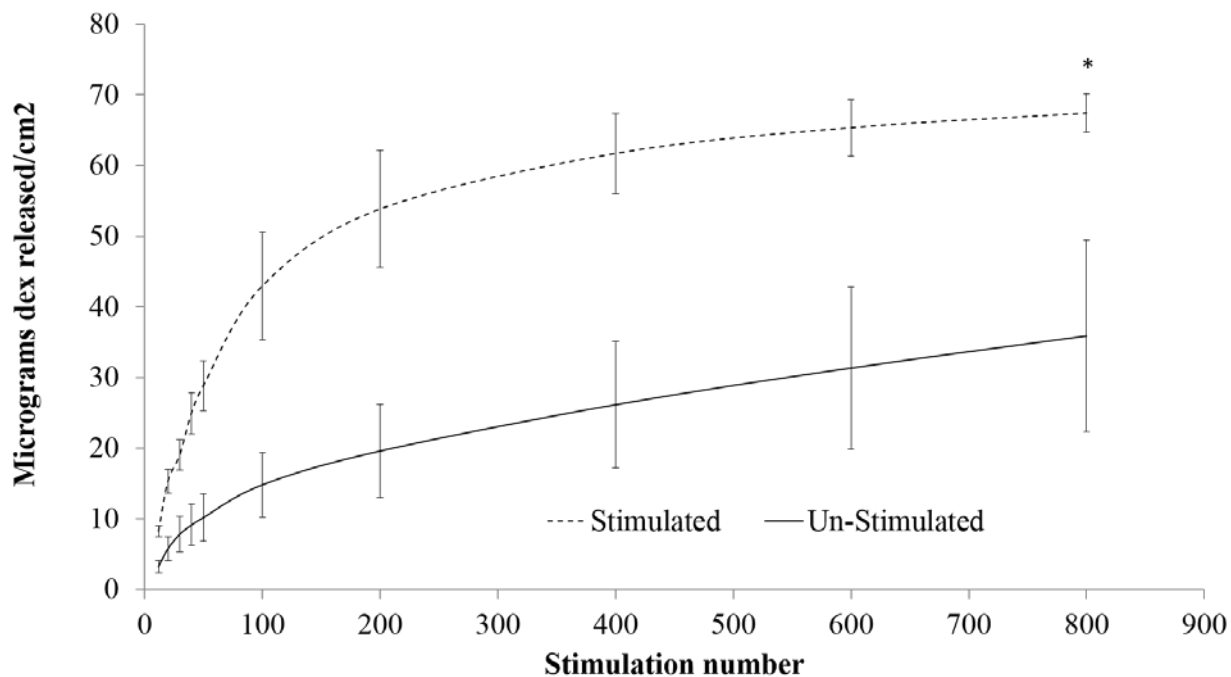


Figure 3-5: Powered drug release. Dex release resulting from applied reducing potential on PEDOT/GO/Dex Mg and drug release from PEDOT/GO/Dex Mg without stimulation. (* $p > 0.05$, all other data $p < 0.05$)

3.4.6 Corrosion triggered drug release

Here, corrosion of the exposed Mg facilitates an expedited reduction of the film and consequently increased drug release rates. As can be seen in Fig. 3-6. The samples with greater exposed Mg had a greater release rate than those with only a small portion of Mg exposed. Long

exposed samples had an average drug release rate of $3.36 \mu\text{g}/\text{cm}^2 \cdot \text{min}$ for the first five minutes while short exposed samples had a release rate of $1.5 \mu\text{g}/\text{cm}^2 \cdot \text{min}$. For the following 10 minutes long exposed samples had an average drug release rate of $3.19 \mu\text{g}/\text{cm}^2 \cdot \text{min}$ while short exposed samples had a rate of $1.3 \mu\text{g}/\text{cm}^2 \cdot \text{min}$. At the end of the experiment long exposed samples maintained an increased release rate at $1.16 \mu\text{g}/\text{cm}^2 \cdot \text{min}$ while short exposed samples had a release rate of $0.73 \mu\text{g}/\text{cm}^2 \cdot \text{min}$. The total release per surface area of the long exposed samples was significantly greater than that of the short exposed samples for the initial 30 min of the release experiment due to the excess current generated by the Mg corrosion. The remaining 2.5 hr of the release experiment showed that the long exposed samples trended to release more although not statistically significant. This is firstly due to the stabilization of the corrosion of the exposed Mg. Initial time points see a rapid corrosion of the exposed Mg while after 1 hr the corrosion has begun to stabilize. Additionally at these later time points it is likely that some of the media has diffused through the PEDOT/GO/Dex coating and also begun driving release. Both the long and short exposed Mg has the same total coated area, and therefore the total possible drug release from the two samples would be the same. At later time points the corrosion under the PEDOT/GO/Dex film is likely driving increased release of the short exposed Mg. PEDOT/GO/Dex on gold samples showed virtually no release of Dex.

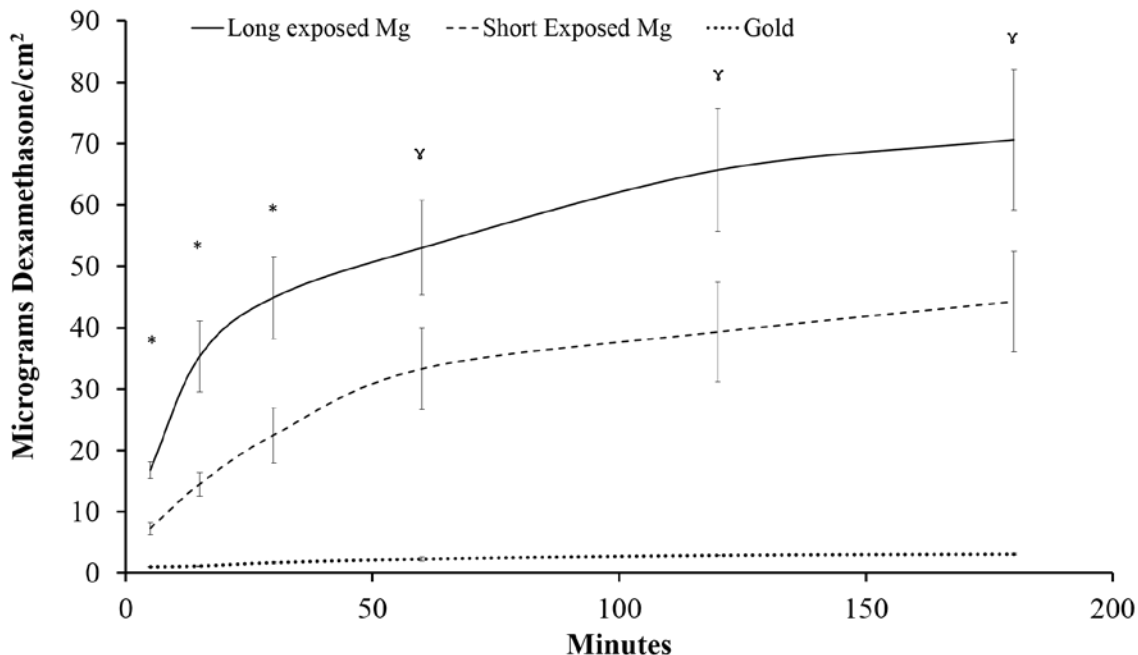


Figure 3-6: Corrosion powered drug release. Dex release from PEDOT/GO/Dex films on Mg where drug release is powered by Mg corrosion. Mg samples had different amounts of exposed Mg but the same amount covered by the PEDOT/GO/Dex coating. Gold samples had the same amount covered by PEDOT/GO/Dex and an equivalent amount of uncoated gold. (* $p < 0.05$, $\gamma p < 0.08$)

3.4.7 Bioactivity of release Dex

To confirm the Bioactivity of Dex released from the PEDOT/GO coatings, microglia derived HAPI cells were stimulated with LPS[288]. Microglia stimulation with pro-inflammatory LPS results in the release of a variety of inflammatory products including NO and pro-inflammatory cytokines. Dex quenches the HAPI cell activation and decreases the release of NO through inhibiting expression of inflammatory mediators[289]. Released Dex was compared to as-purchased Dex (this was the same source of Dex that was added to the polymerization solution for the polymerization of PEDOT/GO/Dex films) in its ability to suppress activity of the microglia. Fig. 3-7 displays Nitric Oxide production determined by griess reagent assay.

Microglia stimulated with LPS bacterial derived peptide are activated to produce a fivefold increase in NO production as can be seen in Fig. 3-7. Treatment with both, released and as-purchased Dex at 5 μ M suppresses microglia activation decreasing NO production. The released Dex applied at the same concentration as the purchased Dex shows the same ability to suppress microglia activity. This indicates that entrapment of Dex in the PEDOT/GO film on Mg and subsequent release did not damage the drug.

Additionally, there was no significant difference between HAPI cells exposed to released or as-purchased Dex without the presence of LPS. This indicates that the PEDOT/GO/Dex samples are not releasing monomers, short mer units, or GO during the stimulation that could generate confounding toxicity.

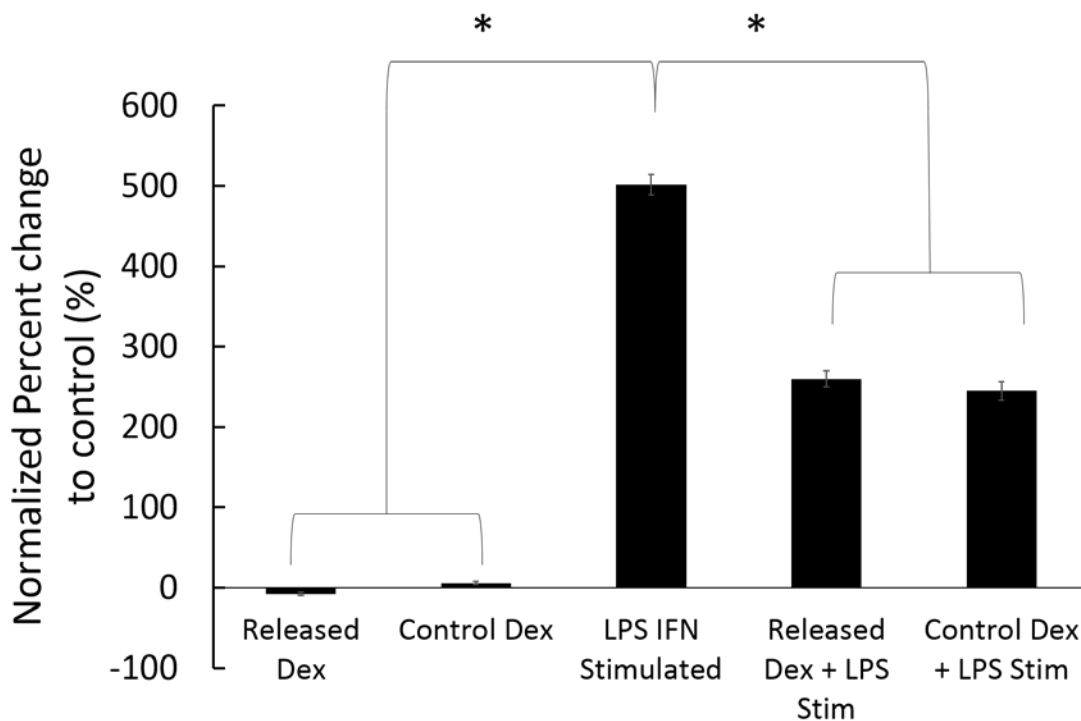


Figure 3-7: Dex Bioactivity. Assessment of Dex bioactivity through quantification of NO generated by HAPI cells due to LPS stimulation using Griess Assay. n=4 for each group (* p < 0.05)

3.5 DISCUSSION

Here we utilize a PEDOT/GO/Dex composite coating to both control Mg corrosion as well as release bioactive cues in a smart self-powered way. A coating with these two properties, corrosion control and smart self-powered drug release, could aid in the clinical implementation of Mg based implants. Our composite coating takes advantage of the beneficial properties of both of these components for use as a responsive corrosion control and drug releasing coating. The coating prevents corrosion as an initial barrier layer. Following eventual diffusion of the corrosion media through the film, the properties of the film will both passivate the corroding location, as described in chapter 2, and locally release anti-inflammatory drugs in the area of corrosion. The galvanic coupling of PEDOT/GO/Dex to the Mg corrosion current facilitates the release of Dex in the areas where corrosion is occurring. This PEDOT/GO/Dex coating system aims to combat the potential negative effects of increasing pH local to the corroding Mg implant as well as gas pockets resulting from the evolved hydrogen by both decreasing corrosion and improving tissue health near sites when corrosion does occur.

Polymerizing the PEDOT/GO/Dex film directly on the Mg allows it to act as a corrosion inhibitor similarly to the PEDOT/GO coating discussed in Chapter 2. The PEDOT/GO/Dex coating showed improved barrier properties over uncoated Mg as indicated by EIS measurements (Fig. 3-2). Tafel scan data (Fig. 3-3) also showed corrosion protection provided by PEDOT/GO/Dex coatings, albeit not as significant as PEDOT/GO alone. The lower corrosion protection provided by PEDOT/GO/Dex is also noted in the hydrogen evolution experiments (Fig. 3-4) where 75% the PEDOT/GO/Dex films showed film delamination within the first 24 hours of immersion in PBS. Despite this delamination, over the following 17 days, the PEDOT/GO/Dex films maintained a decreased rate of hydrogen evolution (Fig. 3-4). This

indicates that the electrochemical coupling of the PEDOT/GO/Dex films and the Mg was maintained. This electrochemical coupling provides improved corrosion protection even if areas of the film begin to delaminate. The combination of expedited film delamination observed during hydrogen evolution experiments as well as decreased corrosion protection assessed through EIS and Tafel scans indicates that the PEDOT/GO/Dex coating is not as effective at preventing corrosion as the PEDOT/GO coatings without Dex. This is due to the imperfect barrier layer of the PEDOT/GO/Dex film resulting from the added Dex. The Dex is incorporated into the film both by being trapped in the polymer matrix during polymerization, as well as being carried into the film by GO discussed below. This results in a barrier film that has Dex interrupting the PEDOT/GO film. These disruptions are vulnerable locations where the corrosion media can more easily diffuse through the coating. The barrier properties are likely further decreased as the Dex leaves the film, through diffusion in addition to being driven out by the corrosion current.

Corrosion triggered drug release from CPs has been shown previously with active metals wired to the CP acting as a power source. In one study, CP doped with negatively charged phenol red was electrically connected to a zinc anode and both were placed in aqueous media[290, 291]. Oxidation of the zinc in water generated negative current that reduced the CP and drove drug release. In another study, external coupling of Mg corrosion for drug release was shown when the corroding Mg was wired to a CP/Dex coating and both were placed in an aqueous media[292]. These cases both did not place the CP film directly on the corroding metal, instead the corroding metal was wire connected to the CP film that was deposited on an inert and stable substrate. Controlled release of adenosine triphosphate from CP has been shown where Mg is sputtered onto the polymer film and the corrosion of the thin Mg layer drives the

release[293, 294]. Here however, the Mg was purely sacrificial and served only to power release from the CP.

Different from the above studies, PEDOT/GO/Dex was directly deposited on active Mg and self-powered drug release was achieved. Common CP drug releasing systems often utilize a negatively charged drug that is incorporated with the positively charged backbone of the CP. Upon reduction, the CP backbone is neutralized and the positive charge that prevented diffusion out of the film drug in is eliminated allowing the drug to diffuse out of the film. Here however we were unable to use a negatively charged drug molecule due to the induced aggregation of the GO sheets due to the positive charge of the drug salt, in this case dexamethasone 21-phosphate disodium salt[100, 102]. The positive charge results in a shrinking of the electric double layer that keeps the GO sheets suspended in solution resulting in GO aggregation[295]. To prevent aggregation, Polymerization of the PEDOT/GO/Dex films was accomplished using a non-salt form of Dex in the ethanol based PEDOT/GO solution discussed in chapter 2. Without the negative charge, the Dex will not be loaded and released from the polymer film in the traditional CP dopant release paradigm.

Here, incorporation of the Dex into the polymer is facilitated both by entrapment during the polymerization as well as bonding of Dex with the GO sheets. The bonding is possibly facilitated by hydrophobic π - π stacking between the aromatic rings on the Dex and GO as well as hydrogen bonding between hydroxyl groups of Dex and GO. Once attached, the Dex can be carried into the PEDOT film with the GO that acts as the dopant[278, 280-282].

Application of external voltage stimuli resulted in well controlled Dex release (Fig. 3-5). This externally powered reduction of the PEDOT/GO/Dex film releases the entrapped uncharged Dex through multiple mechanisms. Firstly, reduction can interfere with the π - π stacking of the

Dex and GO[296]. Here the reduction interferes with the quadrupole established by the aromatic rings which drive π - π stacking[297]. Also, reduction of the polymer may reduce some of the GO resulting in less hydroxyl groups expressed. This could minimize hydrogen bonding between the Dex and GO[278]. Both the interference of the π - π stacking and loss of hydrogen bonds eliminate the forces holding the Dex in the film causing it to be released. Additionally, reduction of CP films causes significant volume changes as solvent is transported in the film changing the arrangement of the polymer chains and causing ion transport in and out of the film to compensate for the charge change[298]. This volume change has also been shown to release drug from CP films [113, 299], and may be another method for the release of non-charged Dex from the PEDOT/GO/Dex film.

Drug release was also accomplished without the application of external power, but through the coupling of the PEDOT/GO/Dex coatings and current generated by Mg oxidation. As can be seen in Fig. 3-6, samples with more exposed Mg showed increased total drug release as well as increased drug release rates. This is due to greater amount of exposed Mg providing more surface area for corrosion. More electrons are therefore generated on large exposed Mg samples and these electrons further reduce the polymer resulting in greater drug release. Self-powered on demand drug release of anti-inflammatory Dex in the area of Mg corrosion could help combat local tissue response to increase pH and gas pocket formation that can prevent proper healing and tissue interfacing with the device. The increase in drug release with increasing exposed Mg did not however did not correlate with the total exposed surface area. Those samples with 1 mm exposed Mg did not have 11 times less drug release than those samples with 11 mm exposed Mg. This is likely due to the poor barrier properties of the PEDOT/GO once the Dex is added. Consequently, while corrosion is occurring at the exposed

Mg, there is also corrosion occurring underneath the PEDOT/GO/Dex film. This corrosion drives drug release and this local corrosion may be more efficient at driving release from the polymer as opposed to the more distant corrosion of the exposed Mg. For those reasons, the short exposed Mg samples did result in increased drug release compared to controls while releasing ~50% less drug than the long exposed Mg samples.

Of paramount importance with drug releasing systems is the viability of the drug following release[100]. During electropolymerization, Dex is exposed to ethanol and oxidizing potentials that could damage the bioactivity of the drug release from the PEDOT/GO/Dex coating. The quenching of the activity of HAPI cells exposed to LPS by the released Dex confirms that the bioactivity of Dex in the PEDOT/GO/Dex coating is maintained. While the LPS stimulation of HAPI cells shows the Dex is bioactive, the pathway activated by the LPS stimulation is that of the Pathogen-Associated Molecular Pattern (PAMP)[300]. It may be useful to also look at the effect of released Dex on the Damage-Associated Molecular Patter (DAMP) which may be more representative of the cellular response around an implanted device[300]. This self-powered drug releasing paradigm has the potential to also be used for other drugs such as bisphosphonate molecules for orthopedic implants[301] and Sirolimus and Paclitaxel for stent applications[302-304]. In addition, the drug release rate could be tuned to provide optimal release paradigm for each specific application through sonication of the GO to alter the amount of drug that is loaded into the film as well as the release kinetics[102].

3.6 CONCLUSION

Mg corrosion, while being ideally safe, has shown local tissue damage through increases in pH and gas pockets resulting from hydrogen evolution if corrosion is too fast or if the byproducts cannot be cleared easily. The PEDOT/GO/Dex coating developed here provides both corrosion protection and as serves as a smart drug release system that actively responds to Mg corrosion. This PEDOT/GO/Dex coating controls corrosion through initial barrier properties followed by coupling of the redox properties of film to generate a more corrosion resistant intermediate. In addition to corrosion protection, when corrosion inevitably does occur, anti-inflammatory drugs are locally released to minimize detrimental effects on the surrounding tissue. This single layer dual function approach will serve to bring Mg closer to clinical applications by providing corrosion control and the ability to locally release biologically relevant molecules

4.0 PEDOT/GO COATINGS AS A METHOD FOR ADDING BIO-FUNCTIONAL SURFACE CUES

4.1 ABSTRACT

Magnesium's corrosion in vivo has the potential to make it a useful material for constructing biomedical implants that do not need to be surgically removed but simply degrade away once the tissue has healed. Magnesium however lacks a versatile method of functionalizing the surface with biomolecules that could guide improved local tissue response. Here we report on the coating of Mg with conducting polymer 3,4-ethylenedioxythiophene (PEDOT) and graphene oxide (GO) composite coating. This coating provides carboxylic acid groups on its surface that can be used to facilitate attachment of biomolecules with primary amines through carbodiimide crosslinking chemistry. Here we explore the attachment of different molecules to the surface in order to determine if this coating could function as a versatile platform for adding various surface cues on Mg implants. Albumin-fluorescein protein complex, amine functionalized poly ethylene glycol(PEG), nerve growth factor (NGF), and a novel super oxide dismutase mimic with amine functionalization (iSODm) were covalently attached through this carbodiimide crosslinking chemistry. Attachment of fluorescently tagged albumin confirmed the covalent attachment of molecules to the surface. PEG functionalized surfaces showed decreases in attachment of both fibroblast cells and *Escherichia coli* (E. coli) bacteria. Surfaces

functionalized with NGF showed the ability to increase neurite outgrowth of PC12 cells. Attachment of iSODm was confirmed as its antioxidant behavior was maintained and it resulted in increased mortality of bacteria attached to the surface. These results suggest that the PEDOT/GO coating has the potential to be a versatile method of attaching surface cues to Mg implants to help guide tissue response and improve patient outcomes.

4.2 INTRODUCTION

4.2.1 Problems that can be addressed by surface functionalization

Biomedical implants suffer from multiple issues in regards to integration with the host tissue. Firstly, as with all medical implants, there is an inherent risk of infection. Complications associated with implant infection often lead the need for implant removal[305]. In addition to infection, implanted devices suffer from both acute and chronic inflammation. Acute inflammation, resulting from the trauma of implantation procedure can, in some cases, be severe enough to warrant removal of the device[306]. Chronic inflammation has been the target of recent research to prevent the loss of implants which are designed to remain *in vivo* for the patient's lifetime[307]. The chronic foreign body reaction (FBR) is classified by persistent inflammation and recruitment of macrophages, monocytes, and lymphocytes to the implant location and can be another cause for implant removal[308, 309]. In addition to infection and inflammation, which are applicable to all implanted devices, there are certain device and tissue specific issues that result device failure. Stent failure results from restenosis and thrombosis [310], orthopedic implant failure is caused by a lack of osseointegration[311], and the slow rate

of axonal regeneration in nerve conduits prevents functional recovery for long gap injuries [312-316]. One method that can be utilized to combat these complications is the use of surface immobilized bioactive factors to improve tissue specific reactions local to the implant[317-320].

4.2.2 Prevention of infection

Bacterial or fungal colonization of the device can be introduced during the implantation operation from sources including ambient air, contamination from the surgical staff or equipment, bacteria residing on the patient's skin, and bacteria found in the patient's body[321, 322]. These organisms adhered to the implant are often embedded in an extracellular matrix which shields them from the host's immune systems as well as decreases the potency of administered antibiotics[311]. To prevent bacteria or fungi colonization, surface coatings that prevent attachment are being developed. Most notably is the use of polyethylene glycol (PEG). Kingshott *et al.* showed that the technique used to covalently immobilize PEG played a significant roll in the resulting the effectiveness of PEG at preventing bacterial adhesion[323]. PEG Coatings with utilizing a combination of steric hindrance and anti-adhesion surface charge have shown the ability to prevent bacterial adhesion[324]. Coatings incorporating PEG while also presenting the RGD (Arg-Asp-Gly) adhesion peptide prevented bacterial (*staphylococcus aureus*) adhesion while maintaining fibroblast and osteoblast cell adhesion[325]. These reports suggest that a PEG surface coating could provide antibacterial properties to prevent biofilm formation and decrease infection risk.

4.2.3 Mitigation of inflammation

The FBR is another issue that could potentially be ameliorated by the application of a surface coating on the implant. Upon implantation, the device is immediately covered by proteins from the patient's blood and tissue that nonspecifically adsorb to the surface. The degree of nonspecific adsorption can be correlated with the degree of biocompatibility of the implant[307]. An immune and inflammatory response involving leukocytes and neutrophils then takes place[326]. Monocytes and macrophages begin to interact with the implant, where the composition of the non-specifically adsorbed proteins can affect macrophage phenotype[326]. Macrophages are considered the key mediators of the FBR in that they generate both inflammatory and regenerative products[326]. Chronic presences of the foreign body results in the fusion of macrophages into foreign body giant cells which contribute further to inflammation[327]. Additionally, fibroblasts are recruited to the implant area and generate a fibrous capsule to isolate it from the native tissue[251]. This FBR of chronic inflammation and fibrous encapsulation impedes device-tissue integration.

While coatings that release anti-inflammatory and other drugs to minimize FBR have been investigated [113, 326, 328-330], the finite reservoir of drug contained in a surface coating limits this technology's applications for chronically implanted devices. For this reason different coatings that alter the surface chemistry of the implant have been investigated. These coatings attempt to interfere with the initial nonspecific adsorption of proteins which literature suggests guides the remainder of the FBR[326]. Currently, PEG surfaces, like those used to decrease bacterial adhesion, are one of the more promising surfaces for prevention of the non-specific protein adsorption[331]. Also, coatings of collagen and PLA scaffolds have shown decreased FBR and increased angiogenesis around the implant[332, 333]. A variety of hydrogel coatings

have also been investigated to improve implant performance through decreasing the effects of the FBR[334-336]. While these coatings have shown in vitro promise, in vivo improvements of the FBR have been mixed.

Also, heparin coatings have been shown to reduce adsorption of multiple different proteins in the inflammatory pathway including fibronectin, fibrinogen, kininogen, and complement 3 protein from whole blood[337]. Immobilization of anti-inflammatory peptide Alpha-MHS on neural electrodes reduced inflammation through altering the activity of glia response surrounding the implant[338]. Covalent immobilization of anti-inflammatory cytokines was accomplished with a fusion protein of recombinant human IL-1 receptor antagonist and elastin-like peptide and significantly changed the behavior of LPS stimulated monocytes[339]. Exposure to this protein decreased monocyte differentiation and expression of pro-inflammatory cytokines and caused an increase in anti-inflammatory and pro-wound healing cytokines. Additionally, the surface modification of samples with a superoxide dismutase mimic (SODm) can minimize the harmful environment around an implant by eliminating the powerful oxidant superoxide which is released by macrophage and glia[340, 341]. The acute and chronic tissue response to polyethylene samples modified with SOD displayed decreased inflammatory response characterized by neutrophil migration, presence of foreign body giant cells, and fibrous encapsulation[342].

4.2.4 Implant specific cues

In conjunction with infection and inflammation, implant performance could be enhanced through the addition of further surface cues to encourage appropriated local tissue response to the implant. In the case of orthopedic implants, ossiointegration, or bone growth and remodeling

around the implant, to form a tight junction between the bone and implant is desired. To accomplish this, different surface roughening and calcium based coatings have been investigated[311, 343]. In addition to these non-biologic coatings, surface functionalization of biomolecules has been shown to improve implant outcomes. Adhesion promoter RGD (Arg-Gly-Asp) increased adhesion of osteoblasts in vitro which could facilitate improved bone regrowth around the implant[344]. In vivo RGD surface functionalized samples doubled the amount of bone interfacing with the functionalized implants as well as decreased fibrous tissue formation and increase in bone density surrounding the implant[345]. Implants functionalized with GFOGER, a peptide mimicking a binding loci of collagen, stimulated osteoblast differentiation through $\alpha 2\beta 1$ integrin binding mediated pathway resulting in increased the amount of bone contacting the implant[346]. Growth factors such as bone morphogenic protein (BMP) have also been covalently immobilized and resulted in increased bone density adjacent to the implant[347].

Stents too could benefit from tissue specific surface immobilization to combat issues such as thrombosis, re-stenosis, and endothelialization. Heparin modified stents have a significantly lowered the activation of platelets and coagulation and decreased the expression of GP IIb/IIIa, $\alpha \text{IIb}\beta 3$ on platelets, an integrin required for normal platelet aggregation[348, 349]. Immobilized heparin has also suppressed the adsorption/activation of procoagulant proteins and enhanced the adsorption/activation of anticoagulant proteins[350]. Phosphocholine, a zwitterionic molecule, has been immobilized on stents and resulted in reductions in platelet adhesion and activation[351, 352]. Surface modification with the apyrase enzyme was able to catalytically degrade ADP preventing the recruitment and aggregation of platelets on the surface[353]. Attachment of collagen binding peptides to the surface allowed collagen attach and mask the

implant, preventing platelet adhesion and activation[354]. In addition to preventing thrombosis, surface functionalization has been used to prevent restenosis. Estrogen functionalized surfaces have been shown to increase intracellular cyclic AMP which in turn decreases synthesis rates in vascular smooth muscle cells[355]. Methods for inhibiting platelet-derived growth factor have also been investigated towards decreasing restenosis[356]. In contrast to sequestering restenosis, encouraging proper endothelialization of stents has also been linked to improved outcomes. Surface immobilization of vascular endothelial growth factor significantly increased the attachment of endothelial cells[357]. Attachment of anti-CD34 antibody showed specific adhesion promotion of vascular endothelial cells through binding the CD32 transmembrane protein resulting in increased vascularization of the stents[168]. Immobilization of REDV peptides, complement to endothelial integrin, selectively increased endothelial cell growth on the surface[358].

Similar to the above two applications, peripheral and central nerve regeneration could benefit from implants that degrade over time but also have functional cues to encourage rapid nerve growth as well as guide nerves to the proper target location. A variety of peptide sequences derived from the extracellular matrix have been investigated including CDPGYIGSR, GQAASIKVAV, GRGDS, and PHSRN[359]. Hydrogels modified with CDPGYIGSR and GQAASIKVAV peptides improved adhesion of dorsal root ganglia (DRG) neurons as well as reported neurite growth into the functionalized scaffolds indicating the ability of peptides to promote neurite guidance [360]. Patterns of GRDGS placed on a modified agarose hydrogel encouraged preferential attachment of dorsal root ganglia cells and guided neurite outgrowth along the RGDGS paths [361]. Similarly, IKVAV peptide, bound to a hydrogel via streptavidin-biotin mechanism, encouraged selective adhesion of primary hippocampal neurons with neurons

sprouting neurites along the functionalized route and developing functional synapses[362]. In addition to adjusting the substrate surface to promote neural health, gradients of the extracellular matrix protein laminin have been immobilized on surfaces to directing neurite growth up the concentration gradient [363]. These surface functionalization techniques provide promising outlook for the implementation of nerve regeneration materials that not only can improve neuron interaction with the device, but can functionally guide neurons to the correct target.

4.2.5 EDC-NHS linking

One convenient method for attaching different biomolecules to a surface is through the use of carbodiimide crosslinking. Here the carbodiimide group 1-ethyl-3-(3-dimethylaminopropyl) carbodiimide hydrochloride (EDC) serves to link primary amine ($-NH_2$) groups present on many biomolecules, to a carboxylic acid group ($-COOH$) on the substrate surface[364]. The carbodiimide reacts with the surface bound $-COOH$ to form an O-acylisourea, which is easily displaced by the primary amine resulting in an amide bond. This O-acylisourea intermediate is however not stable, so the addition of N-hydroxysuccinimide (NHS) has been added to the linking step. The NHS group reacts with the O-acylisourea to form a more stable ester that still allows the anchoring of primary amines. This technique has been used to attach many bioactive molecules including proteins[365, 366], peptides (IKVAV, RGD, or YIGSR)[367, 368], active enzymes[369], and aptamers[370] to name a few. Here we utilize the CP coating PEDOT/GO on Mg to provide the $-COOH$ groups that can be utilized for EDC-NHS chemistry. The $-COOH$ groups are present on the surface of the PEDOT/GO film due to the edges of the GO sheets being exposed at the surface[103]. EDC-NHS chemistry can then be conducted linking the $-COOH$ on the surface to primary amines of different bioactive molecules.

Here we report on the exploration of different functional groups attached to PEDOT/GO on Mg through EDC-NHS that may be used in the future to improve implant performance. PEG functionalization of the PEDOT/GO film showed significant decrease in the number of fibroblast cells and E. coli bacteria attached. Functionalization of the PEDOT/GO surface with Nerve Growth Factor (NGF) promoted neurite outgrowth from PC12 cells. Additionally, the immobilization of a novel super oxide dismutase mimic (iSODm) showed the ability of the functionalized surface to decrease the presence of harmful super-oxide reactive oxygen species and suppress inflammation. The iSODm surface also caused an increase in mortality of E. Coli on the surface. These results show that the PEDOT/GO coating on Mg can provide a variety of surface cues to guide implant specific tissue responses.

4.3 MATERIALS AND METHODS

4.3.1 Materials

Single layer graphene oxide sheets were purchased from Cheap Tubes (Cambridgeport, VT). 200 proof ethanol was purchased from Decon Labs Inc. (King of Prussia, PA). Magnesium ribbon $\geq 99.5\%$ (3 mm wide x 0.2 mm thick), 3,4-Ethylenedioxythiophene (EDOT) monomer, xanthine, xanthine oxidase from bovine milk, catalase from bovine liver, cytochrome C from equine heart, N-(3-Dimethylaminopropyl)-N'-ethylcarbodiimide hydro-chloride, N-Hydroxysuccinimide, and albumin-fluorescein isothiocyanate conjugate were purchased from Sigma-Aldrich. Amine functionalized poly ethylene glycol (2000 molecular weight) with a hydroxyl terminal was purchased from JenKem Technologies (Beijing, China). Kwiksil silicone

elastomer was purchased from World Precision Instruments(Sarasota, FL). PBS 10x concentrate (136 mM NaCl, 2.7 mM Potassium chloride, 10 mM Phosphate Buffer) was purchased from EMD Millipore (Billerica, MA) and diluted using de-ionized water from a Millipore Milli-Q system. BacLight bacterial Live/Dead stain, Live/Dead Viability/Cytotoxicity for mammalian cells stain, yeast extract, tryptone, and sodium chloride were purchased from Fisher Scientific. NIH-3T3 fibroblasts (CRL-1658), Dulbecco's Modified Eagle's Medium (30-2002), Bovine calf serum, PC12 cells (CRL-1721), RPMI-1640 Medium (30-2001), heat- inactivated horse serum, fetal bovine serum, *Escherichia coli* (11775) were purchased from ATCC (Manassas, VA). iSODm was custom synthesized in our lab by Dr. Noah Snyder[371].

4.3.2 Polymerization of PEDOT/GO film

GO was added to ethanol at a concentration of 10 mg/ml and the resulting solution was sonicated for 30 minutes in a bath sonicator FS110H (Fisher Scientific). Following sonication, 20 μ l/ml EDOT and 35 μ l/ml deionized water were added into the GO ethanol solution to create the polymerization solution. The Mg ribbon was cut into 2 cm long strips, rinsed with ethanol, and blotted dry. Polymerizations, and all electrochemical measurements, were conducted on a Gamry Potentiostat FAS2/Femtostat using Gamry Framework Software (Warminster, PA). Polymerization consisted of a two-electrode system with Mg ribbon working electrode and a gold counter/reference electrode. Polymerization was conducted in 300 μ l of fresh polymerization solution and a potential of 0.6 V vs. counter was applied until a charge of 10 mC was reached. Coated length was 9 mm. Following polymerization, electrodes were gently dipped in ethanol then dried at -20°C for two days, followed by drying at 3°C for one day.

Following this drying process, the PEDOT/GO forms a thin adherent black film on the Mg ribbon. Samples were stored at ambient temperature following drying process.

4.3.3 EDC-NHS functionalization

EDC-NHS functionalization was conducted in a 50% ethanol solution with 0.1 M EDC and 0.1 M NHS. Functionalization was carried out for 15 minutes followed by an ethanol rinse and a brief air dry. The samples were then exposed to the moiety desired for attachment for another 15 minutes. For albumin-fluorescein isocyanate conjugate, 20 $\mu\text{g/ml}$ in DiH_2O was exposed to the surface, followed by a rinse with DiH_2O . NGF functionalized samples were exposed to 20 $\mu\text{g/ml}$ NGF.

iSODm and PEG were functionalized in one step where the EDC-NHS solution also contained the moiety for attachment for a total of 30 minutes. Amine functionalized PEG was added to the EDC-NHS solution at 40 $\mu\text{g/ml}$. iSODm was added to the EDC-NHS solution at 0.8 mg/ml . Following functionalization, samples were rinsed with ethanol and air dried.

4.3.4 NIH-3T3 fibroblast

NIH-3T3 cells were cultured in Dulbecco's Modified Eagle's Media supplemented with 10% bovine calf serum. Cells were maintained in 75 cm^2 culture flasks and passaged at ~80% confluence.

PEDOT/GO on Mg samples were functionalized with PEG as described in section 4.3.3. Non-functionalized PEDOT/GO on Mg was used as the control. 2 cm long Mg strips coated 9 mm with PEDOT/GO, either PEG functionalized or non-functionalized, were cut to a total length

of 10mm resulting in 9mm of PEDOT/GO coating with 1mm of exposed Mg for handling. Mg samples were individually placed into 24 well plates. The samples were affixed to the base of the plate using Kwiksil silicone ensuring to completely cover the 1mm exposed section.

10 μ l culture media containing 10,000 cells were placed on the samples and allowed to sit for 15 minutes. Following this 1.5 ml of culture media was added to the well. Cells were cultured for 24 hr and then stained with live dead staining.

4.3.5 Live dead stain

Mg samples were removed from the well plate and placed in to the staining solution of 2 μ M calceinAM and 2 μ M ethidium homodimer-1 in PBS and incubated for 10 min. After incubation, images at 10x were taken on a Zeiss Axioskop 2 Mat Fluorescent microscope. Cells were counted manually using ImageJ and 'Cell Counter' add-on by Kurt De Vos.

4.3.6 PC12 cell culture

PC12 cells were cultured in ATCC RPMI-1640 media supplemented with 10% heat inactivated horse serum and 5% fetal bovine serum. Prior to plating on samples for analysis of neurite extension, PC12 cells were cultured in the flask for two days with 10ng/ml NGF added to the media. This serves to prep the cells prior to plating on the samples so that the response to NGF can be expedited. PEDOT/GO on Mg was functionalized with NGF as described in section 4.3.3. Samples were then cut, resulting in 1 cm long samples with 9 mm PEDOT/GO coated and 1 mm uncoated. The samples were affixed to the bottom of a 24 well plate using Kwiksil silicone ensuring to cover completely the small uncoated portion. Control cells were plated on

collagen IV coated 24 well plates. Throughout the 4 day experiment, samples were then either stained with live dead stain 4.3.5 or fixed for SEM 4.3.7.

4.3.7 Cell Fixation for SEM

PC12 cells cultured on PEDOT/GO Mg substrates with and without EDC-NHS functionalization of NGF were fixed in 4% paraformaldehyde for 30 minutes. Following fixation cells were rinsed with ethanol three times allowing each rinsing solution to sit for 10 minutes. Ethanol was removed and the samples were allowed to air dry overnight. Samples were placed in a desiccator for 12 hours followed by a vacuum desiccator for 12 hours prior to SEM imaging. The cells were sputtered with 3 nm gold prior to imaging and were imaged using JEOL JSM 6330F.

4.3.8 Cytochrome C assay

Reaction solution consisted of 1 mg/ml cytochrome C, 0.5 mg/ml Catalase, 0.05 mg/ml xanthine, and 0.05 mg/ml xanthine oxidase. Control solution was the reaction solution without xanthine oxidase. Solutions were placed in a 96 well plate and monitored using Spectromax i3x at the characteristic absorbance of ferrocytochrome C 550nm. After ~5 min, when the control solution absorbance had plateaued, PEDOT/GO coated Mg samples, with and without iSODm functionalization, were placed in the well. Every 5 min for the next 20 min samples were removed from the wells and absorbance was tested.

4.3.9 Bacteria culture

Lysogeny Broth consisted of 10 g tryptone, 5 g yeast extract, and 10 g NaCl in 950 mL deionized water and was autoclaved prior to use. *E. coli* bacteria powder was placed into ~9 ml of Lysogeny Broth and cultured in a Forma Orbital Shaker incubator overnight. *E. coli* were diluted to reach an optical density of 0.8 at 600nm, assessed on Spectromax i3x. They were then plated on PEDOT/GO Mg samples with and without iSODm functionalization that had been affixed to the base of a 24 well plate as described in section 4.3.4 in 300 μ l total volume. Following a 12 hour static settlement, samples were stained with Live/Dead BacLight stain by removing 50% of the culture media in the wells and replacing it with the staining solution as per the manufacturer's instructions (6 μ M SYTO 9 stain and 30 μ M propidium iodide in PBS). Following 15 min incubation, the media was removed and rinsed three times with PBS. Mg samples were then removed from the well plate and dipped three times in PBS to remove any loosely adhered cells. Excess PBS was then wicked away with kimwipe. Imaging was conducted immediately using a Leica DMI 4000 B inverted fluorescent microscope. Cells were counted manually using ImageJ and 'Cell Counter' add-on by Kurt De Vos.

4.4 RESULTS

4.4.1 Albumin-Fluorescein

To demonstrate the ability of EDC-NHS chemistry to covalently attach components with amine functional groups, albumin-fluorescein complex was tested. Here the albumin has amine groups

on the N-terminus of the peptide chains as well as on amino acids lysine, asparagine, and glutamine. As can be seen in Fig. 4-1 below, the PEDOT/GO sample without EDC-NHS treatment has only areas where large aggregates of protein adsorbed to the surface. The sample that treated with EDC-NHS prior to protein exposure is completely covered in the green fluorescent glow due to the attached albumin. This suggests that the EDC-NHS functionalization covalently attached the amine groups of the albumin to the exposed carboxylic acid groups of GO sheets protruding from the polymer surface.

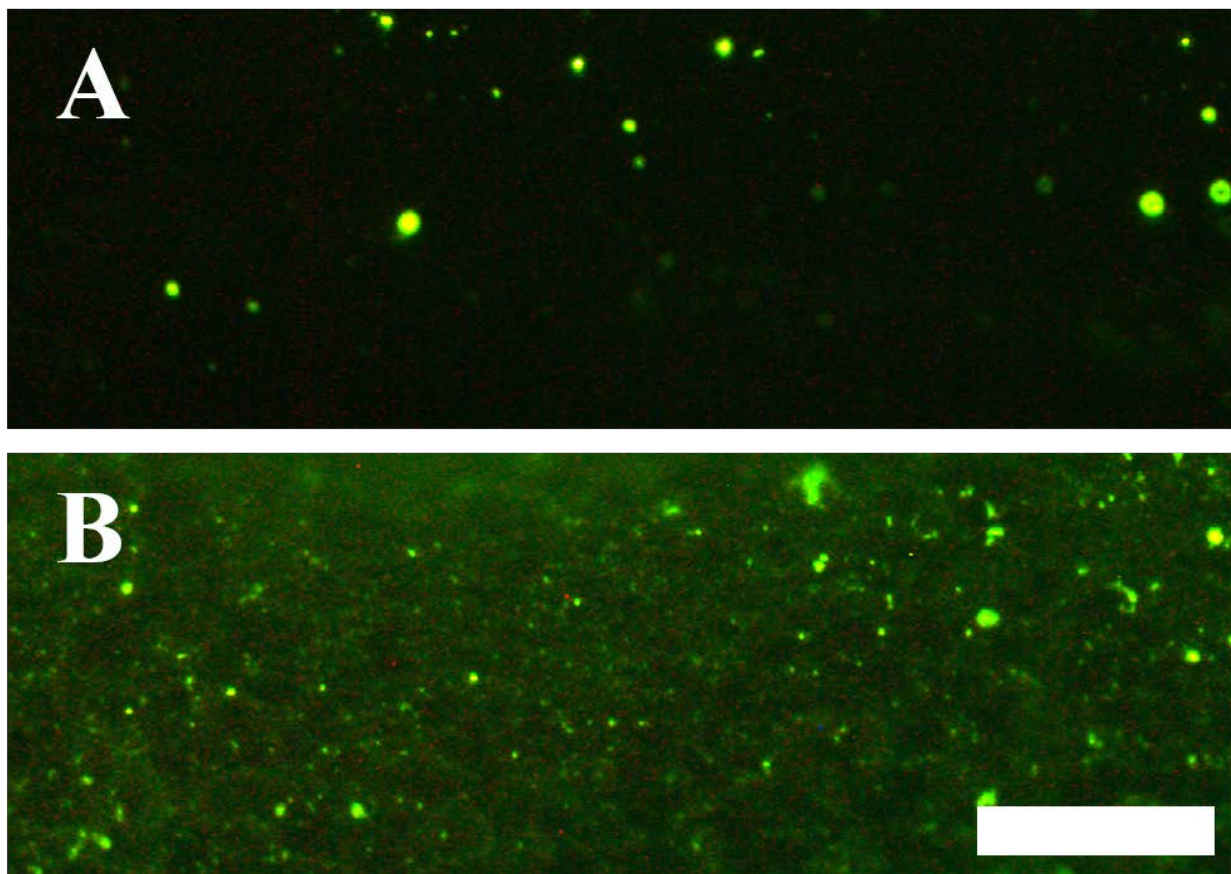


Figure 4-1: Albumin-Fluorescein surface attachment. (A) PEDOT/GO on Mg that did not have EDC-NHS treatment prior to exposure to Albumin tagged with fluorescein. (B) PEDOT/GO on Mg that did have EDC-NHS treatment prior to exposure to Albumin tagged with fluorescein. Scale bar 20 μm

4.4.2 NIH 3T3 Fibroblast attachment

To test the ability of PEG functionalized PEDOT/GO to prevent cell attachment, the adhesion of Fibroblast cells was tested. Fibroblasts plated on PEG functionalized PEDOT/GO Mg samples showed an 81% decrease in the number of attached cells. Additionally those cells that did attach showed less extending of processes indicating that the PEG functionalized surface was not conducive to cell attachment and spreading.

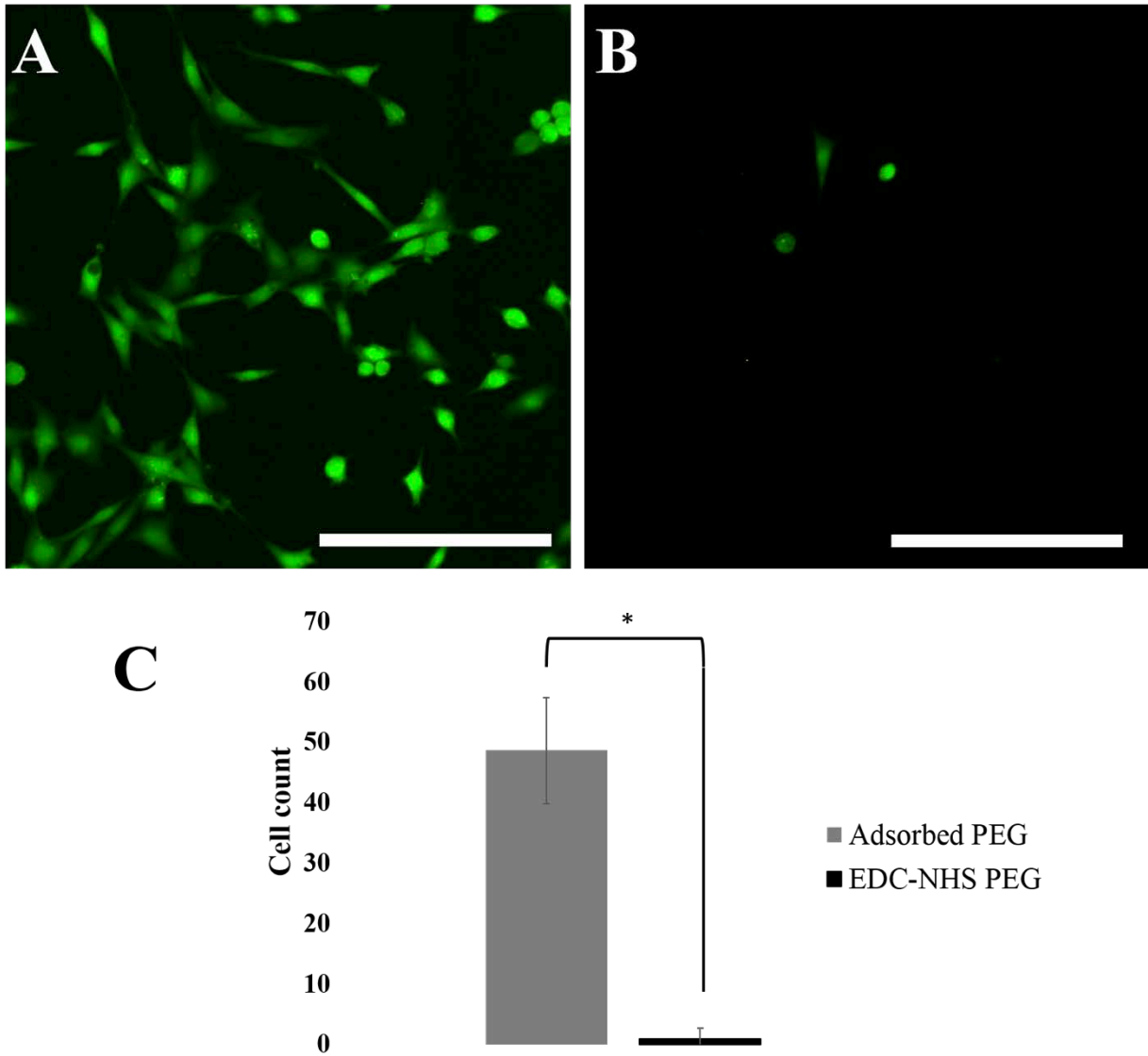


Figure 4-2: NIH 3T3 on PEG surface. (A) 10x image showing fibroblasts attached to adsorbed PEG PEDOT/GO Mg samples stained with calcein AM (B) 10x image showing fibroblasts attached to EDC-NHS attached PEG PEDOT/GO Mg samples (C) Counting of cells on PEG adsorbed and PEG functionalized samples. Scale bar 250 μm (* $p < 0.05$)

4.4.3 PC12 cell attachment and neurite sprouting

Representative images illustrating the neurite sprouting from PC12 cells on collagen IV with and without NGF supplemented culture media can be seen in Fig. 4-3. Without NGF exposure, the PC12 cells exhibited very little spreading and process extension (Fig. 4-3). In contrast, PC12 cells with NGF supplemented media displayed increased spreading, neurite sprouting, and increased neurite length. NGF also increased the number of cells extending multiple processes (Fig. 4-3 B).

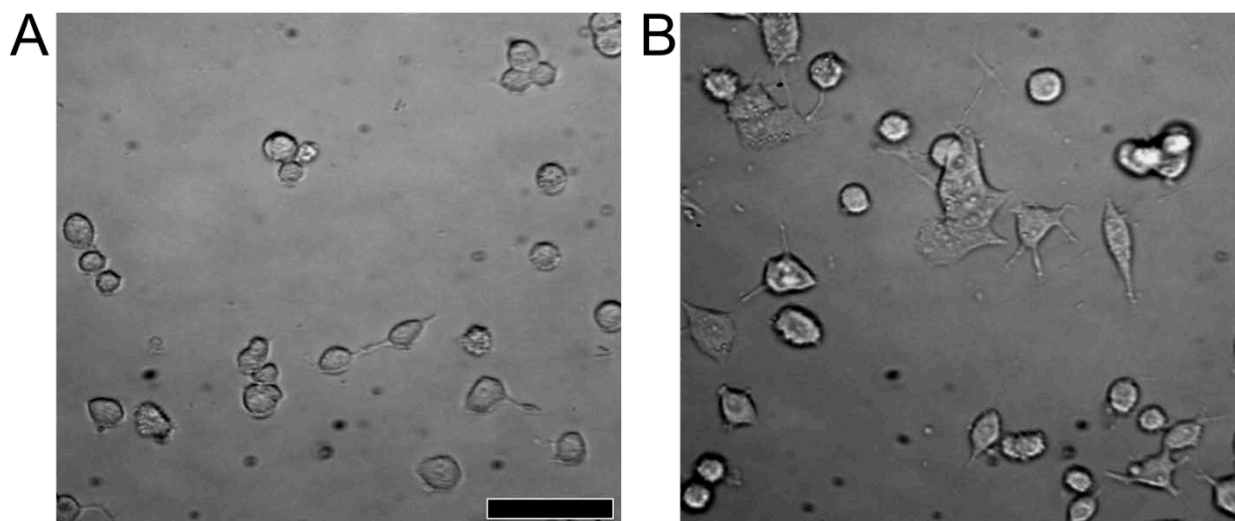


Figure 4-3: PC12 control culture. Images of PC12 cells culture on collagen IV coated wells (A) without NGF in the culture media, and (B) with the addition of 10 ng/ml NGF in the culture media after 3 days in culture. Scale bare = 50 μ m

To investigate the ability of surface cues immobilized on PEDOT/GO to drive cell specific behavior, NGF was attached to the PEDOT/GO through the EDC-NHS protocol. PC12 cells cultured on NGF functionalized PEDOT/GO substrates showed sprouting of processes

indicative of their response to the surface immobilized NGF. Over the course of 4 days PC12 cells showed increasing process outgrowth as can be seen in Fig. 4-3. Cells on NFG functionalized PEDOT/GO imaged at 1 day (4-3 A) showed no process sprouting while at 2 days (4-3 C) processes can be seen and at 4 days (4-3 E and F) multiple processes and processes of increasing length can be observed. Cells on non-functionalized PEDOT/GO did not show evidence of neurite sprouting (Fig 4-3 B, D, and G).

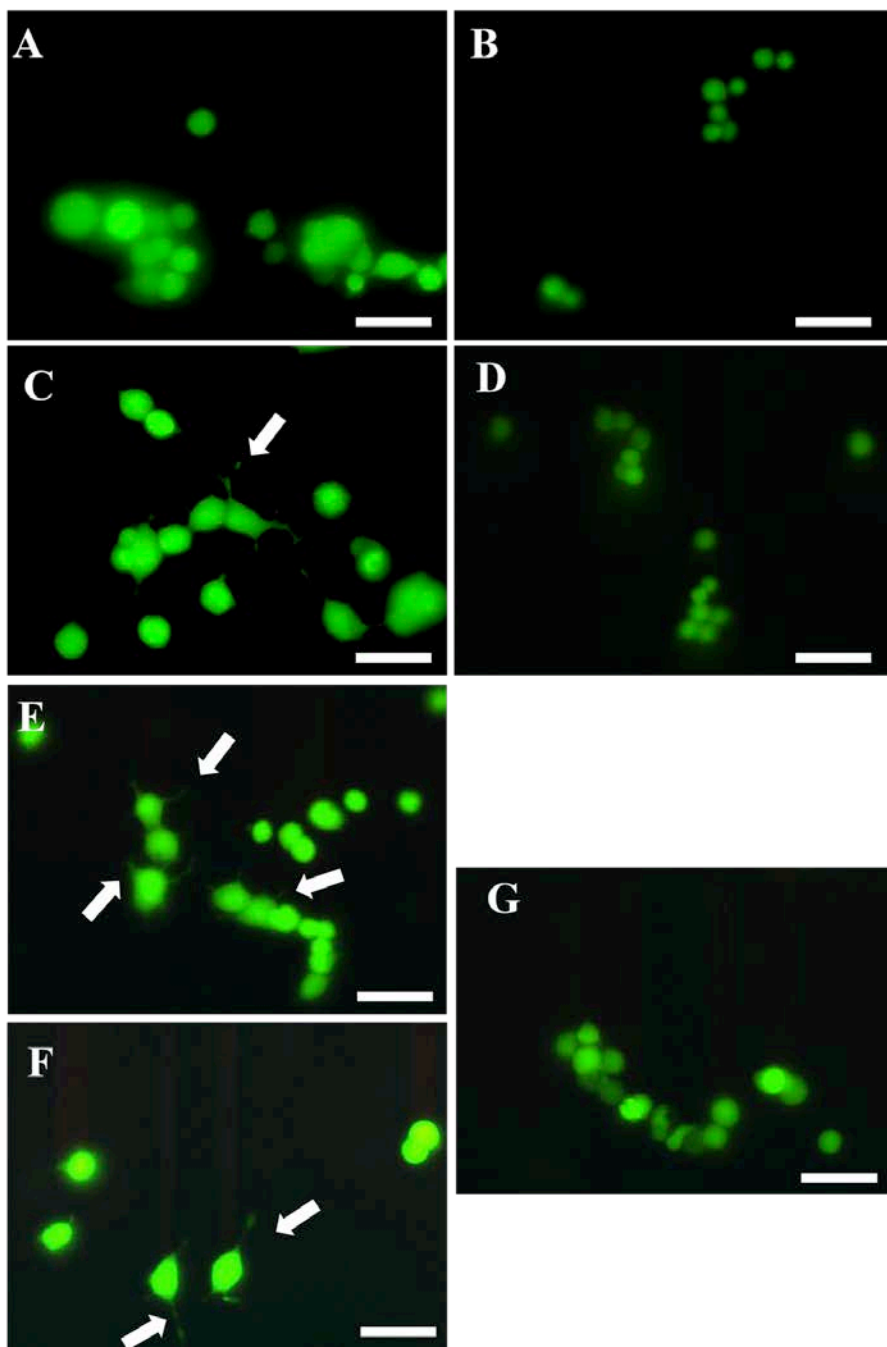


Figure 4-4: PC12 Cell culture. PC12 cells cultured on NGF functionalized and adsorbed PEDOT/GO Mg samples over the course of 4 days imaged with calcein AM stain. (A) Cells imaged after 1 day in culture on NGF functionalized samples. (B) Cells imaged after 1 day in culture on NGF adsorbed samples. (C) Cells imaged after 2 days in culture on NGF functionalized samples. (D) Cells imaged after 2 days in culture on NGF adsorbed samples. (E & F) Cells imaged after 4 days in culture on NGF functionalized samples, and (G) samples cells imaged after 4 days in culture on NGF adsorbed samples. Scale bar 50 μ m

SEM imaging was used to more closely observe the PC12 cell morphology and neurite sprouting on the surface of NGF functionalized and NGF adsorbed PEDOT/GO surfaces. Images of the PC12 cells on NGF functionalized substrates can be seen in Fig. 4-5 (A, C, and E). In Fig. 4-5 A, a larger cluster of PC12 cells on an NGF functionalized surface exhibit increased spreading as well as increased neurite sprouting compared to the cluster of cells on the NGF adsorbed surface (4-5 B) which are more rounded with less spreading and less neurite sprouting. This lack of neurite sprouting and more rounded morphology is again seen on the NGF adsorbed surface in Fig. 4-5 D. Figure 4-5 C and E show additional examples of neurite sprouting on the NGF functionalized surface. In 4-5 C, it can be seen that the cell in the lower portion of the image is extending a neurite upward while several smaller neuritis are extending downward. In 4-5 E, the remains of a larger neurite process can be seen. While a cell fixation method has been developed to preserve cell structure under the high vacuum of the SEM, these protocols involve extended duration soaking in a variety of media. To prevent excessive corrosion of the samples during the fixation, the procedure was expedited which may have resulted in destabilization of the cells on the surface of the substrate causing some cells to be removed from the surface. This is likely the reason that only portions of neurites can be found on the surface in Fig. 4-5 E.

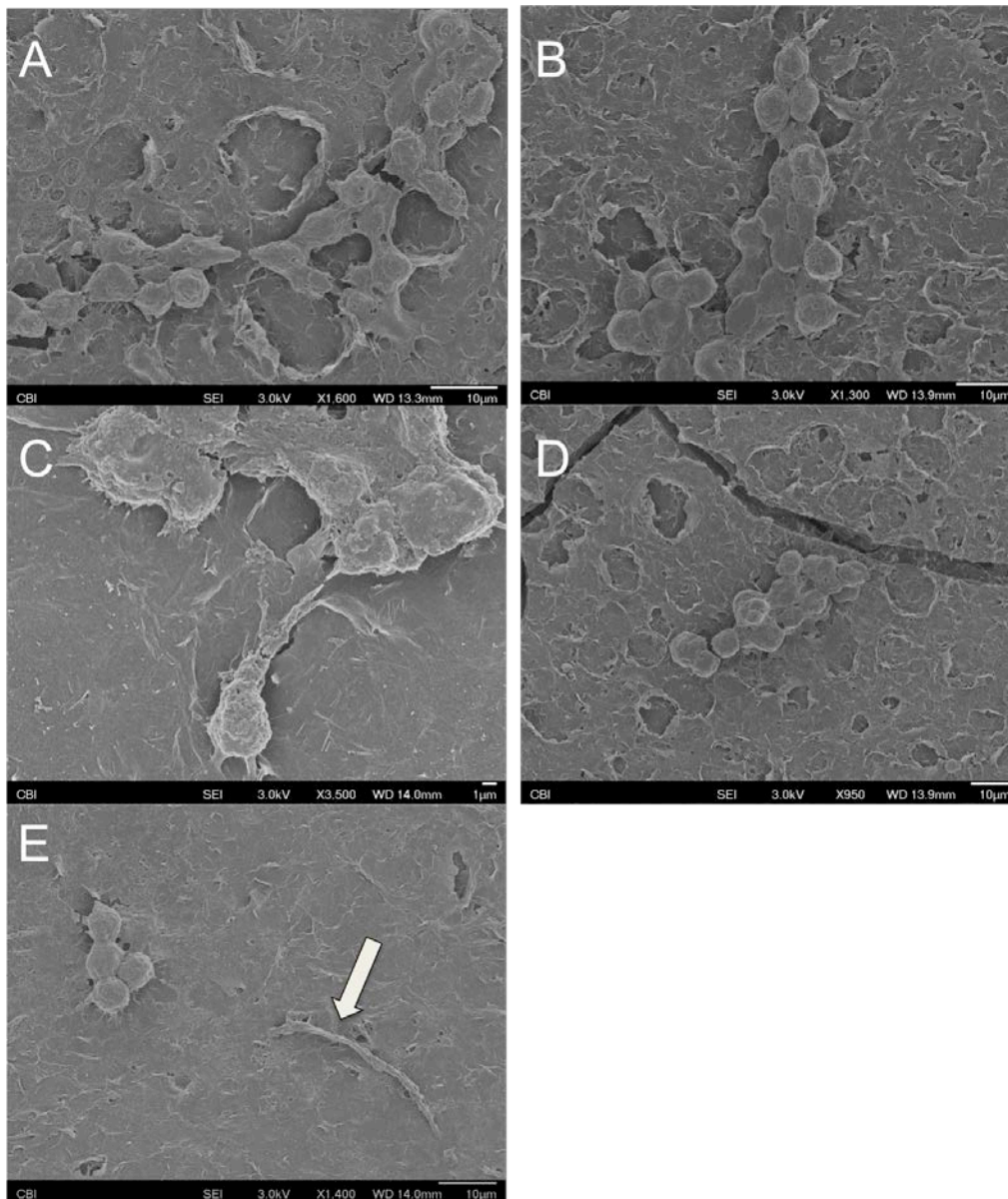


Figure 4-5: PC12 SEM. SEM images of PC12 cells cultured on EDC-NHS functionalized or adsorbed PEDOT/GO substrates for 3 days. (A) Cluster of cells on NGF surface showing increased cell spreading and increased neurite sprouting. (B) Cluster of cells on adsorbed surface where cells are more rounded indicating less spreading and display less neurite sprouting. (C) Image on NGF surface showing neurite sprouting between cells. (D) Cells on NGF adsorbed surface showing less neurite sprouting. (E) A larger neurite remaining on the NGF-functionalized surface. In this case, the cell body was likely removed during the expedited drying process that was used to minimize corrosion during fixation and drying.

4.4.4 Cytochrome C Assay

Testing the activity of PEDOT/GO functionalized with iSODm requires the generation of superoxide as well as its quantification which is difficult due to superoxide's short half-life and reactivity[372]. The reaction of xanthine with xanthine oxidase results in the production of superoxide which can be quantified as the superoxide reduces cytochrome c to ferrocytochrome c which has a characteristic absorbance at 550 nm[373]. As a result of iSODm immobilized on the surface of the PEDOT/GO Mg samples, the amount of cytochrome C that was reduced decreased when a PEDOT/GO/iSODm sample was placed in the superoxide generating and cytochrome C containing solution. This can be seen in Fig. 4-3 where the absorbance recorded when iSODm functionalized samples were placed is significantly lower than both those solutions that had no sample as well as those solutions that had non functionalized PEDOT/GO Mg. After just 5 minutes of the iSODm functionalized sample being immersed in the superoxide generating solution, the amount of superoxide that had been generated decreased 55.5%. Over the course of the experiment the iSODm functionalized PEDOT/GO samples showed a 72% decrease in the amount of super-oxide generated compared to non-functionalized PEDOT/GO. Linear regression of the data in Fig. 4-4 revealed a 12 fold decrease in the rate of cytochrome C reduction by super-oxide. This suggests that the iSODm functionalized surface intervened by converting superoxide to less reactive groups.

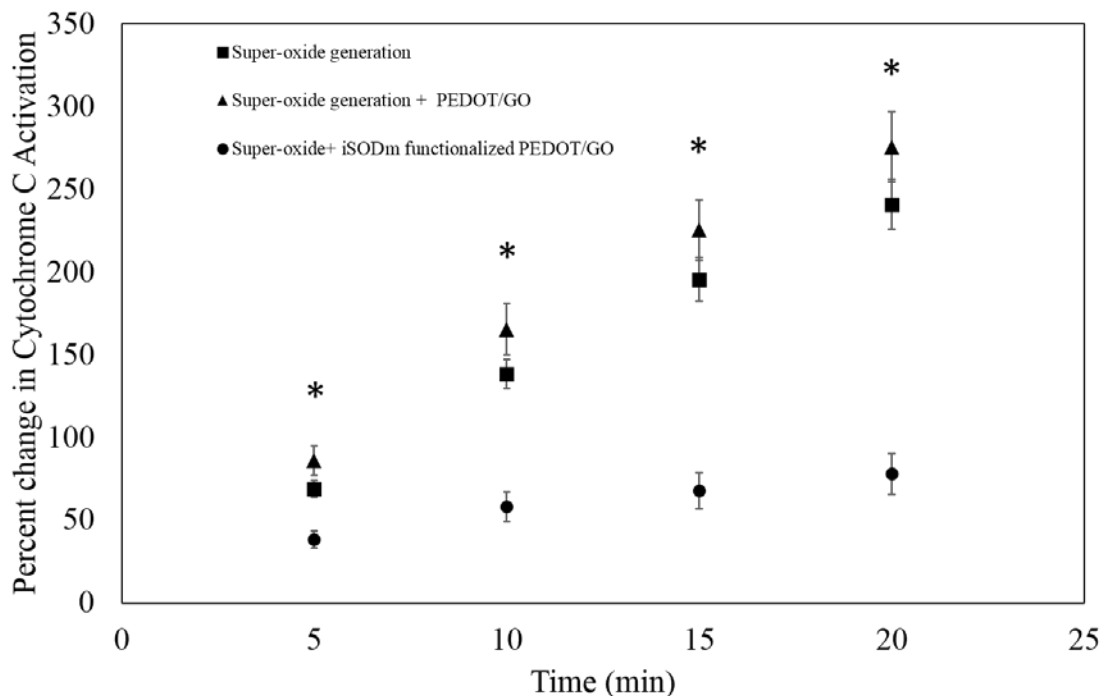


Figure 4-6: Cytochrome C Assay. Percent change in absorbance of Cytochrome C, catalase, xanthine, xanthine oxidase solutions over time. PEDOT/GO Mg samples with and without iSODm functionalization were soaked in the solution and removed for each absorbance measurement then returned to the solution. (* $p < 0.05$)

4.4.5 Bacteria Culture

E. coli attachment and viability on PEG and iSODm functionalized PEDOT/GO substrates were compared to non-functionalized coatings after 12 hour incubation period. PEG functionalized surfaces showed a significant 54% decrease in cell attachment. Despite reducing cell attachment, the PEG functionalized surfaces did not show a significant decrease in the viability of the attached cells (Fig. 4-5B). iSODm functionalized surfaces also showed a significant 46% decrease in the number of *E. coli* attached after 12 hours. iSODm functional surfaces also showed an 8.5% decrease in the viability of those cells that did attach. This toxicity is likely

derived from the amine functional groups added to the iSODm which can disrupt the membranes of bacteria[374].

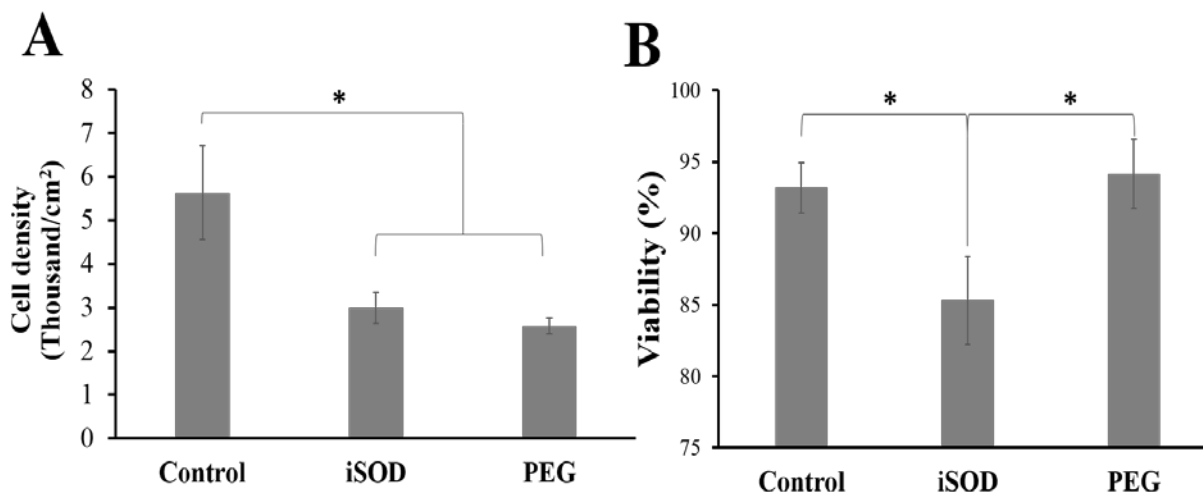


Figure 4-7: E coli attachment and viability. (A) Total cell count of adhered bacteria to PEDOT/GO functionalized Mg. (B) viability of the attached cells. (* p <0.05)

4.5 DISCUSSION

Surface functionalization provides the ability to tailor the PEDOT/GO coating to fit a variety of needs which could be useful for improving Mg implant performance including; anti-bacterial, anti-inflammatory, and promoting tissue specific responses from the cells local to the implant surface. To functionalize the surface of the PEDOT/GO coating, EDC-NHS chemistry was used covalently linking primary amines of the functionalizing molecule to the carboxylic acid groups of the exposed GO sheets exposed at the surface of the PEDOT/GO film[103].

EDC-NHS linking chemistry normally takes place in an aqueous solution, often at physiological or acidic pH[375, 376]. While the PEDOT/GO coating can act as initial barrier minimize corrosion upon immersion into phosphate buffers at physiological pH, the protection is less in acidic media due to the ionizing power driving rapid corrosion. To minimize the effect of the EDC-NHS chemistry on the coated Mg sample, alternate solvents were investigated. Replacing the aqueous media while resulting in decreased corrosion may also result in a decrease in the rate of hydrolysis of the EDC[377]. This would consequently reduce the surface functionalization rate. Nam *et al* showed that EDC-NHS crosslinking chemistry occurred optimally in a water and ethanol co-solvents with a mole ration of 0.12:1(ethanol:water) [377]. Various concentrations from 100% ethanol to the reported optimal ratio reported by Nam et al were investigated. Functionalization occurred effectively when using 1:1 (ethanol:water), which could be a result of the high EDC-NHS concentrations compensating somewhat for the slower reaction speed.

The EDC-NHS covalent attachment method was confirmed through the attachment of fluorescently tagged albumin proteins. Proteins have multiple primary amines located at the N-terminus of each poly peptide chain as well as on amino acids lysine, asparagine, and glutamine, which can participate in the covalent linkage. These amines facilitate attachment to the –COOH of the GO edges exposed at the surface of the PEDOT/GO film[103]. Effective attachment of these fluorescently tagged proteins suggests that the EDC-NHS reaction in 50% ethanol was sufficient to drive the surface functionalization of the PEDOT/GO films and facilitate covalent attachment of amine containing molecules.

EDC-NHS chemistry was also used to attach of an amine functionalized PEG. PEG is a versatile molecule in that it has been shown to decrease attachment of bacteria and fungi in

addition to being antithrombogenic[168, 378, 379]. The PEG functionalized surface was tested for its ability to prevent both bacteria and mammalian cells from attaching.

E coli bacteria adhesion was tested to determine if PEG functionalized PEDOT/GO had the ability to decrease bacterial attachment. Low bacterial attachment is an important factor for medical implants as bacterial growth on the implant and subsequent patient infection can often require the premature removal of the device. Previously PEG functionalized surfaces have been shown to prevent bacterial attachment[323, 378]. PEG functionalized PEDOT/GO surfaces showed a significant 47% decrease in the attachment of *E coli* (Fig. 4-5). While significant, this decrease is not as dramatic as previously reported 80% decrease in bacterial adhesion following PEG functionalization [378] , these data suggest the PEG functionalized PEDOT/GO coating may be an effective method to minimize bacterial infection risk of Mg implants.

Attachment of PEG to the surface is reliant on exposed edges of GO protruding from the PEDOT/GO surface. As shown in Fig. 2-2 C and 3-1 C, the edges of the GO sheets protrude from the surface of the PEDOT leaving exposed areas of PEDOT between the protruding sheets. In these PEDOT areas without exposed GO, there would be no PEG functionalization. The small size of *e coli* (~0.5 μm diameter and ~ 2 μm length) could allow for their attachment in these exposed PEDOT locations resulting in an increase in attachment when compared to literature values for the decrease in bacterial attachment afforded by PEG coatings.

In addition to bacterial adhesion, PEG functionalized PEDOT/GO films were tested for their ability to prevent attachment of fibroblasts. Fibroblasts play an important role in the wound healing process and contribute to the fibrous tissue encapsulation that is synonymous with the FBR[380]. By preventing fibroblast attachment to the surface of the implant, the amount of fibrous tissue that forms around the implant could potentially be decreased. PEG functionalized

surfaces showed a significant decrease in the number of fibroblasts adhered to the surface following 24 hr incubation as indicated by Live/Dead staining in Fig. 4-2. This prevention of cell attachment is likely due to multiple factors. Firstly, PEG results in the surface being more hydrophilic. Hydrophilic surfaces decrease protein attachment through the formation of an interfacial layer of water molecules that are tightly bound to the surface[381], and non-specific protein adhesion, from the culture media in this case, is the initial necessary step for cell attachment. In addition to the prevention of protein adsorption and binding, the mobility of PEG chains around a single bonding point as well as the absence of ionic interactions with incoming cells may also prevent cellular attachment[379].

The more complete prevention of fibroblast attachment compared to *E. coli* attachment could be due to the distribution of GO, and consequently functional groups, on the surface of the PEDOT/GO film. The size of fibroblasts are reported at $\sim 15 \mu\text{m}$ [382] while *e coli* have a diameter of $\sim 0.5 \mu\text{m}$ and length of $\sim 2 \mu\text{m}$. This smaller size could allow the *e coli* to infiltrate the PEG surface while the larger size of the fibroblasts may result in the level of PEG functionalization being sufficient to prevent attachment.

While preventing the attachment of bacteria and certain cells is important for implants, attachment and guidance of other cell types could improve tissue interaction with the implant. PEDOT/GO surfaces functionalized with NGF were evaluated for their ability to guide PC12 cell neurite sprouting. PC12 cells are rat pheochromocytoma cells which closely resemble neurons and have a broad set of past research in use as a neuron model for studying the exocytosis of neural signaling[383]. PC12 cells also have a characteristic response to NGF exposure in that they sprout neurites and begin forming synapses with one another and can even develop neural networks[384-387]. Immobilization of NGF on other substrates has been shown to promote

neurite outgrowth and gradients of NGF can even guide neurite direction[388-390]. Following EDC-NHS functionalization of PEDOT/GO Mg with NGF, PC12 cells showed neurite sprouting and growth over four days(Fig. 4-4). After 24 hours minimal neurite sprouting was visible, following 48 hours, neurites could be seen sprouting from the cells, and after 4 days, cells showed multiple neurites sprouting as well as increased neurite length (Fig. 4-4). SEM images also revealed increased cell spreading and neurite extension on NGF functionalized samples (Fig. 4-5). These results indicate that the functionalization of PEDOT/GO can be used guide the behavior of specific cells, and could be used for other biologics.

The immobilization of a novel anti-inflammatory component iSODm (MnIII TEA-2-Pyp5+(manganese(III)-5,10,15,20-tetrakis(N-(2-aminoethyl)pyridinium-2-yl)porphyrin)), developed in our lab, was also tested. This molecule consists of a metalloporphyrin core that facilitates the catalytic reduction and oxidation of the superoxide to less harmful molecular oxygen and H₂O₂. It accomplishes this by having a redox potential of ($E_{1/2} = 230$ mV vs. NHE) which lies roughly halfway between the oxidation (-160 mV) and reduction (890 mV) of superoxide. Additionally, four amine functional groups were added to the periphery which did not show an effect on the catalysis of superoxide to less harmful components[371]. These added amines allow iSODm to be immobilized on to the surface through EDC-NHS chemistry. Reactive oxygen species (ROI), like superoxide, have been implicated in the foreign body response as being released by macrophages and foreign body giant cells in their “frustrated phagocytosis” phase as they try to degrade the implant[391]. High concentrations of ROS cause inflammation and cell death, iSODm serves to eliminate the harmful superoxide molecules around the implant through its catalytic reduction and oxidation of superoxide into molecular oxygen and hydrogen peroxide making the environment surrounding the implant more hospitable to healthy tissue.

iSODm activity following immobilization was quantified using xanthine and xanthine oxidase to generate superoxide, and cytochrome C to quantify the amount of superoxide generated. The iSODm on the surface catalyzes the reduction and/or oxidation of superoxide preventing it from reducing the cytochrome C. iSODm functionalized PEDOT/GO samples soaked in the reaction solution showed a 12 fold decrease rate of superoxide generation indicating that the attached iSODm is active on the surface(Fig. 4-6). This iSODm surface treatment could be used to improve the environment around implanted Mg devices by decreasing the concentration of superoxide local to the implant, which could allow healthy tissue to more easily interact with the implant.

iSODm functionalized surfaces also resulted in a decrease in the viability of *E. coli* plated on the surface (Fig. 4-7). This is likely due to the presence of multiple amine terminated functional groups on the iSODm. While some of these amine functional groups are utilized for the covalent attachment to the PEDOT/GO surface, it is expected that others would be free to interact with the Bacteria. Cationic antimicrobial agents, like amine, have kill bacteria through adsorption and penetration of the cell wall resulting in membrane disruption and leakage of intracellular material followed by degradation of proteins and nucleic acids[374]. Here it is likely that the exposed amine groups of the iSODm serve to kill the bacteria that have adhered to the surface through this membrane disruption mechanism. This antimicrobial property could be useful for minimizing bacterial colonization of implanted medical devices. These data suggest that iSODm surface functionalization has the potential to both decrease bacterial adhesion to the implant surface as well as continually improve the environment around the implant by mitigating superoxide to better facilitate the interaction of healthy tissue with the implant.

4.6 CONCLUSION

Biological proteins, synthetic polymer, and small molecule compounds have all been successfully immobilized on the PEDOT/GO surface via a modified EDC-NHS chemistry. PEG functionalized surfaces showed a decrease in the attachment of fibroblasts, which contribute to fibrous tissue encapsulation around implants. NGF functionalized surfaces supported the sprouting of neurites from PC12 cells. iSODm functionalized PEDOT/GO decreased superoxide concentrations and decreased the viability of attached bacteria. These results demonstrate that the PEDOT/GO coating is a versatile platform for surface immobilization, which could guide tissue. Future work in designing applications with specific functionalization goals could use this study to guide their efforts.

5.0 CONCLUSION

5.1 SUMMARY OF RESULTS

This dissertation describes the development of a conducting polymer graphene oxide (GO) composite coating on magnesium and the investigation of this coating's ability to delay corrosion, add drug releasing properties, and provide surface functionalization for magnesium implants. In *Chapter 2* the conducting polymer poly 3,4-ethylene dioxythiophene (PEDOT) was electropolymerized on Mg in the presence of GO resulting in a PEDOT/GO composite film. Electropolymerization was conducted in an ethanol based solution that minimizes the corrosion of the underlying Mg. The resulting PEDOT/GO film displayed uniform coverage of the Mg substrate as well as a rough surface morphology resulting from the GO sheets at the surface of the film. Tafel scans of the PEDOT/GO coated Mg displayed decreased corrosion current and a noble shift in the corrosion potential when compared to untreated Mg, both indicating the PEDOT/GO coating improved corrosion resistance. During long term corrosion analysis, the PEDOT/GO coated Mg exhibited decreased production of three Mg corrosion byproducts, Mg^{2+} , OH^- , and H_2 . In addition to assessing corrosion byproducts, electrochemical analysis investigated the electrode electrolyte interface at the surface of the Mg. PEDOT/GO coated samples showed an increased resistance to corrosion throughout the long term corrosion experiment indicated by both electrochemical impedance spectroscopy (EIS) data as well as

equivalent circuit analysis. Scanning electron microscope analysis post corrosion revealed a distinct morphology difference between uncoated Mg and Mg exposed beneath PEDOT/GO coatings. Uncoated Mg displayed an amorphous morphology post corrosion while areas of Mg exposed beneath the PEDOT/GO coating showed a scale like morphology. Elemental analysis through Energy Dispersive X-ray Spectroscopy indicated the uncoated Mg samples were predominantly covered in a $\text{Mg}(\text{OH})_2$ layer, while a magnesium phosphate layer was formed on the Mg exposed beneath the PEDOT/GO coating. PEDOT/GO corrosion protection is attributed to initially acting as a barrier layer, followed by electrochemical coupling of the PEDOT/GO to Mg corrosion to generate a more protective magnesium phosphate layer. The corrosion protection afforded by the PEDOT/GO also served to improve the neuronal biocompatibility of the Mg. Primary neuron viability was significantly improved for cells exposed to PEDOT/GO Mg corrosion media when compared to culture media exposed to uncoated Mg samples. These results suggest that the PEDOT/GO coating is effective at decreasing Mg corrosion through its barrier properties as well as its redox coupling, and that this protection afforded improved biocompatibility.

In *Chapter 3* the PEDOT/GO coating previously developed was tested for its ability to serve as a drug releasing platform. Anti-inflammatory drug Dexamethasone (Dex) was incorporated into the film during polymerization resulting in a PEDOT/GO/Dex film. This PEDOT/GO/Dex film exhibited similar, albeit less significant than PEDOT/GO alone, abilities to prevent corrosion suggesting that the redox coupling described in *Chapter 2* was maintained but the barrier properties were diminished due to the addition of Dex. The PEDOT/GO/Dex film displayed an ability to release Dex through externally powered reduction of the film. Additionally, Dex release was accomplished through the use of current generated during Mg

corrosion whereby increasing the area of exposed Mg increased the corrosion current and drove increased Dex release. Dex bioactivity following release from PEDOT/GO/Dex films was also confirmed through the quenching of activity of microglia derived cells upon exposure to bacterial lipopolysaccharide. *Chapter 3* describes the use of the PEDOT/GO film as a combination corrosion inhibiting and a smart self-powered drug releasing platform that could be utilized to both control corrosion and affect tissue around Mg implants.

Chapter 4 explored the ability of PEDOT/GO films, developed in *Chapter 2*, to be utilized as a method of adding biofunctional surface cues on to Mg. Here, edges of the GO sheets are exposed at the surface of the PEDOT/GO film, which reveals the carboxylic acid groups of the GO. These carboxyl groups were functionalized using carbodiimide crosslinking chemistry facilitating the addition of components with primary amines forming an amide bond. Functionalization was confirmed through the attachment of fluorescently tagged albumin protein that remained only on the functionalized samples following rinsing. Additionally, amine terminated polyethylene glycol functionalization of PEDOT/GO on Mg decreased the attachment of both *Escherichia coli* bacteria and NIH-3T3 fibroblast cells. Attachment of nerve growth factor to the surface of PEDOT/GO facilitated increased neurite sprouting of PC12 cells suggesting that the functionalization protocol can be utilized for driving specific cellular responses that may improve implant tissue interactions. This work suggests that the PEDOT/GO coating can be a versatile method for adding functional groups on the surface of Mg to better guide tissue regeneration around the implant.

This dissertation explored the ability to utilize a novel PEDOT/GO composite coating for improving Mg performance for implantable devices. The PEDOT/GO coating decreased corrosion through unique electrochemical coupling with the underlying Mg, and improved

biocompatibility of Mg when exposed to primary neurons. Additionally, Dex incorporation into the PEDOT/GO film provided a self-powered drug release mechanism. Lastly, the edges of the GO sheets exposed at the surface of the PEDOT/GO film provided functional groups for the immobilization of bioactive molecules. These results suggest that the PEDOT/GO coating could be a versatile platform for improving corrosion resistance and adding of bioactive cues to Mg for improving performance as an implantable material.

5.2 FUTURE DIRECTIONS

Chapter 2 illustrated a mechanism by which the PEDOT/GO coating could improve Mg corrosion resistance in a phosphate buffered solution. The PEDOT/GO film described was polymerized to a total charge of 10 mC and in a 10 mg/ml GO solution. Future work could investigate the potential of altering both the total charge used during electropolymerization as well as the concentration of GO in the film. Altering the total charge would result in a change in the thickness of the PEDOT/GO film from the current 50 μm and presumably a change in the corrosion protection afforded by the film. Similarly, altering the concentration of GO in the film could not only change the barrier properties of the film, but also result in changes in surface morphology and corrosion protection due to the entrapped GO providing added negative charges which prevent negatively charged ions from reaching the underlying Mg surface. A detailed investigation into the role of polymer thickness and GO concentration and their effects on corrosion resistance would provide a framework for the ability to design of the PEDOT/GO coating to meet the needs of the different Mg implant applications. This improved corrosion rate modulation would allow for the PEDOT/GO coating to be tuned so as to prevent degradation for

the specific duration required for tissue healing. Following the appropriate healing during, the implant could then begin to degrade.

In addition, future work may look towards improving the degradability of the PEDOT/GO coating. While literature suggests conducting polymers are biocompatible and that GO can be degraded *in vivo*, potential issues may arise as pieces of the PEDOT/GO coating delaminate during corrosion of the underlying Mg. To address these issues, degradable conducting polymers [392] may be investigated. To that end, our lab has begun research with degradable conducting polymers developed in conjunction with outside industrial partners.

The effects of the coating thickness and GO concentration on the mechanical properties of the film may also be investigated to minimize potential shedding of the polymer film. The current PEDOT/GO film protocol results in a film that while well adhered to the surface, is relatively brittle. This is likely due to the high concentration of GO in the film. Improving the flexibility of the film could minimize potential complications from delamination as well as improve the longevity of the film *in vivo*.

Chapter 3 Investigated the ability to use corrosion current generated by Mg oxidation to drive drug release from the PEDOT/GO film. This work only investigated dexamethasone release. In the future, other anti-inflammatory molecules as well as tissue specific molecules such as bisphosphonate molecules for orthopedic applications[301] and Sirolimus and Paclitaxel for stent applications could be investigated. Multi-layer techniques using a layer of PEDOT/GO without drug followed by a topcoat of PEDOT/GO with drug could also be investigated as a way to improve the corrosion resistance of the self-powered drug releasing system. In addition, further investigation into the correlation of exposed Mg and its effect on the drug release profile

could improve the ability to tune the drug release profile for the needs of each tissue and the specific drug being released.

Chapter 4 provided an initial exploration into the ability to surface functionalize the PEDOT/GO Mg surface with bioactive cues. While this work suggests that the PEDOT/GO coating could serve as an effective method for immobilizing bioactive cues, more characterization and optimization need to be conducted prior to initiating in vivo testing. A more detailed analysis of the binding and coverage of the bound moiety should be conducted using Fourier Transform Infrared Spectroscopy (FTIR) and X-ray photoelectron spectroscopy (XPS). This analysis would allow for a better understanding of the method of attachment and coverage required to elicit a biologic response. This type of surface analysis would likely be required for each specific moiety attached to the surface. Analysis in this way could also allow for further optimization of the coating protocol to maximum tissue response as well as retain maximum bioactivity of the functionalized moiety.

Lastly, the combination of corrosion protection, drug release, and surface functionalization through PEDOT/GO coatings could be analyzed. This work largely focused on each component individually with the intent to bolster the basic knowledge so as to allow for the future development of coatings. Using methods outlined in this work future investigation into the use of a single coating that provides improved corrosion resistance, decreased hydrogen evolution, self-powered drug release, and a method to add surface cues could be used to improve Mg implant performance.

BIBLIOGRAPHY

1. Zheng, Y.F., X.N. Gu, and F. Witte, *Biodegradable Metals*. Materials Science and Engineering: R: Reports, 2014. **77**: p. 1-34.
2. Hornberger, H., S. Virtanen, and A. Boccaccini, *Biomedical coatings on magnesium alloys- A review*. Acta Biomaterialia, 2012. **8**: p. 2442-2455.
3. Walker, J., et al., *Magnesium biomaterials for orthopedic application: A review from a biological perspective*. J Biomed Mater Res Part B, 2014.
4. *Dietary Reference Intakes: Calcium, Phosphorus, Magnesium, Vitamin D and Fluoride*, I.o.M. (IOM), Editor. 1997, National Academy Press: Washington, DC.
5. Touyz, R., *Magnesium in clinical medicine*. Frontiers in Bioscience, 2004. **9**: p. 127-1293.
6. Saris, N.-E.L., et al., *Magnesium: An update on physiological, clinical and analytical aspects*. Clinica Chimica Acta, 2000. **294**(1-2): p. 1-26.
7. Hartwig, A., *Role of magnesium in genomic stability*. Mutation Research/Fundamental and Molecular Mechanisms of Mutagenesis, 2001. **475**(1-2): p. 113-121.
8. Rude, R., *Magnesium*, in *Modern Nutrition in Health and Disease*, A. Ross, et al., Editors. 2012, Lippincott Williams & Wilkins: Baltimore. p. 159-175.
9. Kuhlmann, J., et al., *Fast escape of hydrogen from gas cavities around corroding magnesium implants*. Acta Biomaterialia, 2013. **9**: p. 8714-8721

10. Nordlien, J., S. Ono, and N. Masuko, *Morphology and structure of oxide films formed on magnesium by exposure to air and water*. J. Electrochem. Soc., 1995. **142**(10): p. 3320-3322.
11. Song, G. and A. Atrens, *Understanding magnesium corrosion: a framework for improved alloy performance* Advanced Engineering Materials, 2003. **5**(12): p. 837-858.
12. Atrens, A., M. Liu, and N.I. Zainal Abidin, *Corrosion mechanism applicable to biodegradable magnesium implants*. Materials Science and Engineering: B, 2011. **176**(20): p. 1609-1636.
13. Zhang, L.-n., et al., *The effect of selected alloying element additions on properties of Mg-based alloy as bioimplants: A literature review*. Front. Mater. Sci., 2013. **7**(3): p. 227-236.
14. Blaine, J., M. Chonchol, and M. Levi, *Renal Control of Calcium, Phosphate, and Magnesium Homeostasis*. Clinical Journal of the American Society of Nephrology, 2014.
15. Staiger, M., et al., *Magnesium and its alloys as orthopedic biomaterials: A review*. Biomaterials, 2006. **27**(9): p. 1728-1734.
16. K, V.d.V. and P. Kiekens, *Biopolymers: overview of several properties and consequences on their applications*. Polymer Testing, 2002. **21**: p. 433-442.
17. Song, G., *Control of biodegradation of biocompatible magnesium alloys*. Corrosion Science, 2007. **49**: p. 1696-1701.
18. Witte, F., *The history of biodegradable magnesium implants: A review*. Acta Biomaterialia, 2010. **6**: p. 1680–1692.
19. Andrews, E., *Absorbable metal clips as substitutes for ligatures in wound closure*. JAMA, 1917. **28**: p. 278-281.
20. Stone, P. and J. Lord, *An experimental study of the thrombogenic properties of magnesium-aluminum wire in the dog's aorta*. Surgery, 1951. **30**(6): p. 987-993.
21. Hussl, H., et al., *Resorption time and tissue reaction with magnesium rods in rats and rabbits*. Chirurgia Plastica, 1981. **6**(2): p. 117-126.

22. Jun, J.-H., *Damping behavior of Mg–Zn–Al casting alloys*. Materials Science and Engineering: A, 2016. **665**: p. 86-89.
23. Park, G.H., et al., *Development of lightweight MgLiAl alloys with high specific strength*. Journal of Alloys and Compounds, 2016. **680**: p. 116-120.
24. Li, X., et al., *Effect of nano TiN/Ti refiner addition content on the microstructure and properties of as-cast Al-Zn-Mg-Cu alloy*. Journal of Alloys and Compounds, 2016. **675**: p. 201-210.
25. Zheng, J., Z. Li, and B. Chen, *Segregation of rare earth atoms in Mg-Gd-Y-Zr alloy after a 6-year natural ageing at room temperature: Atomic-scale direct imaging*. Materials Letters, 2016. **174**: p. 86-90.
26. Li, J.L., et al., *Superplasticity of multi-directional impact forged Mg–Gd–Y–Zr alloy*. Journal of Alloys and Compounds, 2016. **672**: p. 27-35.
27. Song, G., *Recent Progress in Corrosion and Protection of Magnesium Alloys*. Advanced Engineering Materials, 2005. **7**(7): p. 563-586.
28. Estrin, Y., et al., *New hot rolled Mg-4Li-1Ca alloy: A potential candidate for automotive and biodegradable implant applications*. Materials Letters, 2016. **173**: p. 252-256.
29. Liu, X., et al., *Microstructure, mechanical properties, in vitro degradation behavior and hemocompatibility of novel Zn–Mg–Sr alloys as biodegradable metals*. Materials Letters, 2016. **162**: p. 242-245.
30. Zhao, C., et al., *Microstructure, mechanical properties, bio-corrosion properties and cytotoxicity of as-extruded Mg-Sr alloys*. Materials Science and Engineering: C, 2016.
31. D, H., et al., *In vitro degradation and cytotoxicity response of Mg-4% Zn-0.5% Zr (ZK40) alloy as a potential biodegradable material*. Acta Biomaterialia, 2013. **9**(10): p. 8534-8547.
32. Chou, D., et al., *In vitro and in vivo corrosion, cytocompatibility and mechanical properties of biodegradable Mg-Y-Ca-Zr alloys as implant materials*. Acta Biomaterialia, 2013. **9**: p. 8518-8533.

33. Li, Z., et al., *The development of binary Mg–Ca alloys for use as biodegradable materials within bone*. *Biomaterials*, 2008. **29**(10): p. 1329-1344.
34. Bowen, P., et al., *Metallic zinc exhibits optimal biocompatibility for bioabsorbable endovascular stents*. *Materials Science and Engineering: C*, 2015. **56**: p. 467-472.
35. Seal, C., K. Vinsce, and M. Hodgson, *Biodegradable Surgical Implants based on Magnesium Alloys - A Review of Current Research*. *Material Science and Engineering*, 2009. **4**.
36. Persaud-Sharma, D. and A. McGoron, *Biodegradable Magnesium Alloys: A Review of Material Development and Applications*. *Journal of Biomimetics, Biomaterials & Tissue Engineering*, 2011. **12**.
37. Makar, G. and J. Kruger, *Corrosion of Magnesium*. *International Materials Reviews*, 1993. **38**(3): p. 138-153.
38. Gu, X., et al., *In vitro corrosion and biocompatibility of binary magnesium alloys*. *Biomaterials*, 2009. **30**(4): p. 484-498.
39. Witte, F., et al., *Degradable biomaterials based on magnesium corrosion*. *Current Opinion in Solid State and Materials Science*, 2008. **12**(5-6): p. 63-72.
40. Mueller, W.-D., et al., *Degradation of magnesium and its alloys: Dependence on the composition of the synthetic biological media*. *Journal of Biomedical Materials Research Part A*, 2009. **90A**(2): p. 487-495.
41. Reifenrath, J., D. Bormann, and A. Meyer-Lindenberg, *Magnesium alloys - corrosion and surface treatments*, F. Czerwinski, Editor. 2011, INTECH.
42. Zberg, B., P. Uggowitzer, and J. Löffler, *MgZnCa glasses without clinically observable hydrogen evolution for biodegradable implants*. *Nature Materials*, 2009. **8**: p. 887-891.
43. *Transluminal Technologies Receives CE Mark Approval for Velox CD Vascular Closure Device*. 2014 [cited 2016 May 1]; Available from: <http://www.dicardiology.com/content/transluminal-technologies-receives-ce-mark-approval-velox-cd-vascular-closure-device>.

44. *Magnezix-The revolution in orthopedic surgery.* [cited 2016 May 1]; Available from: <http://www.syntellix.de/en/doctor/product-information/>.
45. Gupta, R., K. Mensah-Darkwa, and D. Kumar, *Corrosion protective conversion coatings on Magnesium Disks Using a Hydrothermal Technique.* Journal of Materials Science & Technology, 2014. **30**(1): p. 47-53.
46. Retting, R. and S. Virtanen, *Composition of corrosion layers on magnesium rare-earth alloy in simulated body fluids.* J Biomed Mater Res Part A, 2009. **85**(2): p. 359-369.
47. Rettig, R. and S. Virtanen, *Time-dependent electrochemical characterization of the corrosion of a magnesium rare-earth alloy in simulated body fluids.* J Biomed Mater Res A, 2008. **85**(1): p. 167-175.
48. Chen, X., N. Birbilis, and T. Abbot, *A simple route towards a hydroxy apatite Mg (OH)₂ conversion coating for magnesium.* Corrosion Science, 2011. **53**: p. 2263-2268.
49. Ellingsen, J., *Pre-treatment of titanium implants with fluoride improves their retention in bone.* Journal of Materials Science: Materials in Medicine, 1995. **6**: p. 749-753.
50. Monjo, M., et al., *in vivo expression of osteogenic markers and bone mineral density at the surface of fluoride-modified titanium implants.* Biomaterials, 2008. **29**(28): p. 3771-3780.
51. Chiu, K., et al., *Characterization and corrosion studies of fluoride conversion coating on degradable Mg implants.* Surface & Coatings Technology, 2007. **202**(3): p. 590-598.
52. Yan, T., et al., *Fluoride treatment and in vitro corrosion behavior of an AZ31B magnesium alloy.* Materials Science and Engineering: C, 2010. **30**(5): p. 740-748.
53. Thomann, M., et al., *Influence of a magnesium-fluoride coating of magnesium-based implants (MgCa0.8) on degradation in a rabbit model.* Journal of Biomedical Materials Research Part A, 2010: p. 1609-1619.
54. Cano-Iranzo, F., et al., *Chromium-free conversion coating.* U.S. Patent 8,298,350, issued December 30, 2012.

55. Huo, H., Y. Li, and F. Wang, *Corrosion of AZ91D magnesium alloy with chemical conversion coating and electroless nickel layer*. Corrosion Science, 2003. **46**: p. 1467-1477.
56. Brunelli, K., et al., *Effect of HCl pre-treatment on corrosion resistance of cerium based conversion coatings on magnesium and magnesium alloys*. Corrosion Science, 2005. **47**(4): p. 989-1000.
57. Gupta, R., K. Mensah-Darkwa, and D. Kumar, *Effect of Post Heat Treatment on Corrosion Resistance of Phytic Acid Conversion Coated Magnesium*. Journal of Materials Science and Technology, 2013. **29**(2): p. 180-186.
58. Ismail, K. and S. Virtanen, *Electrochemical behavior of magnesium alloy AZ31 in 0.5 M KOH solution*. Electrochem Solid-State Letter, 2007. **10**(3): p. c9-c11.
59. Zhou, X., et al., *Film formation and detachment during anodizing of Al-Mg alloys*. Corrosion Science, 1999. **41**: p. 1599-1613.
60. Mousa, H.M., et al., *One-step anodization deposition of anticorrosive bioceramic compounds on AZ31B magnesium alloy for biomedical application*. Ceramics International, 2015. **41**(9, Part A): p. 10861-10870.
61. Mousa, H.M., et al., *A novel simple strategy for in situ deposition of apatite layer on AZ31B magnesium alloy for bone tissue regeneration*. Applied Surface Science, 2015. **351**: p. 55-65.
62. Hiromoto, S. and A. Yamamoto, *High corrosion resistance of magnesium coated with hydroxyapatite deirectly synthesized in an aqueous solution*. Electrochimica Acta, 2009. **54**: p. 7085-7093.
63. Zhang, X., et al., *Corrosion and wear resistance of AZ91D magnesium alloy with and without microarc oxidation coating in Hank's solution*. J Mater Sci, 2007. **42**: p. 8523-8528.
64. Xu, X., et al., *Corss-linked gelatin/nanoparticles composite coating on micro-arc oxidation film for corrosion and drug release*. Applied Surface Science, 2010. **256**: p. 2367-2371.

65. Srinivasan, P., et al., *Characterization of calcium containing plasma electrolytic oxidation coating on AM50 magnesium alloy*. Applied Surface Science, 2010. **256**: p. 4017-4022.
66. Yao, Z., L. Li, and Z. Jiang, *Adjustment of the ratio of Ca/P in the ceramic coating on Mg alloy by plasma electrolytic oxidation*. Applied Surface Science, 2009. **255**: p. 6724-6728.
67. Tian, P., X. Liu, and C. Ding, *In vitro degradation behavior and cytocompatibility of biodegradable AZ31 alloy with PEO/HT composite coating*. Colloids and Surfaces B: Biointerfaces, 2015. **128**: p. 44-54.
68. Shi, P., et al., *Improvement of corrosion resistance of pure magnesium in Hanks' solution by microarc oxidation with sol-gel TiO₂ sealing*. J Alloy Compd, 2009. **469**: p. 286-292.
69. White, L., et al., *TiO₂ deposition on az31 Magnesium alloy using plasma electrolytic oxidation*. Journal of Nanomaterials, 2013. **2013**: p. 8.
70. White, L., et al., *Hardness enhancement of PEO-treated Mg alloy for biodegradable implants*. Engineering Materials Research, 2013. **2**(EMR5): p. 291-296.
71. Alabbasi, A., et al., *Performance of pulsed constant current silicate-based PEO coating on pure magnesium in simulated body fluid*. Materials Letters, 2013. **106**: p. 18-21.
72. Ma, J., et al., *Similarities and differences in coatings for magnesium-based stents and orthopaedic implants*. Journal of Orthopaedic Translation, 2014. **2**(3): p. 118-130.
73. Conceicao, T.F., et al., *Corrosion protection of magnesium alloy AZ31 sheets by spin coating process with poly(ether imide) [PEI]*. Corrosion Science, 2010. **52**(6): p. 2066-2079.
74. Scharnagl, N., C. Blawert, and W. Dietzel, *Corrosion protection of magnesium alloy AZ31 by coating with poly(ether imides) (PEI)*. Surface and Coatings Technology, 2009. **203**(10-11): p. 1423-1428.
75. Li, J., et al., *In vitro degradation and cell attachment of a PLGA coated biodegradable Mg-6Zn based alloy*. Journal of Materials Science, 2010. **45**(22): p. 6038-6045.

76. Chen, Y., et al., *Interaction between a high purity magnesium surface and PCL and PLA coatings during dynamic degradation*. *Biomedical Materials*, 2011. **6**(2).
77. Wong, H.M., et al., *A biodegradable polymer-based coating to control the performance of magnesium alloy orthopaedic implants*. *Biomaterials*, 2010. **31**(8): p. 2084-2096.
78. Xu, L. and A. Yamamoto, *Characteristics and cytocompatibility of biodegradable polymer film on magnesium by spin coating*. *Colloids and Surfaces B: Biointerfaces*, 2012. **93**: p. 67-74.
79. Ostrowski, N., et al., *Corrosion protection and improved cytocompatibility of biodegradable polymeric layer-by-layer coatings on AZ31 magnesium alloys*. *Acta Biomaterialia*, 2013. **9**(10): p. 8704-8713.
80. Lu, P., et al., *Corrosion and drug release properties of EN-plating/PLGA composite coating on MAO film*. *Materials Science and Engineering C*, 2011. **31**: p. 1285-1289.
81. Haude, M., et al., *Safety and performance of the drug-eluting absorbable metal scaffold (DREAMS) in patients with de-novo coronary lesions: 12 month results of the prospective, multicentre, first-in-man BIOSOLVE-I trial*. *TheLancet*, 2013. **382**(9869): p. 836-844.
82. Wittchow, E., et al., *Bioresorbable drug-eluting magnesium-alloy scaffold: design and feasibility in a porcine coronary model*. *EuroIntervention*, 2013. **8**(12).
83. Xu, X., et al., *Cross-linked gelatin/nanoparticles composite coating on micro-arc oxidation film for corrosion and drug release*. *Applied Surface Science*, 2010. **256**(8): p. 2367-2371.
84. Kunjukunju, S., et al., *A layer-by-layer approach to natural polymer-derived bioactive coatings on magnesium alloys*. *Acta Biomaterialia*, 2013. **9**(2013): p. 8690-8730.
85. Letheby, H., *XXIX.-On the production of a blue substance by the electrolysis of sulphate of aniline*. *Journal of the Chemical Society*, 1862. **15**(0): p. 161-163.
86. Halls, J.J.M., et al., *Efficient photodiodes from interpenetrating polymer networks*. *Nature*, 1995. **376**(6540): p. 498-500.

87. Feng, C., et al., *One-step fabrication of membraneless microbial fuel cell cathode by electropolymerization of polypyrrole onto stainless steel mesh*. Biosensors and Bioelectronics, 2011. **26**(9): p. 3953-3957.
88. Burke, A., *Ultracapacitors: why, how, and where is the technology*. Journal of Power Sources, 2000. **91**(1): p. 37-50.
89. Tallman, D., et al., *Electroactive conducting polymers for corrosion control Part 1: General introduction*. Journal of Solid State Electrochemistry, 2002. **6**: p. 73-84
90. Tallman, D., et al., *Electroactive conducting polymers for corrosion control Part 2. Ferrous metals*. Journal of Solid State Electrochemistry, 2002. **6**: p. 85-100.
91. Bai, H. and G. Shi, *Gas Sensors Based on Conducting Polymers*. Sensors (Basel, Switzerland), 2007. **7**(3): p. 267-307.
92. Barisci, J., C. Conn, and G. Wallace, *Conducting Polymer Sensors*. Trends in Polymer Science, 1996. **4**(9): p. 307-311.
93. Luo, S.-C., *Conducting polymers as biointerfaces and biomaterials: A perspective for a special issue of polymer reviews*. Polymer Reviews, 2013. **53**(3): p. 303-310.
94. Balint, R., N.J. Cassidy, and S.H. Cartmell, *Conductive polymers: Towards a smart biomaterial for tissue engineering*. Acta Biomaterialia, 2014. **10**(6): p. 2341-2353.
95. Bendrea, A.D., L. Cianga, and I. Cianga, *Review paper: progress in the field of conducting polymers for tissue engineering applications*. J Biomater Appl, 2011. **26**(1): p. 3-84.
96. Cui, X., et al., *Electrochemical deposition and characterization of conducting polymer polypyrrole/PSS on multichannel neural probes*. Sensors and Actuators A: Physical, 2001. **93**(1): p. 8-18.
97. Cui, X., et al., *Surface modification of neural recording electrodes with conducting polymer/biomolecule blends*. Journal of Biomedical Materials REsearch, 2001. **56**(2): p. 261-272.

98. Kolarcik, C., et al., *Evaluation of poly(3,4-ethylenedioxythiophene)/carbon nanotube neural electrode coatings for stimulation in the dorsal root ganglion*. Journal of Neural Engineering, 2015. **12**.
99. Luo, X., et al., *Highly stable carbon nanotube doped poly(3,4-ethylenedioxythiophene) for chronic neural stimulation*. Biomaterials, 2011. **32**(24): p. 5551-5557.
100. Luo, X., et al., *Carbon nanotube nanoreservoir for controlled release of anti-inflammatory dexamethasone*. Biomaterials, 2011. **32**(26): p. 6316-6323.
101. Luo, X.L. and X.T. Cui., *Sponge-like nanostructured conducting polymers for electrically controlled drug release*. Electrochemistry Communications, 2009. **11**(10): p. 1956-1959
102. Weaver, C., et al., *Electrically controlled drug delivery from graphene oxide nanocomposite films*. ACS Nano, 2014. **8**(2): p. 1834-1843.
103. Luo, X., et al., *Pure graphene oxide doped conducting polymer nanocomposite for bio-interfacing*. J. Mater. Chem. B, 2013. **1**: p. 1340-1348.
104. Inzelt, G., *Conducting polymers: a new era in electrochemistry*. 1st ed. 2008, New York: Springer.
105. Guimarda, N.K., N. Gomez, and C.E. Schmidt, *Conducting polymers in biomedical engineering*. Prog. Polym. Sci., 2007. **32**: p. 876-921.
106. Inzelt, G., *Chemical and Electrochemical Syntheses of Conducting Polymers*. 2012, Berlin: Springer.
107. Heinze, J., B.A. Frontana-Urbe, and S. Ludwigs, *Electrochemistry of Conducting Polymers—Persistent Models and New Concepts*. Chemical Reviews, 2010. **110**(8): p. 4724-4771.
108. Wallace, G.G., et al., *Conductive Electroactive Polymers: Intelligent Polymer Systems*. 3 ed. 2008: CRC Press.
109. Bredas, J. and G. Street, *Polarons, bipolarons, and solitons in conducting polymers*. Acc Chem Res, 1985. **18**: p. 309-315.

110. Svirskis, D., et al., *Electrochemically controlled drug delivery based on intrinsically conducting polymers*. Journal of Controlled Release, 2010. **146**: p. 6-15.
111. George, P., et al., *Electrically Controlled Drug Delivery from Biotin-Doped Conducting Polypyrrole*. Advanced Materials, 2006. **18**: p. 577-581.
112. Bidan, G., et al., *Incorporation of sulphonated cyclodextrins into polypyrrole: and approach for the electro-controlled delivering of neutral drugs*. Biosensors and Bioelectronics, 1995. **10**(1-2): p. 219-229.
113. Abidian, M., D.-H. Kim, and D. Martin, *Conducting-Polymer Nanotubes for Controlled Drug Release*. Advanced Materials, 2006. **18**(4): p. 405-409.
114. Ohtsuka, T., *Corrosion protection of steels by conducting polymer coating*. International Journal of Corrosion, 2012. **2012**.
115. Bar-Cohen, Y. *Electroactive Polymers as Artificial Muscles-Reality and Challenges*. in *42nd American Institute of Aeronautics and Astronautics: Structures, Structural Dynamics, and Materials Conference*. 2001. Seattle WA.
116. Smela, E., O. Inganäs, and I. Lundström, *Controlled Folding of Micrometer-size Structures*. Science, 1995. **268**: p. 1735-1738.
117. Jager, E.W.H., O. Inganäs, and I. Lundström, *Microrobots for Micrometer-Size Objects in Aqueous Media: Potential Tools for Single-Cell Manipulation*. Science, 2000. **288**(5475): p. 2335-2338.
118. Spinks, G.M., et al., *Strain response from polypyrrole actuators under load*. Advanced Functional Materials, 2002. **12**(6-7): p. 437-440.
119. Spinks, G.M., et al., *Conducting polymers electromechanical actuators and strain sensors*. Macromolecular Symposia, 2003. **192**(1): p. 161-170.
120. Smyth, C., et al., *Self-maintained colorimetric acid/base sensor using polypyrrole actuator*. Sensors and Actuators B: Chemical, 2008. **129**(2): p. 518-524.
121. Sapp, S.A., et al., *Rapid switching solid state electrochromic devices based on complementary conducting polymer films*. Advanced Materials, 1996. **8**(10): p. 808-811.

122. Sapp, S.A., G.A. Sotzing, and J.R. Reynolds, *High contrast ratio and fast-switching dual polymer electrochromic devices*. Chemistry of Materials, 1998. **10**(8): p. 2101-2108.
123. Schwendeman, I., et al., *Enhanced contrast dual polymer electrochromic devices*. Chemistry of materials, 2002. **14**(7): p. 3118-3122.
124. Nambiar, S. and J.T. Yeow, *Conductive polymer-based sensors for biomedical applications*. Biosensors and Bioelectronics, 2011. **26**(5): p. 1825-1832.
125. Weaver, C., et al., *A graphene oxide/conducting polymer nanocomposite for electrochemical dopamine detection: origin of improved sensitivity and specificity*. Journal of Materials Chemistry B, 2014. **2**: p. 5209-5219.
126. Mawad, D., et al., *A single component conducting polymer hydrogel as a scaffold for tissue engineering*. Advanced Functional Materials, 2012. **22**(13): p. 2692-2699.
127. Li, M., et al., *Electrospinning polyaniline-contained gelatin nanofibers for tissue engineering applications*. Biomaterials, 2006. **27**(13): p. 2705-2715.
128. Collier, J.H., et al., *Synthesis and characterization of polypyrrole-hyaluronic acid composite biomaterials for tissue engineering applications*. Journal of biomedical materials research, 2000. **50**(4): p. 574-584.
129. Zhou, D.D., et al., *Conducting polymers in neural stimulation applications*, in *Implantable Neural Protheses 2*. 2009, Springer. p. 217-252.
130. Yang, W.-W. and E. Pierstorff, *Reservoir-Based Polymer Drug Delivery Systems*. Journal of Laboratory Automation, 2011. **17**(1): p. 50-58.
131. Green, R., et al., *Conducting polymers for neural interfaces: Challenges in developing an effective long-term implant*. Biomaterials, 2008. **29**: p. 3393-3399.
132. Kim, D.-H., et al., *Soft, fuzzy, and bioactive conducting polymers for improving the chronic performance of neural prosthetic devices*. Indwelling neural implants: Strategies for contending with the in vivo environment, 2008: p. 165-207.

133. Wadhwa, R., C.F. Lagenaur, and T. Cui, *Electrochemically controlled release of dexamethasone from conducting polymer polypyrrole coated electrode*. Journal of Controlled Release, 2006. **110**: p. 531-541.
134. Stauffer, W. and T. Cui, *Polypyrrole doped with 2 peptide sequences from laminin*. Biomaterials, 2006. **11**: p. 2305-2313.
135. Novoselov, K.S., et al., *Electric Field Effect in Atomically Thin Carbon Films*. Science, 2004. **306**(5696): p. 666-669.
136. Novoselov, K.S., et al., *Two-dimensional atomic crystals*. Proceedings of the National Academy of Sciences of the United States of America, 2005. **102**(30): p. 10451-10453.
137. Geim, A.K. and K.S. Novoselov, *The rise of graphene*. Nat Mater, 2007. **6**(3): p. 183-191.
138. Ovid'ko, I., *Mechanical properties of graphene*. Rev. Adv. Mater. Sci., 2013. **34**: p. 1-11.
139. Falkovsky, L.A., *Optical properties of graphene*. Journal of Physics: Conference Series, 2008. **129**(1): p. 012004.
140. Dreyer, D., et al., *The chemistry of graphene oxide*. Chemical Society Reviews, 2010. **39**: p. 228-240.
141. Lerf, A., et al., *Structure of Graphite Oxide Revisited*. The Journal of Physical Chemistry B, 1998. **102**(23): p. 4477-4482.
142. Dreyer, D.R., H.P. Jia, and C.W. Bielawski, *Graphene oxide: a convenient carbocatalyst for facilitating oxidation and hydration reactions*. Angewandte Chemie, 2010. **122**(38): p. 6965-6968.
143. Jung, H.S., et al., *Nanographene Oxide–Hyaluronic Acid Conjugate for Photothermal Ablation Therapy of Skin Cancer*. ACS Nano, 2014. **8**(1): p. 260-268.
144. Lu, C.-H., et al., *A Graphene Platform for Sensing Biomolecules*. Angewandte Chemie International Edition, 2009. **48**(26): p. 4785-4787.

145. Wang, Y., et al., *Aptamer/Graphene Oxide Nanocomplex for in Situ Molecular Probing in Living Cells*. Journal of the American Chemical Society, 2010. **132**(27): p. 9274-9276.
146. Chen, D., H. Feng, and J. Li, *Graphene Oxide: Preparation, Functionalization, and Electrochemical Applications*. Chemical Reviews, 2012. **112**(11): p. 6027-6053.
147. Chen, S., et al., *Graphene Oxide–MnO₂ Nanocomposites for Supercapacitors*. ACS Nano, 2010. **4**(5): p. 2822-2830.
148. Wang, H., et al., *Graphene oxide doped polyaniline for supercapacitors*. Electrochemistry Communications, 2009. **11**(6): p. 1158-1161.
149. Eda, G. and M. Chhowalla, *Chemically Derived Graphene Oxide: Towards Large-Area Thin-Film Electronics and Optoelectronics*. Advanced Materials, 2010. **22**(22): p. 2392-2415.
150. Kim, J., et al., *Graphene Oxide Sheets at Interfaces*. Journal of the American Chemical Society, 2010. **132**(23): p. 8180-8186.
151. Prasai, D., et al., *Graphene: corrosion-inhibiting coating*. ACS Nano, 2012. **6**(2): p. 1102-1108.
152. Lih, E.T.Y., et al., *Facile corrosion protection coating from graphene*. International Journal of Chemical Engineering and Applications, 2012. **3**(6): p. 453-455.
153. Krishnamurthy, A., et al., *Passivation of microbial corrosion using graphene coating*. Carbon, 2013. **56**: p. 45-49.
154. Prabakar, R., et al., *Graphene oxide as a corrosion inhibitor for the aluminum current collector in lithium ion batteries*. Carbon, 2013. **52**: p. 128-136.
155. Singh, B.P., et al., *Development of oxidation and corrosion resistance hydrophobic graphene oxide-polymer composite coating on copper*. Surface and Coatings Technology, 2013. **232**: p. 475-481.
156. Liu, J., L. Cui, and D. Losic, *Graphene and graphene oxide as new nanocarriers for drug delivery applications*. Acta biomaterialia, 2013. **9**(12): p. 9243-9257.

157. Sun, X., et al., *Nano-graphene oxide for cellular imaging and drug delivery*. Nano Research, 2008. **1**(3): p. 203-212.
158. Yang, X., et al., *High-efficiency loading and controlled release of doxorubicin hydrochloride on graphene oxide*. J. Phys. Chem. C, 2008. **112**: p. 17554-17558.
159. Lu, Y.-J., et al., *Improving thermal stability and efficacy of BCNU in treating glioma cells using PAA-functionalized graphene oxide*. Int. J. Nanomed, 2012. **7**: p. 1737-1747.
160. Seabra, A.B., et al., *Nanotoxicity of graphene and graphene oxide*. Chemical research in toxicology, 2014. **27**(2): p. 159-168.
161. Akhavan, O., E. Ghaderi, and A. Akhavan, *Size-dependent genotoxicity of graphene nanoplatelets in human stem cells*. Biomaterials, 2012. **33**(32): p. 8017-8025.
162. Yue, H., et al., *The role of the lateral dimension of graphene oxide in the regulation of cellular responses*. Biomaterials, 2012. **33**(16): p. 4013-4021.
163. Kotchey, G.P., et al., *The enzymatic oxidation of graphene oxide*. ACS nano, 2011. **5**(3): p. 2098-2108.
164. Kurapati, R., et al., *Dispersibility-Dependent Biodegradation of Graphene Oxide by Myeloperoxidase*. Small, 2015. **11**(32): p. 3985-3994.
165. Yang, Y., et al., *Electrochemically synthesized polypyrrole/graphene composite film for lithium batteries*. Advanced Energy Materials, 2012. **2**(2): p. 266-272.
166. Zhang, Y., et al., *A novel nano-sulfur/polypyrrole/graphene nanocomposite cathode with a dual-layered structure for lithium rechargeable batteries*. Journal of Power Sources, 2013. **241**: p. 517-521.
167. De Oliveira, H.P., S.A. Sydlik, and T.M. Swager, *Supercapacitors from free-standing polypyrrole/graphene nanocomposites*. The Journal of Physical Chemistry C, 2013. **117**(20): p. 10270-10276.
168. Chen, J., et al., *Biofunctionalization of titanium with PEG and anti-CD34 for hemocompatibility and stimulated endothelialization*. Journal of colloid and interface science, 2012. **368**(1): p. 636-647.

169. Chandra, V. and K.S. Kim, *Highly selective adsorption of Hg²⁺ by a polypyrrole-reduced graphene oxide composite*. Chemical Communications, 2011. **47**(13): p. 3942-3944.
170. Gao, Y.-S., et al., *Overoxidized polypyrrole/graphene nanocomposite with good electrochemical performance as novel electrode material for the detection of adenine and guanine*. Biosensors and Bioelectronics, 2014. **62**: p. 261-267.
171. Bose, S., et al., *In-situ synthesis and characterization of electrically conductive polypyrrole/graphene nanocomposites*. Polymer, 2010. **51**(25): p. 5921-5928.
172. Si, P., et al., *An electrochemically formed three-dimensional structure of polypyrrole/graphene nanoplatelets for high-performance supercapacitors*. Rsc Advances, 2011. **1**(7): p. 1271-1278.
173. Kirkland, N.T., N. Birbilis, and M.P. Staiger, *Assessing the corrosion of biodegradable magnesium implants: A critical review of current methodologies and their limitations*. Acta Biomaterialia, 2012. **8**: p. 925-936.
174. Wang, J., et al., *A surface-eroding poly(1,3-trimethylene carbonate) coating for fully biodegradable magnesium-based stent applications: Toward better biofunction, biodegradation and biocompatibility*. Acta Biomaterialia, 2013. **9**(10): p. 8678-8689.
175. Shaw, B., E. Sikora, and S. Virtanen, *Fix, Heal and Disappear: A new approach to using metals in the human body*. The Electrochemical Society Interface, 2008(45-49).
176. Witte, F., et al., *In vivo corrosion of four magnesium alloys and the associated bone response*. Biomaterials, 2005. **26**: p. 3557-3563.
177. Erbel, R., et al., *Temporary scaffolding of coronary arteries with bioabsorbable magnesium stents: a prospective, non-randomized multicenter trial*. The Lancet, 2007. **369**: p. 1869-1875.
178. Doepke, A., et al., *Corrosion of organosilane coated Mg4Y alloy in sodium chloride solution evaluated by impedance spectroscopy and pH changes*. Electrochimica Acta, 2012. **70**: p. 165-170.
179. Muir, K., *Magnesium for neuroprotection in ischaemic stroke*. CNS Drugs, 2001. **15**(12): p. 921-930.

180. Pan, H., et al., *Magnesium supplement promotes sciatic nerve regeneration and down-regulates inflammatory response*. Magnesium Research, 2011. **24**(2): p. 54-70.
181. Elin, R., *Assessment of magnesium status for diagnosis and therapy*. Magnesium Research, 2010. **23**(4).
182. Song, G. and S. Song, *A possible biodegradable magnesium implant material*. Advanced Engineering Materials, 2007. **9**: p. 298-302.
183. Kraus, T., et al., *Magnesium alloys for temporary implants in osteosynthesis: In vivo studies of their degradation and interaction with bone*. Acta Biomaterialia, 2012. **8**: p. 1230-1238.
184. Paliwoda-Porebska, G., et al., *On the development of polypyrrole coatings with self-healing properties for iron corrosion protection*. Corrosion Sciences, 2005. **47**: p. 3216-3233.
185. Kowalski, D., M. Ueda, and T. Ohtsuka, *Self-healing ion-permselective conducting polymer coating*. Journal of Materials Chemistry, 2010. **20**: p. 7630-7633.
186. Luo, X., *Electrochemical deposition of conducting polymer coatings on magnesium surfaces in ionic liquid*. Acta Biomaterials, Xinyan Tracy Cui. **7**(1): p. 441-446.
187. Truong, V., et al., *Corrosion protection of magnesium by electroactive polypyrrole/paint coatings*. Synthetic Materials, 2000. **110**: p. 7-15.
188. Kruze, P., *Corrosion and surface protections*, in *Magnesium Technology*, F. Horst and B. Mordike, Editors. 2006, Springer: Berlin Heidelberg.
189. Beck, F. and M. Oberst, *Electrocatalytic deposition and transformation of polypyrrole layers*. Synthetic Materials, 1989. **28**(1-2): p. 43-45.
190. Diaz, A. and J. Bargon, *Electrochemical synthesis of conducting polymers*, in *Handbook of conducting polymers*, T. Skotheim, Editor. 1986, Marcel Dekker Inc: New York. p. 87-90.
191. Diaz, A. and B. Hall, *Mechanical properties of electrochemically prepared polypyrrole films*. IBM Journal of Research and Development, 1983. **27**(4): p. 342-347.

192. Atrens, A., et al., *Advances in Mg Corrosion and Research Suggestions*. Journal of Magnesium and Alloys, 2013. **1**: p. 177-200.
193. Baril, G., et al., *An impedance investigation on the mechanism of pure magnesium corrosion in sodium sulfate solutions* Journal of the Electrochemical Society, 2007. **154**(2): p. C108-C113.
194. Rammelt, U., P. Nguyen, and W. Plieth, *Protection of mild steel by modification with thin films of polymethylthiophene*. Electrochimica Acta, 2001. **46**: p. 4251-4257.
195. Ganash, A., *Effect of current density on the corrosion protection of poly(o-toluidine)-coated stainless steel*. Int. J Electrochem. Sci., 2014. **9**: p. 4000-4013.
196. Li, X., et al., *Analysis of soft coating corrosion performance on carbon steel using electrochemical impedance spectroscopy*. Corrosion Engineering, Science and Technology, 2014. **70**(6): p. 615-626.
197. Bonora, P., F. Deflorian, and L. Fedrizzi, *Electrochemical impedance spectroscopy as a tool for investigating underpaint corrosion*. Electrochimica Acta, 1996. **41**(7/8): p. 1073-1082.
198. Ahn, S., et al., *A study on corrosion resistance characteristics of PVD Cr-N coated steels by electrochemical method*. Surface and Coatings Technology, 2002. **150**(2-3): p. 319-326.
199. Pan, J., D. Thierry, and C. Leygraf, *Electrochemical impedance spectroscopy study of the passive oxide film on titanium for implant application*. Electrochimica Acta, 1996. **41**(7-8): p. 1143-1153.
200. Alsamuraee, A.M.A., et al., *Electrochemical impedance spectroscopic evaluation of corrosion protection properties of polyurethane/polyvinyl chloride blend coatings on steel*. American Journal of Scientific and Industrial Research, 2011. **2**(5): p. 761-768.
201. Sherif, E.-S., *Corrosion behavior of magnesium in naturally aerated stagnant seawater and 3.5% sodium chloride solutions*. International Journal of Electrochemical Science, 2012. **7**: p. 4235-4249.
202. Rudd, A., C. Breslin, and F. Mansfeld, *The corrosion protection afforded by rare earth conversion coatings applied to magnesium*. Corrosion Science, 2000. **42**(2): p. 275-288.

203. Lamaka, S., et al., *Novel hybrid sol-gel coatings for corrosion protection of AZ31B magnesium alloy*. *Electrochimica Acta*, 2008. **53**(14): p. 4773-4783.
204. Bisquert, J., et al., *Impedance of constant phase element (CPE)-blocked diffusion in film electrodes*. *Journal of Electroanalytical Chemistry*, 1998. **452**(2): p. 229-234.
205. Ocon, P., et al., *Corrosion performance of conducting polymer coatings applied on mild steel*. *Corrosion Science*, 2005. **47**: p. 649-662.
206. Nguyen, T., et al., *Mechanism for protection of iron corrosion by intrinsically electronic conducting polymer*. *Journal of Electroanalytical Chemistry*, 2004. **572**: p. 225-234.
207. Li, H.N.T., et al., *Corrosion protection and conducting polymers: polypyrrole films on iron*. *Electrochimica Acta*, 2001. **46**(4259-4272).
208. Hien, N., et al., *Role of doping ions in the corrosion protection of iron by polypyrrole films*. *Electrochimica Acta*, 2005. **50**: p. 1747-1755.
209. Le, H.N.T., et al., *Raman spectroscopy analysis of polypyrrole films as protective coatings on iron*. 2004.
210. Iroh, J. and W. Su, *Corrosion performance of polypyrrole coating applied to low carbon steel by an electrochemical process*. *Electrochimica Acta*, 2000. **46**: p. 15-24.
211. Rammelt, U., P.T. Nguyen, and w. Plieth, *Corrosion protection by ultrathin films of conducting polymers*. *Electrochimica Acta*, 2003. **48**: p. 1257-1262.
212. Schaftinghen, T.V., et al., *Influence of the surface pre-treatment prior to the film synthesis, on the corrosion protection of iron with polypyrrole films*. *Electrochimica Acta*, 2006. **51**: p. 1695-1703.
213. Troch-Nagels, G., et al., *Electron conducting organic coating of mild steel by electropolymerization*. *Journal of applied electrochemistry*, 1992. **22**: p. 756-764.
214. Shaw, B., *Corrosion resistance of magnesium alloys*. *ASM Handbook*, 2003. **13A**: p. 692-696.

215. Salman, S. and M. Okido, *Anodization of magnesium (Mg) alloys to improve corrosion resistance*, in *Corrosion Prevention of Magnesium Alloys*, G.-L. Song, Editor. 2013, Woodhead Publishing Limited. p. 199.
216. Kinlen, P., V. Menon, and Y. Ding, *A mechanistic investigation of polyaniline corrosion protection using the scanning reference electrode technique*. Journal of the Electrochemical Society, 1999. **146**(10): p. 3690-3695.
217. Wessling, B., *Corrosion prevention with an organic metal (polyaniline): surface ennobling, passivation, corrosion test results*. Materials and Corrosion, 1996. **47**: p. 439-445.
218. Wessling, B., *Passivation of metals by coating with polyaniline: Corrosion potential shift and morphological changes*. Advanced Materials, 1994. **6**(3): p. 226-228.
219. Talo, A., et al., *Polyaniline/epoxy coatings with good anti-corrosion properties*. Synthetic Metals, 1997. **85**: p. 1333-1334.
220. Lu, W., R. Elsenbaumer, and B. Wessling, *Corrosion protection of mild steel by coatings containing polyaniline*. Synthetic Materials 1995. **71**: p. 2163-2166.
221. Li, P., T. Tan, and J. Lee, *Corrosion protection of mild steel by electroactive polyaniline coatings*. Synthetic Metals, 1997. **88**: p. 237-242.
222. Murakami, K., et al., *Mechanism of corrosion protection of anodized magnesium alloys*. Materials Transactions, 2008. **49**(5): p. 1057-1064.
223. Chong, K. and T. Shih, *Conversion-coating treatment for magnesium alloys by a permanganate-phosphate solution*. Materials Chemistry and Physics, 2003. **80**(1): p. 191-200.
224. Ishizaki, T., et al., *Magnesium hydroxide/magnesium phosphate compounds composite coating for corrosion protection of magnesium alloy by a combination process of chemical conversion and steam curing*. Materials Letters, 2012. **68**(1): p. 122-125.
225. Lin, C., et al., *Formation of phosphate/permanganate conversion coating on AZ31 magnesium alloy*. Journal of the Electrochemical Society, 2006. **153**(3): p. B90-B96.

226. Morks, M., *Magnesium phosphate treatment for steel*. Materials Letters, 2004. **58**(26): p. 3316-3319.
227. Zang, H., et al., *A chrome-free conversion coating for magnesium-lithium alloy by a phosphate-permanganate solution*. Surface and Coatings Technology, 2008. **202**(9): p. 1825-1830.
228. Zhou, W., et al., *Structure and formation mechanism of phosphate conversion coating on die-cast AZ91D magnesium alloy*. Corrosion Science, 2008. **50**(2): p. 329-337.
229. Arrabl, R., et al., *Corrosion resistance of WE43 and AZ91D magnesium alloys with phosphate PEO coatings*. Corrosion Science, 2008. **50**(6): p. 1744-1752.
230. Zhang, H., et al., *A chrome-free conversion coating for magnesium-lithium alloy by a phosphate-permanganate solution*. Surface and Coatings Technology, 2008. **202**(9): p. 1825-1830.
231. Xu, L., et al., *In vitro corrosion behavior of Mg alloys in a phosphate solution for bone implant application*. Journal of Material Science: Materials in Medicine, 2008. **19**: p. 1017-1025.
232. Xin, Y., et al., *Influence of aggressive ions on the degradation behavior of biomedical magnesium alloy in physiological environment*. Acat Biomaterialia, 2008. **4**: p. 2008-2015.
233. Yagi, S., et al., *Formation of self-repairing anodized film on ACM522 magnesium alloy by plasma electrolytic oxidation*. Corrosion Science, 2013. **73**: p. 188-195.
234. Song, G., et al., *The anodic dissolution of magnesium in chloride and sulphate solutions*. Corrosion Science, 1997. **39**(10-11): p. 1981-2004.
235. Vennemeyer, J., et al., *Effects of elevated magnesium and substrate on neuronal numbers and neurite outgrowth of neural stem/progenitor cells in vitro*. Neuroscience Research, 2014. **84**: p. 72-78.
236. Vennemeyer, J., et al., *Initial observations on using magnesium metal in peripheral nerve repair*. J Biomater Appl, 2015. **29**(8): p. 1145-1154.

237. Weaver, C. and X.T. Cui, *Directed neural stem cell differentiation with a functionalized graphene oxide nanocomposite*. *Advanced Healthcare Materials*, 2015. **Accepted**.
238. Dribben, W., L. Eisenman, and S. Mennerick, *Magnesium induces neuronal apoptosis by suppressing excitability*. *Cell Death and Disease*, 2011. **1**(63).
239. Huang, T., et al., *Microelectrode Array-evaluation of Neurotoxic Effects of Magnesium as an Implantable Biomaterial*. *Journal of Materials Science & Technology*, 2016. **32**(1): p. 89-96.
240. Dash, A. and G.C. II, *Theraoeutic Applications of Implantable Drug Delivery Systems*. *Journal of Pharmacological and Toxicological Methods*, 1988. **40**: p. 1-12.
241. Alvarez-Lorenzo, C. and A. Concheiro, *Intelligent Drug Delivery Systems: Polymeric Micelles and Hydrogels*. *Mini-Reviews in Medicinal Chemistry*, 2008. **8**.
242. LaVan, D., T. McGuire, and R. Langer, *Small-scale systems for in vivo drug delivery*. *Nature Biotechnology*, 2003. **21**(10): p. 1184-1191.
243. Bettinger, C., *Materials Advances for Nex-Generation Ingestible Electronic Medical Devices*. *Trends in Biotechnology*, 2015. **33**(10): p. 575-585.
244. Munoz, F., G. Alici, and W. Li, *A review of drug delivery systems for capsule endoscopy*. *Advanced Drug Delivery Reviews*, 2014. **71**: p. 77-85.
245. Li, Y., et al., *In vivo release from a drug delivery MEMS device*. *Journal of Controlled Release*, 2004. **100**(2): p. 211-219.
246. Mahnama, A., A. Nourbakhsh, and G. Ghorbaniasl, *A survey on the applications of implantable micropump systems in drug delivery*. *Current Drug Delivery*, 2014. **11**: p. 123-131.
247. Nisar, A., et al., *MEMS-based micropumps in drug delivery and biomedical applications*. *Sensors and Actuators B*, 2008. **130**: p. 917-942.
248. Shawgo, R., et al., *BioMEMS for drug delivery*. *Current Opinion in Solid State and Materials Science*, 2002. **6**(4): p. 329-334.

249. Staples, M., et al., *Application of Micro- and Nano- Electrochemical Devices to Drug Delivery*. *Pharmaceutical Research*, 2006. **23**(5): p. 847-863.
250. Ratner, B., *Reducing capsular thickness and enhancing angiogenesis around implant drug release systems*. *Journal of Controlled Release*, 2002. **78**(1-3): p. 211-218.
251. Park, H. and K. Park, *Biocompatibility Issues of Implantable Drug Delivery Systems*. *Pharmaceutical Research*, 1996. **13**(12): p. 1770-1776.
252. Hatefi, A. and B. Amsden, *Biodegradable injectable in situ forming drug delivery systems*. *Journal of Controlled Release*, 2002. **80**: p. 9-28.
253. Ashley, G., et al., *Hydrogel drug delivery system with predictable and tunable drug release and degradation rates*. *PNAS*, 2012. **100**(6): p. 2318-2323.
254. Schlesinger, A., et al., *A Tunable, Biodegradable, Thin-Film Polymer Device as a Long-Acting Implant Delivering Tenofovir Alafenamide Fumarate for HIV pre-exposure Prophylaxis*. *Pharmaceutical Research*, 2016: p. 1-9.
255. Liu, Y.-C., et al., *Optimization of Subconjunctival Biodegradable Microfilms for Sustained Drug Delivery to the Anterior Segment in a Small Animal Model*. *Investigative Ophthalmology & Visual Science*, 2013. **54**: p. 2607-2615.
256. Tao, H., et al., *Silk-based resorbable electronic devices for remotely controlled therapy and in vivo infection abatement*. *PNAS*, 2014. **111**(49): p. 17385-17389.
257. Irimia-Vladu, M., et al., *Green and biodegradable electronics*. *Materials Today*, 2012. **15**(7-8): p. 340-346.
258. irima-Vladu, M., et al., *Biocompatible and Biodegradable Materials for Organic Field-Effect Transistors*. *Advanced Functional Materials*, 2010. **20**: p. 4069-4076.
259. Bettinger, C. and Z. Bao, *Organic Thin-Film Transistors Fabricated on Resorbable Biomaterial Substrates*. *Advanced Materials*, 2010. **22**: p. 651-655.
260. Wei, X. and J. Liu, *Power sources and electrical recharging strategies for implantable medical devices*. *Frontiers of Energy and Power Engineerin in China*, 2008. **2**(1): p. 1-13.

261. Wang, J., *In vivo glucose monitoring: Towards 'Sense and Act' feedback-loop individualized medical systems*. Talanta, 2008. **75**(3): p. 636-641.
262. Kim, Y., et al., *Biologically derived melanin electrodes in aqueous sodium-ion energy storage devices*. PNAS, 2013. **110**(52): p. 20912-20917.
263. Kim, Y., et al., *Self-deployable current sources fabricated from edible materials*. Journal of Materials Chemistry B, 2013. **31**: p. 3781-3788.
264. Heller, A., *Potentially implantable miniature batteries*. Analytical and bioanalytical chemistry, 2006. **385**(3): p. 469-473.
265. Gill, P., et al., *Corrosion and Biocompatibility Assessment of Magnesium Alloys*. Journal of Biomaterials and Nanobiotechnology, 2012. **3**: p. 10-13.
266. Tsang, M., et al., *Development of Electroplated Magnesium Microstructures for Biodegradable Devices and Energy Sources*. Journal of Microelectromechanical systems, 2014. **23**(6): p. 1281-1289.
267. Yin, L., et al., *Materials, Designs, and Operational Characteristics for Fully Biodegradable Primary Batteries*. Advanced Materials, 2014. **26**: p. 3879-3884.
268. Tsang, M., et al., *Biodegradable magnesium/iron batteries with polycaprolactone encapsulation: a Microfabricated power source for transient implantable devices*. Microsystems & Nanoengineering, 2015. **1**.
269. Kong, Y., et al., *A battery composed of a polypyrrole cathode and a magnesium alloy anode-Toward a bioelectric battery*. Synthetic Metals, 2012. **162**: p. 584-589.
270. Lu, P., et al., *Controllable biodegradability, drug release behavior and hemocompatibility of PTX-eluting stents*. Colloids and Surfaces B: Biointerfaces, 2011. **83**: p. 23-28.
271. Campos, C., et al., *Bioresorbable Drug-eluting Magnesium-Alloy Scaffold for Treatment of Coronary artery disease*. Int J Mol Sci, 2013. **14**(12): p. 24492-24500.
272. Borck, A. and N. Adden, *Biocorrosible implant with a coating containing drug eluting polymer matrix*, USPTO, Editor. 2010, A Borck, N Adden: USA.

273. Moravej, M. and D. Mantovani, *Biodegradable metals for cardiovascular stent applicatoin: interests and New Oppertunities*. Int J Mol Sci, 2011. **12**(7): p. 4250-4270.
274. Witte, F., et al., *In vitro and in vivo corrosion measurements of magnesium alloys*. Biomaterials, 2006. **27**: p. 1013-1018.
275. Zhou, Q., L. Miller, and J. Valentine, *Electrochemicallay controlled binding and release of protonated dimethyldopamine and other cations from poly(N-methyl-pyrrole)/polyanion composite redox polymers*. Journal of Electroanalytic Chemistry and Interfacial Electrochemistry, 1989. **261**(1): p. 147-164.
276. Lien, M., W. Smyrl, and M. Morita, *Cation and anion insertion in separate processes in poly(pyrrole) composite films*. Journal of Electroanalytic Chemistry and Interfacial Electrochemistry, 1991. **309**(1-2): p. 333-340.
277. Hepel, M. and F. Mahdavi, *Application of the electrochemical quartz crystal microbalance for electrochemically controlled binding and release of chlorpromazine from conductive polymer matrix*. Microchemical Journal, 1997. **56**: p. 54-64.
278. Liu, H., et al., *Characterization and drug release behavior of highly responsive electrically modulated reduced graphene oxide-poly(vinyl alcohol) membranes*. Journal of Materials Chemistry, 2012. **22**: p. 17311-17320.
279. Zhang, R., et al., *Real time monitoring of the drug release of rhodamine B on graphene oxide*. Carbon, 2011. **49**: p. 1126-1132.
280. Bao, H., et al., *Chitosan-functionalized graphene oxide as a nanocarrier for drug and gene delivery*. Small, 2011. **7**(11): p. 1569-1578.
281. Sun, X., et al., *Nano-graphene oxide for cellular imaging and drug delivery*. Nano Res, 2008. **1**(3): p. 203-212.
282. Tao, C., et al., *Fabrication of pH-sensitive graphene oxide-drug supramolecular hydrogels as contorlld release systems*. Journal of Materials Chemistry, 2012. **22**: p. 24856-24861.

283. Qiu, Z., et al., *Graphene oxide as a corrosion-inhibitive coating on magnesium alloys*. RSC Advances, 2015. **5**(55): p. 44149-44159.
284. Herrero-Vanrella, R., J. Cardillo, and B. Kuppermann, *Clinical applications of the sustained release dexamethasone implant for treatment of macular edema*. Clinical Ophthalmology, 2011. **5**: p. 139-146.
285. Patil, S., F. Papadimitrakopoulos, and D. Burgess, *Concurrent delivery of dexamethasone and VEGF for localised inflammation control and angiogenesis*. Journal of Controlled Release, 2007. **117**(1): p. 68-79.
286. Hickey, T., et al., *In vivo evaluation of dexamethasone/PLGA microsphere system to suppress the inflammatory tissue response to implantable medical devices*. Journal of Biomedical Materials Research 2002. **61**(2): p. 180-187.
287. Zhong, Y. and R. Bellamkonda, *Dexamethasone Coated Neural Probes Elicit Attenuated Inflammatory Response and Neuronal Loss Compared to Uncoated Neural Probes*. Brain Research, 2007. **1148**: p. 15-27.
288. Cheepsunthorn, P., et al., *Characterization of a novel brain-derived microglial cell line isolated from neonatal rat brain*. Glia, 2001. **35**: p. 53-62.
289. Abraham, S., et al., *Antiinflammatory effects of dexamethasone are partly dependent on induction of dual specificity phosphatase*. The Journal of Experimental Medicine, 2006. **203**(8): p. 1883-1889.
290. Wang, C., et al., *A galvanic cell driven controlled release system based on conducting polymers*. Sensors and Actuators B, 2008. **129**: p. 605-611.
291. Wang, C., et al., *Ionic liquid as electrolyte in a self-powered controlled release system*. Sensors and Actuators B, 2009. **141**: p. 452-457.
292. Moulton, A., et al., *Galvanic coupling conducting polymers to biodegradable Mg initiates autonomously powered drug release*. Journal of Materials Chemistry, 2008. **18**: p. 3608-3613.
293. Ge, D., et al., *Coating metals on cellulose-polypyrrole composites: A new route to self-powered drug delivery system*. Electrochemistry Communications, 2010. **12**: p. 1367-1370.

294. Ru, X., et al., *Synthesis of polypyrrole nanowire network with high adenosine triphosphate release efficiency*. *Electrochimica Acta*, 2011: p. 9887-9892.
295. Gudarzi, M.M., *Colloidal Stability of Graphene Oxide: Aggregation in Two Dimensions*. *Langmuir*, 2016. **32**(20): p. 5058-5068.
296. Schlosser, F., et al., *Redox-Switchable Intramolecular pi-pi stacking of Perylene Bismide Dyes in a Cyclophane*. *Adv. Mater.*, 2013. **25**: p. 410-414.
297. Sinnokrot, M.O., E.F. Valeev, and C.D. Sherrill, *Estimates of the Ab Initio Limit for π - π Interactions: The Benzene Dimer*. *Journal of the American Chemical Society*, 2002. **124**(36): p. 10887-10893.
298. Suárez, M.F. and R.G. Compton, *In situ atomic force microscopy study of polypyrrole synthesis and the volume changes induced by oxidation and reduction of the polymer*. *Journal of Electroanalytical Chemistry*, 1999. **462**(2): p. 211-221.
299. Chen, X., K. Xing, and O. Inganäs, *Electrochemically induced volume changes in poly(3,4-ethylenedioxythiophene)*. *Chem. Mater.*, 1996. **8**: p. 2439-2443.
300. Tang, D., et al., *PAMPs and DAMPs: Signal Os that Spur Autophagy and Immunity*. *Immunological reviews*, 2012. **249**(1): p. 158-175.
301. Cattalini, J., et al., *Bisphosphonate-based strategies for bone tissue engineering and orthopedic Implants*. *Tissue Engineering: Part B*, 2012. **18**(5): p. 323-340.
302. Lu, P., et al., *Controllable biodegradability, drug release behavior and hemocompatibility of PTX-eluting magnesium stents*. *Colloids Surf B Biointerfaces*, 2011. **83**(1): p. 23-28.
303. Burt, H. and W. Hunter, *Drug-eluting stents: A multidisciplinary success story*. *Advanced Drug Delivery Reviews*, 2006. **58**: p. 350-357.
304. Lemos, P., P. Serruys, and J. Sousa, *Drug-Eluting Stents: Cost Versus Clinical Benefit*. *Circulation: Journal of the American Heart Association*, 2003. **107**: p. 3003-3007.
305. von Eiff, C., et al., *Infections Associated with Medical Devices*. *Drugs*, 2005. **65**(2): p. 179-214.

306. Tang, L., T.A. Jennings, and J.W. Eaton, *Mast cells mediate acute inflammatory responses to implanted biomaterials*. Proceedings of the National Academy of Sciences, 1998. **95**(15): p. 8841-8846.
307. Onuki, Y., et al., *A review of the biocompatibility of implanted devices: current challenges to overcome foreign body response*. J Diabetes Sci Technol, 2008. **2**(6): p. 1003-1015.
308. Luttkhuizen, D., M. Harmsen, and M.V. Luyn, *Cellular and Molecular Dynamics in the Foreign Body Reaction*. Tissue Engineering, 2006. **12**(7): p. 1955-1970.
309. Anderson, J.M., A. Rodriguez, and D.T. Chang. *Foreign body reaction to biomaterials*. in *Seminars in immunology*. 2008. Elsevier.
310. Hossfeld, S., et al., *Bioactive coronary stent coating based on layer-by-layer technology for siRNA release*. Acta Biomaterialia, 2013. **9**(5): p. 6741-6752.
311. Goodman, S., et al., *The future of biologic coatings for orthopedic implants*. Biomaterials, 2013: p. 1-10.
312. Yoshii, S., et al., *In vivo guidance of regenerating nerve by laminin-coated filaments*. Experimental neurology, 1987. **96**(2): p. 469-473.
313. Madison, R., et al., *Increased rate of peripheral nerve regeneration using bioresorbable nerve guides and a laminin-containing gel*. Experimental neurology, 1985. **88**(3): p. 767-772.
314. Martini, R., *Expression and functional roles of neural cell surface molecules and extracellular matrix components during development and regeneration of peripheral nerves*. Journal of neurocytology, 1994. **23**(1): p. 1-28.
315. Fawcett, J. and R.J. Keynes, *Peripheral nerve regeneration*. Annual review of neuroscience, 1990. **13**(1): p. 43-60.
316. Zhang, M. and I.V. Yannas, *Peripheral nerve regeneration*, in *Regenerative Medicine II*. 2005, Springer. p. 67-89.

317. Hildebrand, H.F., et al., *Surface coatings for biological activation and functionalization of medical devices*. Surface and Coatings Technology, 2006. **200**(22–23): p. 6318-6324.
318. Xie, J., et al., *Neurite outgrowth on nanofiber scaffolds with different orders, structures, and surface properties*. ACS nano, 2009. **3**(5): p. 1151-1159.
319. Matsumoto, K., et al., *Peripheral nerve regeneration across an 80-mm gap bridged by a polyglycolic acid (PGA)–collagen tube filled with laminin-coated collagen fibers: a histological and electrophysiological evaluation of regenerated nerves*. Brain research, 2000. **868**(2): p. 315-328.
320. Nectow, A.R., K.G. Marra, and D.L. Kaplan, *Biomaterials for the development of peripheral nerve guidance conduits*. Tissue Engineering Part B: Reviews, 2011. **18**(1): p. 40-50.
321. Song, Z., et al., *Prosthesis Infections after Orthopedic Joint Replacement: The Possible Role of Bacterial Biofilms*. Orthopedic Reviews, 2013. **5**(2): p. e14.
322. Ribeiro, M., F.J. Monteiro, and M.P. Ferraz, *Infection of orthopedic implants with emphasis on bacterial adhesion process and techniques used in studying bacterial-material interactions*. Biomatter, 2012. **2**(4): p. 176-194.
323. Kingshott, P., et al., *Covalent Attachment of Poly(ethylene glycol) to Surfaces, Critical for Reducing Bacterial Adhesion*. Langmuir, 2003. **19**(17): p. 6912-6921.
324. Kaper, H., H. Busscher, and W. Norde, *Characterization of poly(ethylene oxide) brushes on glass surfaces and adhesion of Staphylococcus epidermidis*. J Biomater Sci Polymer Edn, 2003. **14**(4): p. 313-324.
325. Harris, L.G., et al., *Staphylococcus aureus adhesion to titanium oxide surfaces coated with non-functionalized and peptide-functionalized poly(l-lysine)-grafted-poly(ethylene glycol) copolymers*. Biomaterials, 2004. **25**(18): p. 4135-4148.
326. Bridges, A. and A. Garcia, *Anti-Inflammatory Polymeric Coatings for Implantable Biomaterials and Devices*. Journal of Diabetes Science and Technology, 2008. **2**(6): p. 984-994.
327. Anderson, J.M., A. Rodriguez, and D.T. Chang, *FOREIGN BODY REACTION TO BIOMATERIALS*. Seminars in immunology, 2008. **20**(2): p. 86-100.

328. Kim, D.-H. and D.C. Martin, *Sustained release of dexamethasone from hydrophilic matrices using PLGA nanoparticles for neural drug delivery*. *Biomaterials*, 2006. **27**(15): p. 3031-3037.
329. Zhong, Y. and R.V. Bellamkonda, *Dexamethasone-coated neural probes elicit attenuated inflammatory response and neuronal loss compared to uncoated neural probes*. *Brain Research*, 2007. **1148**: p. 15-27.
330. Zhong, Y., et al. *A novel dexamethasone-releasing, anti-inflammatory coating for neural implants*. in *Neural Engineering, 2005. Conference Proceedings. 2nd International IEEE EMBS Conference on*. 2005. IEEE.
331. Kingshott, P. and H.J. Griesser, *Surfaces that resist bioadhesion*. *Current Opinion in Solid State and Materials Science*, 1999. **4**(4): p. 403-412.
332. Ju, Y.M., et al., *A novel porous collagen scaffold around an implantable biosensor for improving biocompatibility. I. In vitro/in vivo stability of the scaffold and in vitro sensitivity of the glucose sensor with scaffold*. *Journal of Biomedical Materials Research Part A*, 2008. **87A**(1): p. 136-146.
333. Koschwanez, H.E., et al., *In vitro and in vivo characterization of porous poly-L-lactic acid coatings for subcutaneously implanted glucose sensors*. *Journal of Biomedical Materials Research Part A*, 2008. **87A**(3): p. 792-807.
334. Yu, B., et al., *Use of hydrogel coating to improve the performance of implanted glucose sensors*. *Biosensors and Bioelectronics*, 2008. **23**(8): p. 1278-1284.
335. Quinn, C.P., et al., *Photo-crosslinked copolymers of 2-hydroxyethyl methacrylate, poly(ethylene glycol) tetra-acrylate and ethylene dimethacrylate for improving biocompatibility of biosensors*. *Biomaterials*, 1995. **16**(5): p. 389-396.
336. Quinn, C.A.P., R.E. Connor, and A. Heller, *Biocompatible, glucose-permeable hydrogel for in situ coating of implantable biosensors*. *Biomaterials*, 1997. **18**(24): p. 1665-1670.
337. Weber, N., H.P. Wendel, and G. Ziemer, *Hemocompatibility of heparin-coated surfaces and the role of selective plasma protein adsorption*. *Biomaterials*, 2002. **23**(2): p. 429-439.

338. He, W., et al., *A Novel Anti-inflammatory Surface for Neural Electrodes*. *Advanced Materials*, 2007. **19**(21): p. 3529-3533.
339. Kim, D.-H., et al., *The effect of covalently immobilized rhIL-1ra-ELP fusion protein on the inflammatory profile of LPS-stimulated human monocytes*. *Biomaterials*, 2007. **28**(23): p. 3369-3377.
340. Gao, H.-M., et al., *Synergistic dopaminergic neurotoxicity of MPTP and inflammogen lipopolysaccharide: relevance to the etiology of Parkinson's disease*. *The FASEB Journal*, 2003. **17**(13): p. 1957-1959.
341. Johnston, J.R., C.A. Godzik, and Z.A. Cohn, *Increased superoxide anion production by immunologically activated and chemically elicited macrophages*. *The Journal of experimental medicine*, 1978. **148**(1): p. 115-129.
342. Udipi, K., et al., *Modification of inflammatory response to implanted biomedical materials in vivo by surface bound superoxide dismutase mimics*. *Journal of Biomedical Materials Research*, 2000. **51**(4): p. 549-560.
343. Junker, R., et al., *Effects of implant surface coatings and composition on bone integration: a systematic review*. *Clinical Oral Implants Research*, 2009. **20**: p. 185-206.
344. Auernheimer, J., et al., *Titanium Implant Materials with Improved Biocompatibility through Coating with Phosphonate-Anchored Cyclic RGD Peptides*. *ChemBioChem*, 2005. **6**(11): p. 2034-2040.
345. Elmengaard, B., J.E. Bechtold, and K. Søballe, *In vivo study of the effect of RGD treatment on bone ongrowth on press-fit titanium alloy implants*. *Biomaterials*, 2005. **26**(17): p. 3521-3526.
346. Reyes, C.D., et al., *Biomolecular surface coating to enhance orthopaedic tissue healing and integration*. *Biomaterials*, 2007. **28**(21): p. 3228-3235.
347. Becker, J., et al., *Bone apposition to titanium implants biocoated with recombinant human bone morphogenetic protein-2 (rhBMP-2). A pilot study in dogs*. *Clinical oral investigations*, 2006. **10**(3): p. 217-224.
348. Gurbel, P.A. and K.P. Bliden, *Platelet activation after stenting with heparin-coated versus noncoated stents*. *American heart journal*, 2003. **146**(4): p. 691.

349. Christensen, K., et al., *Heparin coating of the stent graft — effects on platelets, coagulation and complement activation*. *Biomaterials*, 2001. **22**(4): p. 349-355.
350. Du, Y.J., et al., *Protein adsorption on polyurethane catheters modified with a novel antithrombin-heparin covalent complex*. *Journal of Biomedical Materials Research Part A*, 2007. **80**(1): p. 216-225.
351. Ye, S.-H., et al., *Simple surface modification of a titanium alloy with silanated zwitterionic phosphorylcholine or sulfobetaine modifiers to reduce thrombogenicity*. *Colloids and Surfaces B: Biointerfaces*, 2010. **79**(2): p. 357-364.
352. Ye, S.H., et al., *Surface modification of a titanium alloy with a phospholipid polymer prepared by a plasma-induced grafting technique to improve surface thromboresistance*. *Colloids and Surfaces B: Biointerfaces*, 2009. **74**(1): p. 96-102.
353. Nilsson, P.H., et al., *The creation of an antithrombotic surface by apyrase immobilization*. *Biomaterials*, 2010. **31**(16): p. 4484-4491.
354. Paderi, J.E., et al., *The inhibition of platelet adhesion and activation on collagen during balloon angioplasty by collagen-binding peptidoglycans*. *Biomaterials*, 2011. **32**(10): p. 2516-2523.
355. Dimopoulos, G.J. and R.O. Langner, *Inhibition of phosphodiesterase has an additive effect on estrogen's ability to inhibit collagen synthesis in vascular smooth muscle cells*. *Vascular Pharmacology*, 2009. **50**(1–2): p. 78-82.
356. Zhang, K., et al., *Surface modification of implanted cardiovascular metal stents: from antithrombosis and antirestenosis to endothelialization*. *Journal of Biomedical Materials Research Part A*, 2014. **102**(2): p. 588-609.
357. Poh, C.K., et al., *The effect of VEGF functionalization of titanium on endothelial cells in vitro*. *Biomaterials*, 2010. **31**(7): p. 1578-1585.
358. Ceylan, H., A.B. Tekinay, and M.O. Guler, *Selective adhesion and growth of vascular endothelial cells on bioactive peptide nanofiber functionalized stainless steel surface*. *Biomaterials*, 2011. **32**(34): p. 8797-8805.
359. Yu, L.M.Y., N.D. Leipzig, and M.S. Shoichet, *Promoting neuron adhesion and growth*. *Materials Today*, 2008. **11**(5): p. 36-43.

360. Lévesque, S.G. and M.S. Shoichet, *Synthesis of cell-adhesive dextran hydrogels and macroporous scaffolds*. *Biomaterials*, 2006. **27**(30): p. 5277-5285.
361. Luo, Y. and M.S. Shoichet, *A photolabile hydrogel for guided three-dimensional cell growth and migration*. *Nat Mater*, 2004. **3**(4): p. 249-253.
362. Hynd, M.R., et al., *Directed cell growth on protein-functionalized hydrogel surfaces*. *Journal of Neuroscience Methods*, 2007. **162**(1-2): p. 255-263.
363. Dertinger, S.K.W., et al., *Gradients of substrate-bound laminin orient axonal specification of neurons*. *Proceedings of the National Academy of Sciences*, 2002. **99**(20): p. 12542-12547.
364. Sehgal, D. and I.K. Vijay, *A Method for the High Efficiency of Water-Soluble Carbodiimide-Mediated Amidation*. *Analytical Biochemistry*, 1994. **218**(1): p. 87-91.
365. Patel, N., et al., *Immobilization of Protein Molecules onto Homogeneous and Mixed Carboxylate-Terminated Self-Assembled Monolayers*. *Langmuir*, 1997. **13**(24): p. 6485-6490.
366. Fägerstam, L.G., et al., *9th International Symposium on Affinity Chromatography and Biological Recognition Biospecific interaction analysis using surface plasmon resonance detection applied to kinetic, binding site and concentration analysis*. *Journal of Chromatography A*, 1992. **597**(1): p. 397-410.
367. Santiago, L.Y., et al., *Peptide-surface modification of poly(caprolactone) with laminin-derived sequences for adipose-derived stem cell applications*. *Biomaterials*, 2006. **27**(15): p. 2962-2969.
368. Duan, X., et al., *Biofunctionalization of collagen for improved biological response: Scaffolds for corneal tissue engineering*. *Biomaterials*, 2007. **28**(1): p. 78-88.
369. Gooding, J.J. and D.B. Hibbert, *The application of alkanethiol self-assembled monolayers to enzyme electrodes*. *TrAC Trends in Analytical Chemistry*, 1999. **18**(8): p. 525-533.
370. Balamurugan, S., et al., *Surface immobilization methods for aptamer diagnostic applications*. *Analytical and Bioanalytical Chemistry*, 2008. **390**(4): p. 1009-1021.

371. Snyder, N., *Novel method for the prevention of neurodegeneration around neural implants*, in *Bioengineerg*. 2015, The University of Pittsburgh.
372. Rapoport, R., I. Hanukoglu, and D. Sklan, *A Fluorometric Assay for Hydrogen Peroxide, Suitable for NAD(P)H-Dependent Superoxide Generating Redox Systems*. *Analytical Biochemistry*, 1994. **218**(2): p. 309-313.
373. McCord, J.M. and I. Fridovich, *The reduction of cytochrome c by milk xanthine oxidase*. *Journal of Biological Chemistry*, 1968. **243**(21): p. 5753-5760.
374. Carmona-Ribeiro, A.M. and L.D. de Melo Carrasco, *Cationic antimicrobial polymers and their assemblies*. *International journal of molecular sciences*, 2013. **14**(5): p. 9906-9946.
375. Cline, G.W. and S.B. Hanna, *Kinetics and mechanisms of the aminolysis of N-hydroxysuccinimide esters in aqueous buffers*. *The Journal of Organic Chemistry*, 1988. **53**(15): p. 3583-3586.
376. Chen, S.-n. and M.Z. Hoffman, *Rate constants for the reaction of the carbonate radical with compounds of biochemical interest in neutral aqueous solution*. *Radiation research*, 1973. **56**(1): p. 40-47.
377. Nam, K., T. Kimura, and A. Kishida, *Controlling Coupling reaction of EDC and NHS for preraration of collagen gels using ethanol/water co-solvents*. *Macromolecular Bioscience*, 2008. **8**: p. 32-37.
378. Park, K.D., et al., *Bacterial adhesion on PEG modified polyurethane surfaces*. *Biomaterials*, 1998. **19**(7): p. 851-859.
379. Zhang, M., T. Desai, and M. Ferrari, *Proteins and cells on PEG immobilized silicon surfaces*. *Biomaterials*, 1998. **19**(10): p. 953-960.
380. Rolfe, B., et al., *The fibrotic response to implanted biomaterials: implications for tissue engineering*. 2011: INTECH Open Access Publisher.
381. Morra, M., *On the molecular basis of fouling resistance*. *Journal of Biomaterials Science, Polymer Edition*, 2000. **11**(6): p. 547-569.

382. Chen, M., et al., *Role of fiber diameter in adhesion and proliferation of NIH 3T3 fibroblast on electrospun polycaprolactone scaffolds*. Tissue Engineering, 2007. **13**(3): p. 579-587.
383. Westerink, R.H.S. and A.G. Ewing, *The PC12 cell as model for neurosecretion*. Acta physiologica (Oxford, England), 2008. **192**(2): p. 273-285.
384. Tomaselli, K.J., C.H. Damsky, and L.F. Reichardt, *Interactions of a neuronal cell line (PC12) with laminin, collagen IV, and fibronectin: identification of integrin-related glycoproteins involved in attachment and process outgrowth*. The Journal of cell biology, 1987. **105**(5): p. 2347-2358.
385. Drubin, D.G., et al., *Nerve growth factor-induced neurite outgrowth in PC12 cells involves the coordinate induction of microtubule assembly and assembly-promoting factors*. The Journal of Cell Biology, 1985. **101**(5): p. 1799-1807.
386. Takebayashi, M., T. Hayashi, and T.-P. Su, *Nerve growth factor-induced neurite sprouting in PC12 cells involves ζ -1 receptors: implications for antidepressants*. Journal of Pharmacology and Experimental Therapeutics, 2002. **303**(3): p. 1227-1237.
387. Attiah, D.G., R.A. Kopher, and T.A. Desai, *Characterization of PC12 cell proliferation and differentiation-stimulated by ECM adhesion proteins and neurotrophic factors*. Journal of Materials Science: Materials in Medicine, 2003. **14**(11): p. 1005-1009.
388. Kapur, T.A. and M.S. Shoichet, *Immobilized concentration gradients of nerve growth factor guide neurite outgrowth*. Journal of Biomedical Materials Research Part A, 2004. **68**(2): p. 235-243.
389. Achyuta, A.K.H., et al., *Synergistic effect of immobilized laminin and nerve growth factor on PC12 neurite outgrowth*. Biotechnology progress, 2009. **25**(1): p. 227-234.
390. Lee, J.Y., et al., *Nerve growth factor-immobilized electrically conducting fibrous scaffolds for potential use in neural engineering applications*. NanoBioscience, IEEE Transactions on, 2012. **11**(1): p. 15-21.
391. Anderson, J., *Biological Responses to Materials*. Annu. Rev. Mater. Res., 2001. **31**: p. 81-110.

392. Rivers, T.J., T.W. Hudson, and C.E. Schmidt, *Synthesis of a novel, biodegradable electrically conducting polymer for biomedical applications*. *Advanced Functional Materials*, 2002. **12**(1): p. 33-37.